TRANSPORT PHENOMENA IN VISCOELASTIC FLUIDS FLOW

HIROMOTO USUI

December 1974

TRANSPORT PHENOMENA

IN

VISCOELASTIC FLUIDS FLOW

HIROMOTO USUI

December 1974

Contents

CHAPTER 1

INTRODUCTION

1-1 The tendency of contemporary research in the field of non-Newtonian transport phenomena.

For the practical application of rheological knowldge to the industrial engineering, two main approaches are indispensable. One is to find the constitutive equations which are able to discribe precisely the non-Newtonian behavior, and the other is to solve the practical problems concerning transport phenomena which appear in the industrial processes by using an appropriate constitutive equations.

The constitutive equations proposed by many authors are divided into two categories, i.e. purely viscous fluids and viscoelastic fluids. The purpose of this study is not to propose a new constitutive equation, but to make clear the mechanism of non-Newtonian fluid flow and heat tronsfer by using the appropriate constitutive

equations already given by previous investigators. In the research on transport phenomena of non-Newtonian fluids under the condition of forced convection, the extention of the analyses for Newtonian fluid to those for purely viscous non-Newtonian fluids have been widely made, and a great deal of available results have been obtained.

The effects of non-Newtonian viscosity on transport phenomena in simple geometrical flow systems, such as laminar and turbulent pipe flow, boundary layer on a flat plate and cross flow around a submerged sphere or cylinder , have been precisely investigated and good predictions are available for practical design problems. But more detailed studies on the complicated geometrical flow or the other flow systems such as mixed convection and unsteady flow, are still needed.

Recently the transport phenomena of viscoelastic fluids have become to attract the stimulative interests of many investigators. But the complexity of constitutive equations of viscoelastic fluids make the mathematical treatment very difficult except a few example of simple flow, i.e. so-called visco-metric flow. So the more detailed studies on viscoelastic fluid flow are needed even in the simple flow systems.

1-2 Purpose and outline of this study.

Taking into account the discussions mentioned above the author has taken the turbulent transport phenomena and the transprot phenomena in cross flow around a circular cylinder of viscoelastic fluids as the subject of this study. Turbulent flow of viscoelastic fluids is one of the most important subject in the study of non-Newtonian transport phenomena. The constitutive equations for laminar simple shear flow may be insufficient to be applied to turbulent flow. Thus the determination of the rheological constants which should be used in turbulent flow is needed. This study deals with such a problem combining with the mechanism of turbulent shear flow. And also there is a current need to analyze the cross flow of viscoelastic fluids around a circular cylinder. Since the anomalous behavior of hot wire anemometer in the dilute polymer solutions was found, this subject has been discussed concerning with the turbulent measurement technique.

Viscoelastic fluids usualy show also non-Newtonian viscosity, and the constitutive equations which can explain both viscoelasticity and non-Newtonian viscosity become very complicated. This is one of the main difficulty

in the analyses of viscoelastic fluid flow. On the other hand, the very dilute polymer solutions usualy do not show non-Newtonian viscosity, but show only weak viscoelasticity in the laminar simple shear flow. It is well known that Maxwell model can explain the behavior of dilute polymer solutions. Thus the dilute polymer solutions will be used as viscoelastic fluids in this study, and Maxwell model will be taken as the constitutive equation of such fluids. Denn model also will be used in the complementary analyses. These models are the so-called rate equations of viscoelastic fluids, and they can only explain a few effects of viscoelastic fluids. As a results, only a part of viscoelasticity was caught in this study. The author feeled keenly the necessity to use the so-called integral equations. He hopes the appearrance of a simple constitutive equation which can explain the various effects of viscoelasticity.

Consequently, the purpose of this study is to investigate the mechanism of transport phenomena of viscoelastic fluid in turbulent pipe flow, and in cross flow around a circular cylinder.

In Chapter 2, the results of measurements of drag reduction in turbulent pipe flow are described and this phenomena is explained by means of damping factor model

for viscoelastic fluid.

Chapter 3 deals with the heat transfer rate reduction of viscoelastic fluids. Nusselt number and temperature distributions in fully developed flow region are measured by thermo-couples. An extension of damping factor model to heat transfer reduction is shown, and the mechanism of heat transfer reduction is explained by this model.

In Chapter 4, Laser Doppler anemometry will be employed for the measurement of velocity profile of highly elastic fluids in rectangular duct. The results obtained from this experiments ascertain the availability of the visco-elastic damping factor model given in Chapter 2 also for the case of highly elastic fluids.

Numerical solution of Navier-Stokes equation with generalized Maxwell model for the case of a cross flow around a circular cylinder is given in Chapter 5. The results of this calculation is compared with the results obtained by electro-chemical method. The reduction of Nusselt number is explained by this calculation.

In Chapter 6, the final conclusions of this study and recomendation for futher works are given.

CHAPTER 2

DRAG REDUCTION IN TURBULENT PIPE FLOW

2-1 Introduction

2-1-1 Summary of previous works.

In 1948, A.B.Toms (58) expressed the turbulent drag reduction in pipe flow at First International Rheology Congress, Amsterdam. This was the first report about the drag reduction of polymer solutions. The observation of Toms have been confirmed in many subsequent investigators and this phenomenon has been called as Toms phenomenon. From the experimental results of pressure drop measured by many investigators, several kinds of peculiar effects in Toms phenomenon have been clarified. These effects are listed in Table 2-1. To explain these effects, and to interpret physical meaning of Toms phenomenon, various kinds of theoretical approaches have been tried and many useful results were obtained. But, because of the lack of appropriate constitutive equations that are valid in turbulent pipe flow, and because of the complexity of this

Table 2-1

Effects in Toms phenomenon.

1) Concentration effect
2) Polymer molecular weight effect
3) Pipe diameter effect
4) Saturation effect
5) Onset effect

---

phenomenon, its mechanism has not so far been fully explained.

The results obtained up to now for the prediction of friction factor are listed in Table 2-2. The results for velocity distribution are listed in Table 2-3, and those for eddy diffusivity are in Table 2-4.

Dodge and Metzner (14) derived the relationship between friction factor and Reynolds number for the power law model using the dimensional analysis. At first this interpretation based on the unisotropic viscosity was thought as the reason of drag reduction. But later experimental results showed that very dilute polymer solutions which showed no non-Newtonian viscosity also

caused a serious reduction of pressure drop. So the main interest of theoretical researches transferred to the viscoelasticity of dilute polymer solutions. The relaxation time or the elastic modulus were taken as the viscoelastic properties, and Elata (18), Seyer-Metzner (49) and Hasegawa-Tomita (25) gave the predicting equations for viscoelastic fluids shown in Table 2-2. These equations have two demerits. First the rheological constants are generally unknown in a design problem. Second, they cannot fully explain the many effects of drag reduction. The experimental results of friction factor were summarized recently by Virk (62) and Bazilevich (5). The investigations of velocity distribution of viscoelastic turbulent flow are not yet sufficient. The measurements of velocity distribution by means of usual technique are not correct because of the elasticity of polymer solutions. So the special technique, for example, Laser Doppler anemometry or bubble tracer method etc., must be used for the case of highly elastic fluids. Such experiments were carried out by some investigators, i.e. by Seyer-Metzner (49) — bubble tracer method —, by Rudd (48) — Laser Doppler meter —, by Arunahaham-Hummel-Smith (3) — dye injection method — etc. The results of these experimentors showed that the laminar sublayer was thickened and the velocity distribution of turbulent core was parallelly shifted to

Table 2-2

Expression for friction factor of drag reducing system.

Dodge-Metzner (14)

$$\sqrt{\frac{1}{f}} = \frac{4.0}{n^{0.75}} \log\left(N_{Re'} f^{1-\frac{n'}{2}}\right) - \frac{4.0}{n'^{1.4}}$$

where $N_{Re'} = \frac{D^{n'} \bar{u}^{2-n'}}{K' 8^{n-1}}$, $K' = K \left(\frac{3n+1}{4n}\right)^n$,

$$n' = \frac{d\{\log(D \Delta p/L)\}}{d\{\log(8 \bar{u}/D)\}}$$

Elata (18)

$$\sqrt{\frac{1}{f}} = 4.0 \log\left(N_{Re'} f^{\frac{1}{2}}\right) + \frac{\Omega}{\sqrt{2}} \quad 8.6$$

where $\Omega = 11.6 + \beta \log(u^{*2} \lambda_\ell / \nu)$

β : function of concentration of polymer additive

Seyer-Metzner (49)

$$\sqrt{\frac{2}{f}} = 2.5 \{1 - (\frac{y_\ell}{R})\}^2 \ln Re\sqrt{f} + \{1 - (\frac{y_\ell}{R})\}^2$$

$$\times \{B(\tau) - 2.5 \ln 2\sqrt{2}\} - 3.0$$

where y_ℓ : intersection of linear and logarithmic velocity profile

$B(\tau)$: intersept function given by Fig.8 of ref.(49)

$\tau = \theta u^{*2}/\nu$

Table 2-2 (contd.)

Virk (62)

for maximum reduction asymptote,

$$\sqrt{\frac{1}{f}} = 19.0 \log(Re\sqrt{f}) - 32.0$$

Hasegawa-Tomita (25)

$$\frac{1}{\sqrt{(1 + \alpha Ne^*)\lambda}} = \frac{2.0}{n^{0.75}} \log(1 + \alpha Ne^*)^{-\frac{n}{2}} Re^* \lambda^{\frac{1-n}{2}} - \{\frac{2.0}{n^{1.2}} + \frac{1.2}{n^{0.75}}(1 - \frac{n}{2})\}$$

where $Ne^* = \frac{K}{G}(\frac{8\bar{u}}{D})^{n-k}$, $Re^* = \frac{\rho \bar{u}^{2-n} D^n}{K(\frac{3n+1}{4n})^n 8^{n-1}}$

G , k : rheological constants

λ : Darcy friction factor

α : empirical constant

Table 2-3

Various expressions for velocity distribution of viscoelastic fluids.

Wells (65)

$$u^+ = \frac{1}{n\kappa} \ln \left(\frac{\rho\, u^{*2-n}\, y^n}{K}\right) + B$$

where B : thickness of laminar sublayer

$$\kappa(\rho u^{*2-n} B^n/K)^{1/n} = 10$$

Seyer-Metzner (49)

$$u^+ = 2.5 \ln y^+ + B(\tau)$$

$B(\tau)$: see Table 2-?

Poreh-Paz (45)

$$u^+ = y^+ \qquad ; \quad 0 < y^+ < y_1^+$$

$$u^+ = y_1^+ \ln(y^+/y_1^+) + y_1^+ \qquad ; \quad y_1^+ < y^+ < y_2^+$$

$$u^+ = 2.5 \ln(y^+/y_j^+) + u_j^+ \qquad ; \quad y_2^+ < y^+ < R^+$$

where $\ln(y_2^+/y_1^+) = \dfrac{1.32\, y_j^+ - 4.9}{y_j^+ - 5.8}$, $u_j^+ = y_j^+$

y_1^+ : the edge of laminar sublayer.

y_2^+ : the edge of buffer region.

Virk (62)

for maximum reduction asymptote

$$u^+ = 11.7 \ln y^+ - 17.0$$

Table 2-4

Expressions for eddy diffusivity of non-Newtonian fluid.

Krantz-Wassan (30)

$$\frac{\varepsilon_M}{\nu} = \frac{\phi\,\overline{u'v'^+}}{\frac{du^+}{dy^+}}$$

where

$$\phi = \left(\frac{f\,Re}{16}\right)^{\frac{n+1}{n}} \Big/ \left(\frac{3n+1}{4n}\right), \quad \psi = \frac{2(f/2)^{\frac{n-2}{2n}}}{\left(\frac{3n+1}{4}\right) 8^{\frac{n-1}{n}} Re^{1/n}}$$

$$u^+ = \left[1 - \frac{\psi}{2} y^+ - \frac{n-1}{6}\psi^2\right] y^{+2} + U_4^+ y^{+4} + U_5^+ y^{+5} + \ldots$$

$$\overline{u'v'^+} = -\left[U_4^+ + \frac{(2n^2 - 3n + 1)}{24}\psi^3\right] 4n\, y^{+3}$$

$$- \left[5U_5^+ - 4(n-1)U_4^+\psi - \frac{(2n^3 - 9n^2 + 10n - 3)}{24}\psi^{44}\right] \times n\, y^{+4} + \ldots\ldots$$

$$U_4^+ = \frac{3\psi}{4\, y_c^{+2}} + \frac{(n-1)\psi^2}{4\, y_c^+} - \frac{1}{y_c^{+3}} + \frac{3.03}{y_c^{+4}}$$

$$U_5^+ = \frac{3\, y_c^+ - 2\,\psi y_c^{+2} - 0.5(n-1)\psi^2\, y_c^{+3} - 9.68}{5 y_c^{+5}}$$

Spalding (53)

$$\frac{\varepsilon_M}{\nu} = (0.4)^2\, y^{+2} \left(1 - \exp\frac{-y^+}{A'}\right) \frac{d\,u^+}{d\,y^+}$$

where $u^* < U_c$: $A' = 26$

$u^* \geq U_c$: $A' = 26\ \{1 + C \ln(\frac{u^*}{U_c})\}^2$

U_c : onset shear velocity.

C : stability parameter.

upward in u^+ vs. y^+ diagram. Taking account of this fact, Wells (65), Sayer-Metzner (49), Poreh-Paz (45) and Virk (62) proposed the velocity equations shown in Table 2-3. The basic concepts of Wells' and Seyer-Metzner's models are the thickning of laminar sublayer and their models are called as thickened sublayer models. The expression given by Virk is empirical one and it is called as elastic sublayer model. Poreh-Paz modified the equation for velocity profile of Newtonian fluid given by von-Kármán.

The expression of eddy diffusivity such as those commonly used in the analysis of Newtonian turbulent flow is not found except only two paper shown in Table 2-4. Krantz-Wassan (30) developed an equation for the eddy diffusivity of Power Law fluid. Spalding (53) showed the modification of van-Driest's damping factor model for the case of viscoelastic fluid. But he discussed the damping effect only qualitatively. The physical meaning of the constant ; C, appeared in his analysis is not clear.

Recently the measurement of turbulent characteristics, i.e. fluctuating velocity (48), scale of eddy (19), bursting period (35), were carried out by some investigators. These results seem to be very useful for undestanding Toms phenomenon and the accumulation of more results are anticipated.

2-1-2 Purpose and outline of this chapter.

The purpose of this chapter is to obtain a systematic expression of eddy diffusivity for momentum transfer which can explain all the effects in Toms phenomenon given in Table 2-1, and to predict the friction factor of viscoelastic fluids.

For this purpose, velocity distribution and friction factor in turbulent pipe flow of viscoelastic fluid are measured. The damping factor model of viscoelastic fluids for momentum transfer is derived and compared with the experimental results.

2-2 Damping factor model for momentum transfer of viscoelastic fluid.

The previous attempts to obtain the expressions for friction factor or velocity distribution were brifly reviewed in the preceding section. But they have not yet succeeded in explaining the various effects of Toms phenomenon. Moreover there exists some difficulty to estimate the rheological properties which appear in their expressions. So a simple and systematic method for predicting the drag reduction is needed. For this purpose, an analysis similar to the van-Driest's damping factor model (16) was made to obtain a viscoelastic damping factor for turbulent pipe flow of dilute polymer solutions.

Maxwell model will be used as a constitutive equation for dilute polymer solutions;

$$\tau + \lambda \frac{\partial \tau}{\partial t} = \mu \frac{\partial u}{\partial y} \qquad (2\text{-}1)$$

Let us consider the second problem of Stokes shown in Fig. 2-1. Equation of motion in this system can be written as

$$\rho \frac{\partial u}{\partial t} = \frac{\partial \tau}{\partial y} \qquad (2\text{-}2)$$

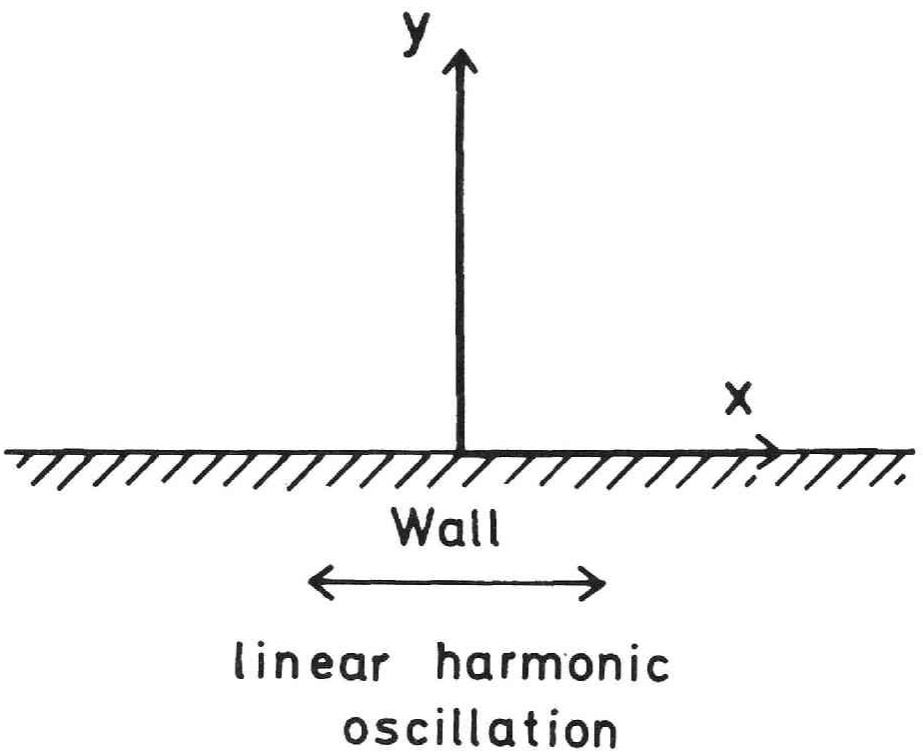

Fig. 2-1 Co-ordinate system

From Eqs.(2-1) and (2-2) one can obtain the basic equation of this analysis,

$$\lambda\frac{\partial^2 u}{\partial t^2} + \frac{\partial u}{\partial t} = \nu\frac{\partial^2 u}{\partial y^2} \qquad (2\text{-}3)$$

The boundary conditions are

$$u(y\ ,\ 0) = 0 \qquad \text{at } t = 0 \qquad (2\text{-}4\text{-}a)$$

$$u(0\ ,\ t) = U\cos\omega t \qquad \text{at } y = 0 \qquad (2\text{-}4\text{-}b)$$

$$u(\infty\ ,\ t) = 0 \qquad \text{at } y = \infty \qquad (2\text{-}4\text{-}c)$$

Eq.(2-3) may finally be rearranged by standard Laplace transformation and with the boundary condition, Eq.(2-4-a), into

$$\frac{d^2F(s)}{dy^2} = \frac{1}{\nu}(\lambda s^2 + s)F(s) \qquad (2\text{-}5)$$

The solution of this equation with the boundary conditions, Eqs.(2-4-b) and (2-4-c), is given as;

$$F(y,s) = F(o,s)\ \exp\left(-y\sqrt{\frac{\lambda s^2 + s}{\nu}}\right) \qquad (2\text{-}6)$$

The transfer function of Eq.(2-6)is written as

$$G(s) = \frac{F(y,s)}{F(o,s)} = \exp\left(-y\sqrt{\frac{\lambda s^2 + s}{\nu}}\right) \qquad (2\text{-}7)$$

Thus the gain of this transfer function is

$$|G(j\omega)| = \left|\exp\left(-y\sqrt{\frac{-\lambda\omega^2 + j\omega}{\nu}}\right)\right|$$

$$= \exp\left[-y\sqrt{\frac{\omega}{2\nu}\left\{-\omega\lambda + \sqrt{(\omega\lambda)^2 + 1}\right\}}\right] \qquad (2\text{-}8)$$

By a similar argument as van-Driest the damping factor of turbulent pipe flow in drag reducing system is given from Eq.(2-8) as;

$$DF_M = 1 \quad \exp\left[-y\sqrt{\frac{\omega}{2\nu}\{-\omega\lambda + \sqrt{(\omega\lambda)^2 + 1}\}}\right] \qquad (2\text{-}9)$$

If λ is put zero, the damping factor becomes;

$$DF_{M_o} = 1 - \exp\left[-y^+/A^+\right] \qquad (2\text{-}10)$$

where

$$A^+ = u^*\sqrt{\frac{2}{\omega\nu}} \qquad (2\text{-}11)$$

If A^+=26, Eq.(2-10) coincides with that of van-Driest. If the value of 26 is assumed to be taken as A^+ also for viscoelastic fluid, Eq. (2-9) becomes;

$$DF_M = 1 - \exp\left(-\frac{y^+}{26}\sqrt{-\alpha + \sqrt{\alpha^2 + 1}}\right) \qquad (2\text{-}12)$$

where

$$\alpha = \frac{2\lambda}{\nu}\left(\frac{u^*}{26}\right)^2 \qquad (2\text{-}13)$$

Then the friction factor of turbulent pipe flow in drag reducing system can be derived from this damping factor. Employing Prandtl's mixing length theory, the total shear stress of turbulent flow is expressed as;

$$\frac{\tau}{\tau_w} = \frac{du^+}{dy^+} + \ell_M^{+2}\left(\frac{du^+}{dy^+}\right)^2 \qquad (2\text{-}14)$$

The distribution of shear stress is linear over the pipe cross section, that is;

$$\frac{\tau}{\tau_w} = 1 - \frac{y^+}{R^+} \tag{2-15}$$

As the mixing length of viscoelastic fluid, the following expression which corresponds to the semiempirical expression of Nikuradse (44) in the Newtonian case is adopted,

$$\ell_M^+ = (0.4y^+ \quad 0.44\frac{y^{+2}}{R^+} + 0.24\frac{y^{+3}}{R^{+2}} - 0.06\frac{y^{+4}}{R^{+3}})$$
$$\times [1 - \exp\{-\frac{y^+}{26}\sqrt{-\alpha + \sqrt{\alpha^2 + 1}}\}] \tag{2-16}$$

From Eqs.(2-14),(2-15) and (2-16) we obtain the velocity distribution as,

$$u^+ = \int_0^{y^+} \frac{2(1 - \frac{y^+}{R^+})\, dy^+}{1 + \sqrt{1 + 4\, f_n(y^+, R^+)^2 DF_M^2 (1 - y^+/R^+)}} \tag{2-17}$$

where

$$fn(y^+,R^+) = 0.4y^+ - 0.44\frac{y^{+2}}{R^+} + 0.24\frac{y^{+3}}{R^{+2}} - 0.06\frac{y^{+4}}{R^{+3}} \tag{2-18}$$

The friction factor of a circular pipe flow is given by,

$$f = \tau_w/(\rho\bar{u}^2/2) = \frac{1}{2}(R^+/\int_0^{R^+} u^+(1-y^+/R^+)dy^+)^2 \tag{2-19}$$

Finally one can obtain the turbulent eddy diffusivity from Eqs.(2-14) and (2-16). The total turbulent shear stress is given in non-dimensional form as,

$$\frac{\tau}{\tau_w} = \frac{du^+}{dy^+} + \frac{\varepsilon_M}{\nu}\frac{du^+}{dy^+} \qquad (2\text{-}20)$$

From Eqs.(2-14),(2-16) and (2-20), the eddy diffusivity is obtained as,

$$\frac{\varepsilon_M}{\nu} = fn(y^+,R^+)^2\ DF_M{}^2\ \frac{du^+}{dy^+} \qquad (2\text{-}21)$$

2-3 Experimental apparatus and procedure.

The flow diagram of experimental apparatus is shown in Fig.2-2. To avoid the mechanical degradation of the polymers, the test liquids were forced to flow only by the difference of height between the test tube and head tank, which was about 190 cm. The test sections were circular tubes of 2.54 cm i.d. and 1.32 cm i.d. with smooth wall made of P.V.C..

The pressure drop in the test section was measured with a U-tube manometer of CCl_4, and the velocity distribution over the cross section was measured by a pitot tube of 1 mm dia.. In the case of high-concentration polymer solutions, the velocity distributions measured by a pitot tube are not correct because of the elasticity of polymer solutions. This anomalous behavior was checked by comparing the integrated flow rate with the directly

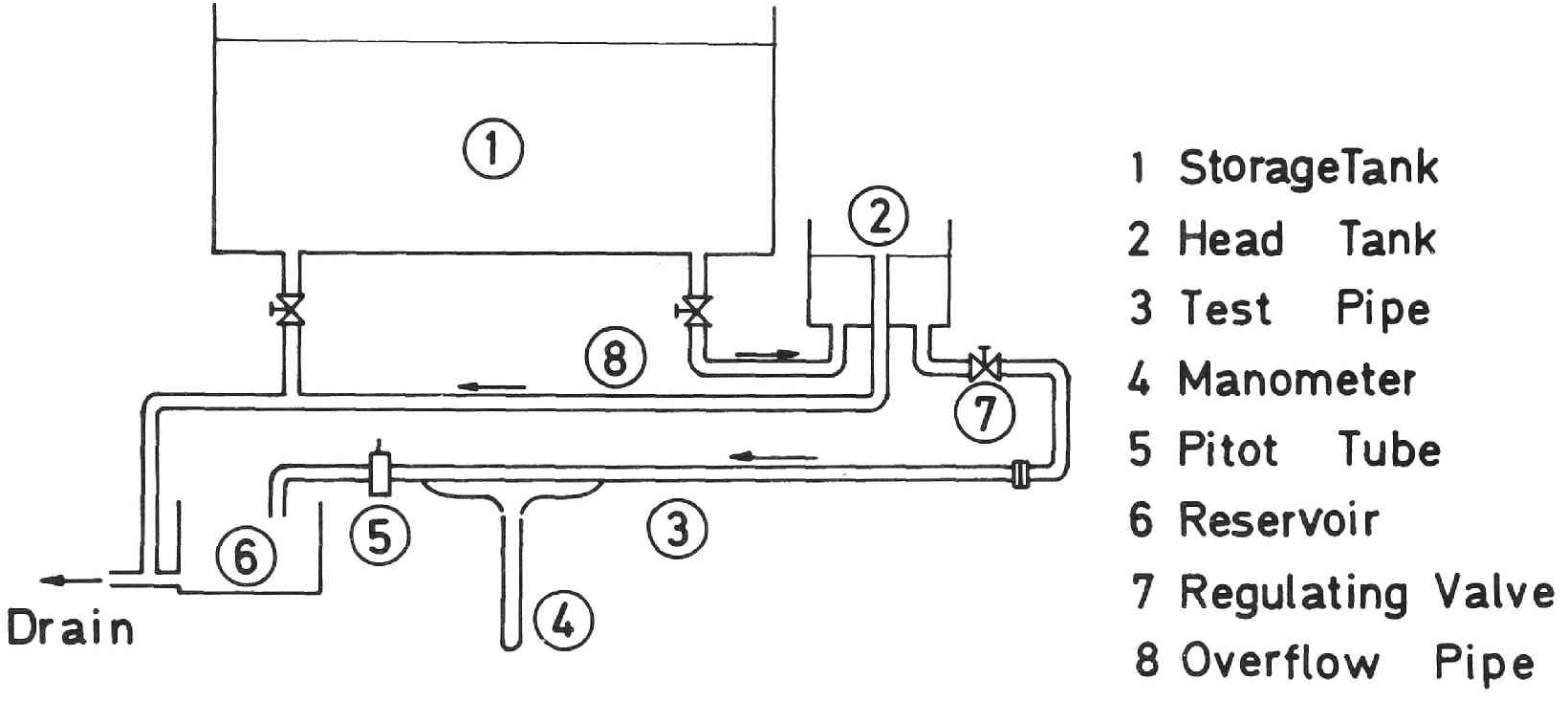

Fig. 2-2 Experimental apparatus.

measured flow rate by the weight-time method. When the error between these two methods was less than ± 1.0 %, the results of the velocity profile were adopted. In the case of highly elastic polymer solutions, it is impossible to measure the velocity distribution by usual methods —— pitot tube or hot wire method. In this study the Laser Doppler anemometry will be adopted to overcome this anomalous behavior of viscoelastic fluids. The results obtained by Laser Doppler meter will be shown in Chapter 4.

The polymer species used in this study were P.E.O. (polyethylene oxide) and P.A.A. (polyacrylamide). The concentration range of polymer solutions were 0 to 300 ppm for P.E.O. and 0 to 3000 ppm for P.A.A.. The intrinsic viscosity of the polymer solutions was measured by an Ostwald viscometer. The molecular weight of the polymer was calculated for polyethlene oxide by the following equation given by Shin (51).

$$[\eta] = 1.03 \times 10^{-4} M^{0.78} \qquad (2\text{-}22)$$

and for polyacrylamide by the following equation given by Collinson (8).

$$[\eta] = 6.80 \times 10^{-4} M^{0.66} \qquad (2\text{-}23)$$

The relaxation time for a laminar simple shear flow was calculated by the following equation, which was derived from the linear viscoelastic theory of Rouse (47) for the

case of laminar simple oscilatory shear flow with low frequency (28).

$$\lambda_\ell = \frac{2}{5} \frac{\eta_s [\eta]^2 M c}{R T} \qquad (2\text{-}24)$$

where R was gas constant and T was absolute temperature of polymer soputions. The range of molecular weight of P.E.O. was $2.41\times10^6 \sim 3.47\times10^6$, and the relaxation time varied $5.0\times10^{-6} \sim 3.2\times10^{-4}$ sec. The molecular weight of P.A.A. was determined as 7.22×10^5, and the relaxation time varied $3.3\times10^{-6} \sim 9.5\times10^{-5}$. None of the dilute polymer solutions used in this study showed a non-Newtonian viscosity, but they showed a weak elasticity.

2-4 Results and discussions.

2-4-1 Unsaturated region.

The analysis of viscoelastic fluid described in Section 2-2 showed that the damping effect of elasticity became greater than that of Newtonian fluid. If the relaxation time λ and the friction velocity u^* are given, the damping factor is able to be calculated by Eq.(2-12). But when the value of λ_ℓ given by Eq.(2-24) is used as

the relaxation time of turbulent pipe flow, the value of α in Eq.(2-13) becomes so small that no effect of viscoelasticity appears in the damping factor. Thus from the experimental results of pressure drop the relaxation time was calculated by using Eqs.(2-12), (2-17) and (2-19). The relaxation time obtained in this way was defined as the turbulent relaxation time, λ_t. The correlation of λ_t thus obtained was found to be

$$\frac{\lambda_t}{\lambda_\ell} = 3.76\times10^{8}\ We^{1.34} \qquad (2\text{-}25)$$

A comparison of this equation with the experimental results is shown in Fig.2-3. This plot includes all the effects of drag reduction in the unsaturated region given in Table 2-1.

Although the effect of viscoelasticity on damping factor seems to appear both in λ and ν of Eq.(2-13), it is very difficult to take into account the variety of ν in turbulent flow, because the viscosity appears not only in Eq.(2-13) but also in Eqs.(2-14),(2-16) and (2-21), etc. So,for simplicity, the effect of viscoelasticity was condensed only in relaxation time.

Before investigating each effects, the validity of the viscoelastic damping factor model must be shown. So the velocity profiles of dilute polymer solutions in turbulent pipe flow were calculated from Eqs.(2-12),(2-

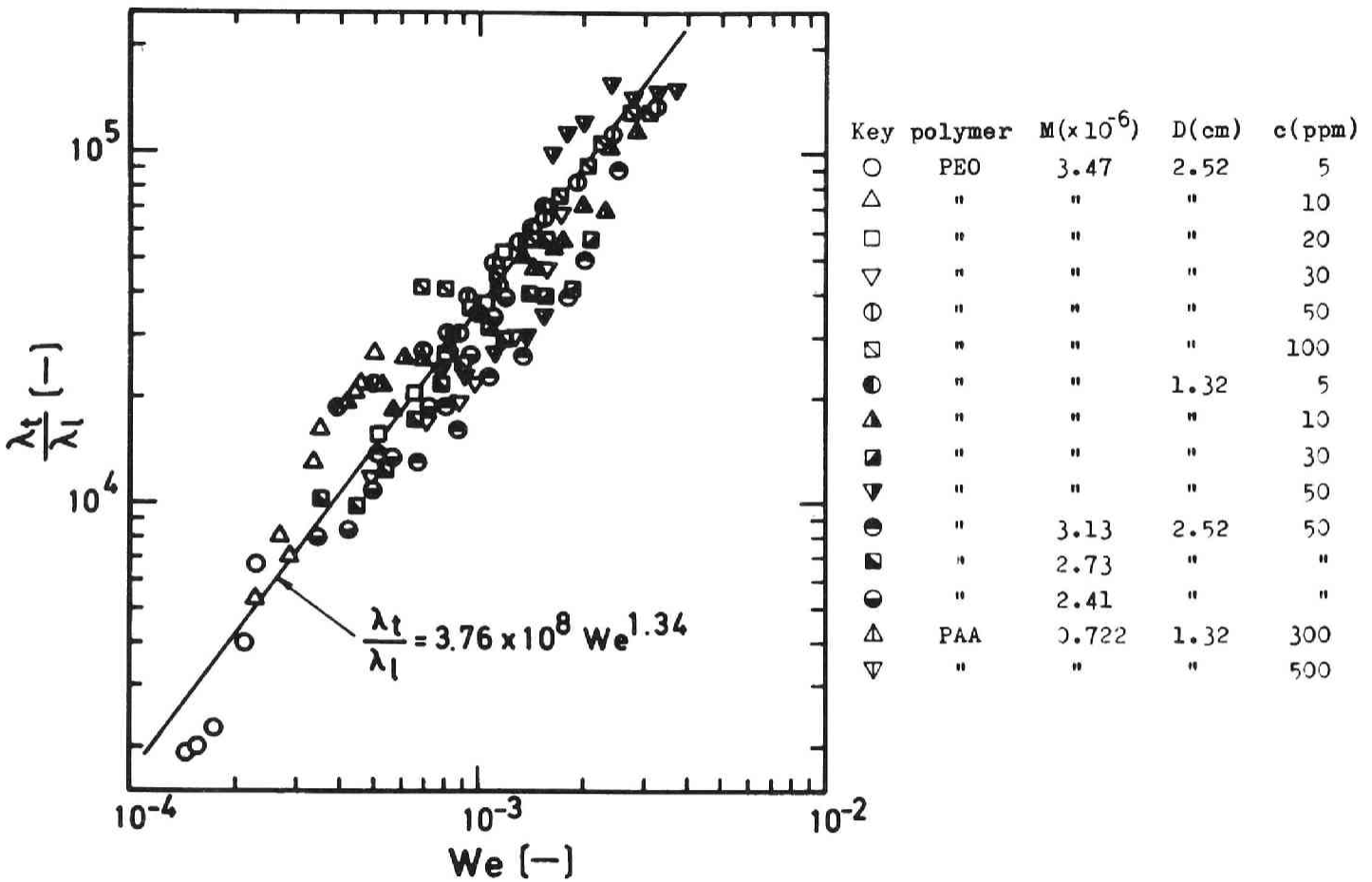

Fig. 2-3 Correlation of turbulent relaxation time.

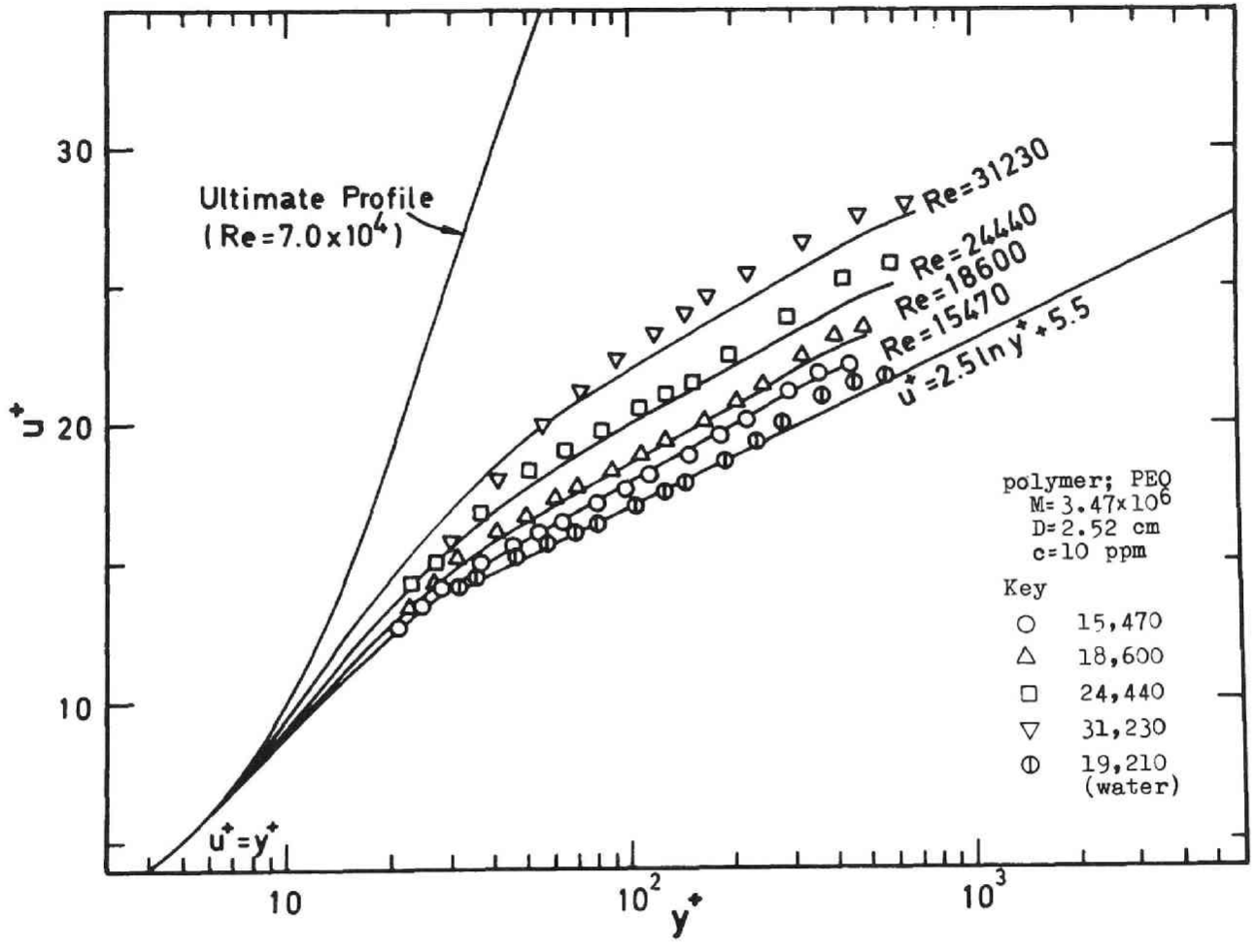

Fig. 2-4 Universal velocity profile of polymer solution.

17) and (2-25) and compared with experimental results as shown in Fig. 2-4. It can be concluded from this diagram that the damping factor model of this study can predict the actual velocity distribution fairly well in the low drag reduction region.

Next, the effects of various sources on drag reduction in the unsaturated region will be examined in Figs. 2-5, 2-6 and 2-7. The concentration effect is shown in Fig. 2-5. The curves of friction factor calculated from Eqs.(2-12),(2-17),(2-19) and (2-25) fit well with experimental results. In the same manner the predicted curves of molecular weight effect are represented in Fig. 2-6. Fig. 2-7 shows that the damping factor model of this study is available for pipe diameter effect. From these diagrams it is clear that the present model is useful to predict the dependence of friction factor on concentration, molecular weight and pipe diameter effect in the unsaturated drag reduction region. Moreover the applicability of this damping factor model to other polymer species was tested for the case of P.A.A.. The friction factor data of P.A.A. solution is represented in Fig. 2-8, and they agree well with the prediction of this model

Finally, it must be emphasized that the onset phenomena of drag reduction, which have been studied by

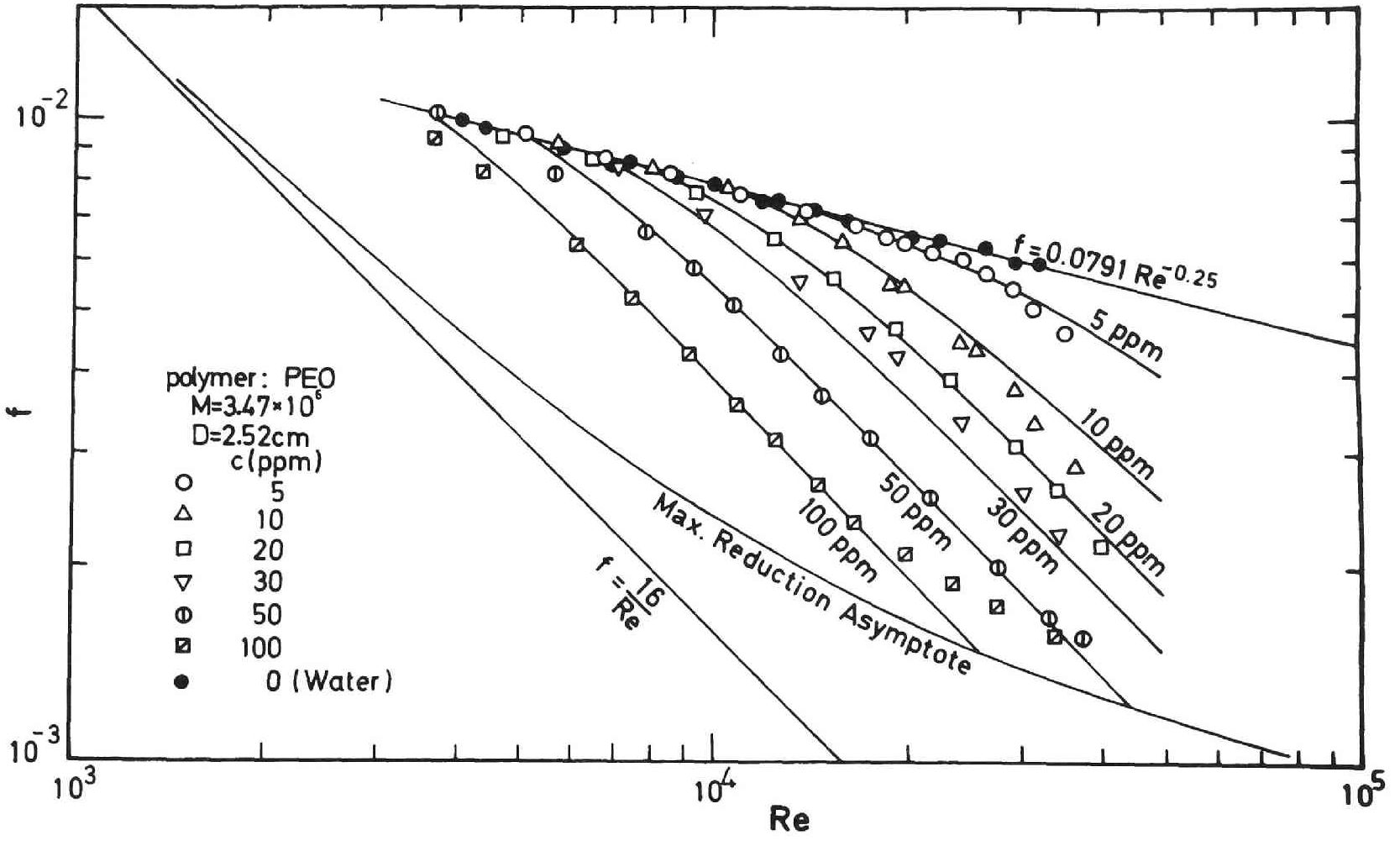

Fig. 2-5 The dependence of friction factor on the polymer concentration.

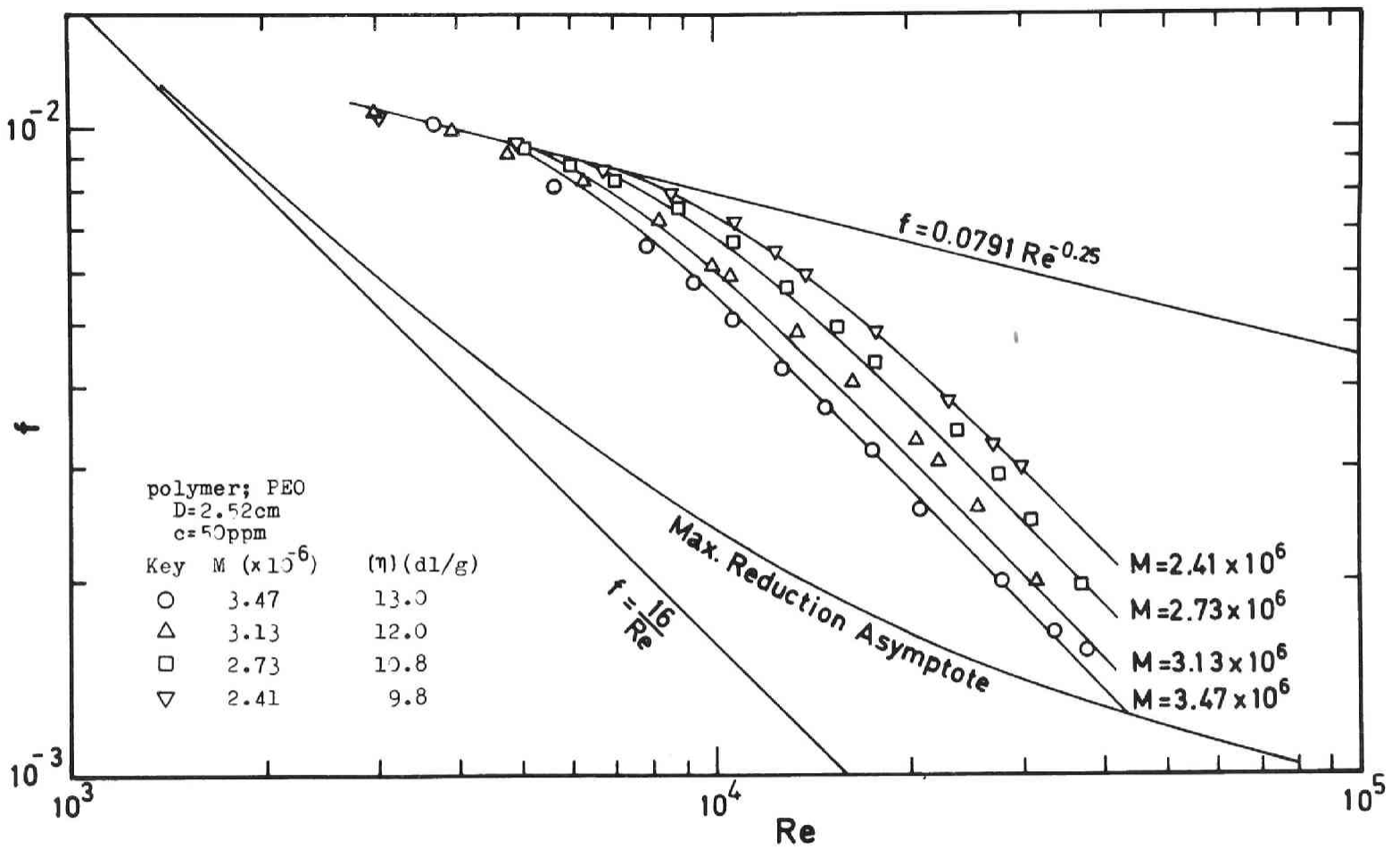

Fig. 2-6 The dependence of friction factor on the molecular weight.

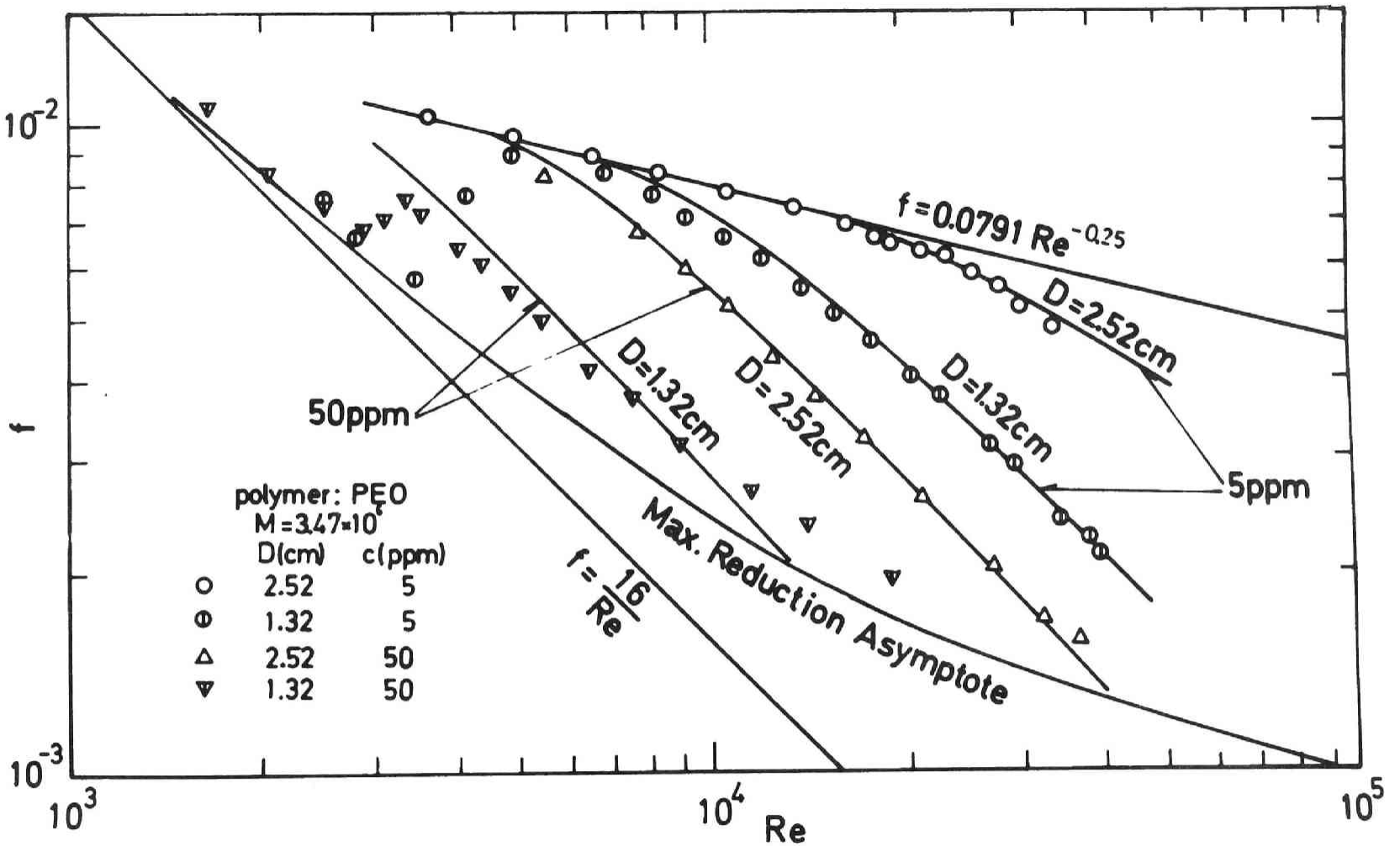

Fig. 2-7 The dependence of friction factor on the pipe diameter.

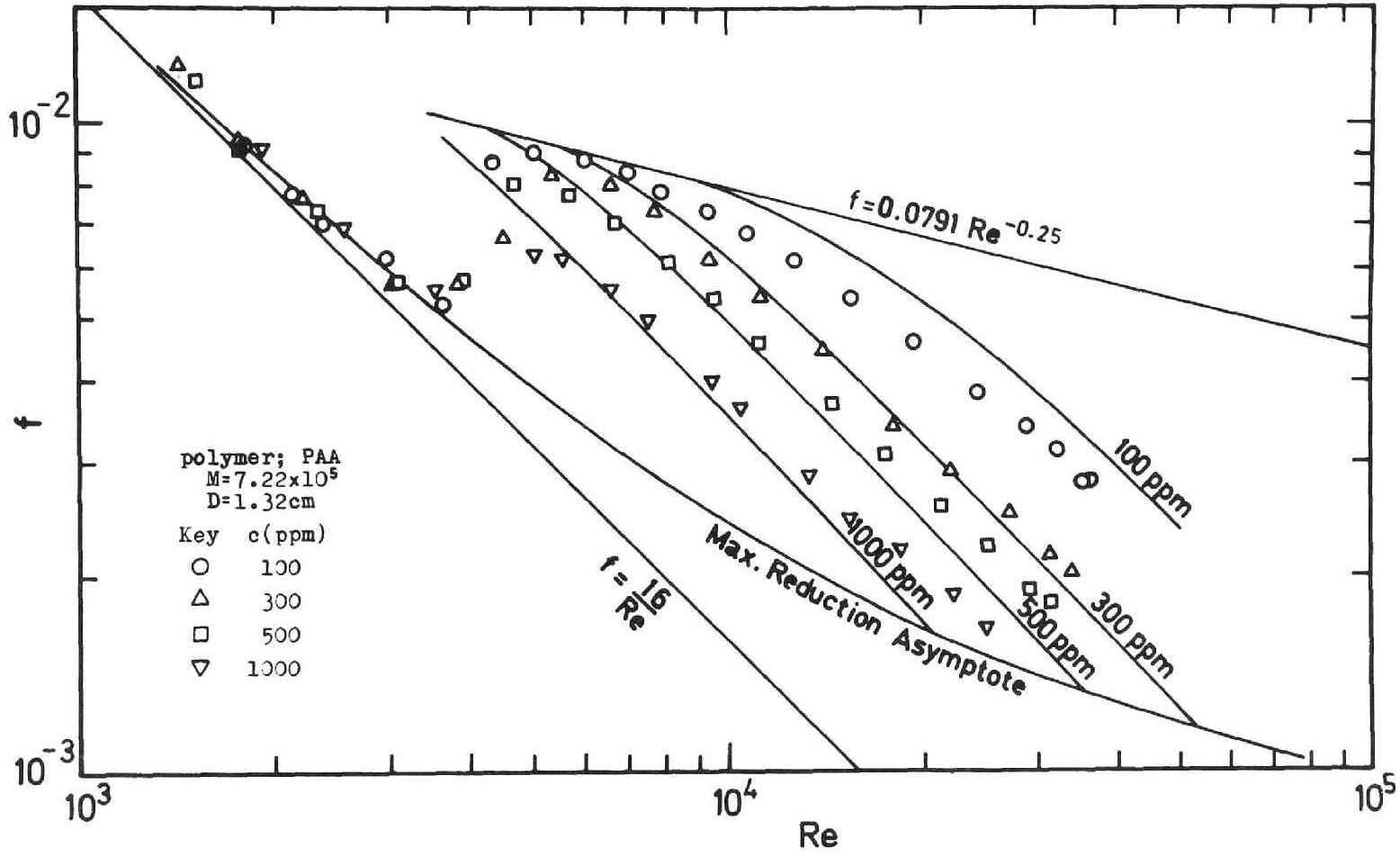

Fig. 2-8 The applicability of damping factor model to other polymer species, (in this case, to P.A.A.) .

some previous investigators (63), is not observed in the results obtained from the damping factor model. Drag reduction seems to occur as soon as the flow field becomes turbulent, although the amount of drag reduction is very small. The amount of drag reduction depends on α in Eq.(2-13), which depends on λ_t and u^* or on Weissenberg number and Reynolds number. Therefore, the position of the point at which the deviation of friction factor curve from the Newtonian one becomes significant is not at one point, the so-called "onset point of drag reduction". The position varies with the above-mentioned effects on drag reduction.

The eddy diffusivity for dilute polymer solutions can be calculated from Eq.(2-21). Both the predicted curves and the experimental results are shown in Fig. 2-9. In this diagram the eddy diffusivity in the turbulent core region for dilute polymer solutions in unsaturated region was calculated also from,

$$\frac{\varepsilon_M}{\nu} = 0.07\ R^+ \qquad (2\text{-}26)$$

, which was a part of the eddy diffusivity model of Mizushina and Ogino (40) for Newtonian fluid. The predicted curves for unsaturated region show good agreement with experimental results. In unsaturated region, the decrease of eddy diffusivity is significant only near the wall and

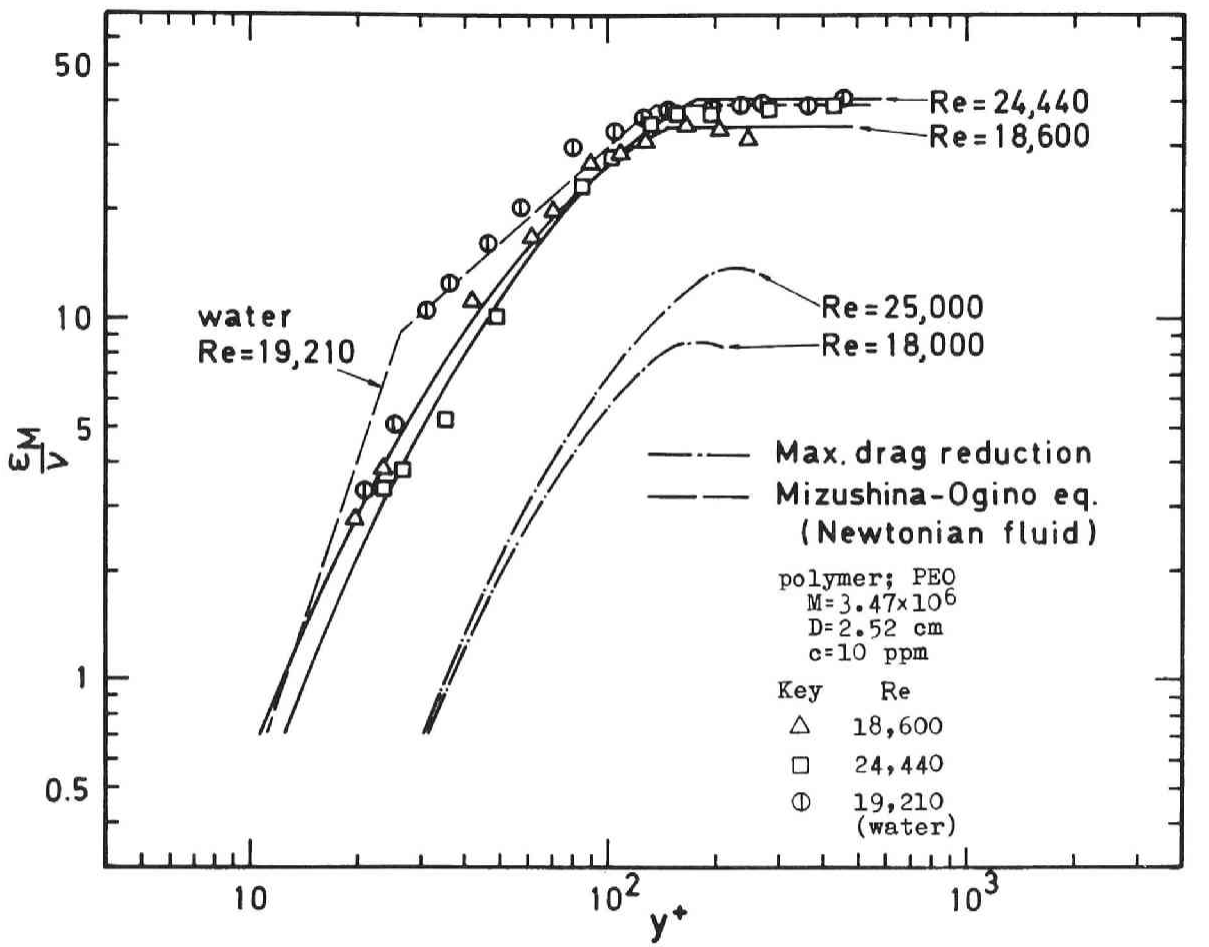

Fig. 2-9 Distribution of the eddy diffusivity for momentum transfer in drag reducing system.

the eddy diffusivity in the turbulent core is almost the same value of Newtonian fluid. On the other hand, the predicted curves at maximum reduction asymptote show a strong decrease in the whole region of pipe flow. This means that the damping effect caused by elasticity reaches the central part of turbulent pipe flow. The results of eddy diffusivity in highly elastic fluids cannot be obtained by usual method, so the Laser Doppler anemometry will be used in Chapter 4. And the discussion about the eddy diffusivity in highly elastic fluids will be given in Chapter 4.

2-4-2 Maximum drag reduction region.

It has been indicated previously by many investigators and is generally accepted that there exists a maximum drag reduction asymptote in Toms phenomenon. Virk (62) recently summarized many data at the maximum drag reduction and pointed out that the friction factor at this asymptote was independent of polymer concentration, the polymer species, the molecular weight of the polymer and pipe diameter.

The experimental results of this study coincide with that of Virk at maximum drag reduction. The value of α can be calculated from the friction factor results.

The value of α calculated at maximum drag reduction asymptote is nearly constant, i.e. $40 \sim 60$, and they are independent of Reynolds number and Weissenberg number. The scatter of α seems to be caused by polymer degradation. Since the experimental error caused by degradation has a tendency to make the value of α smaller, the value 60 is adopted for α as an universal value independent of Weissenberg number and Reynolds number.

Employing this value of α, the velocity profiles at maximum drag reduction asymptote are calculated, and the results are shown in Fig. 2-10. Two other models for maximum drag reduction, i.e. the elastic sublayer model (Virk (62)) and the modified thickened sublayer model (Seyer-Metzner (49)), are also shown in the same diagram. In the elastic sublayer model, the turbulent core of the pipe flow disappears at maximum reduction asymptote, and the whole region except the laminar sublayer becomes the elastic sublayer. On the other hand, the thickened sublayer model shows a parallel shift of the velocity distribution of the turbulent core, so the laminar sublayer is thickened, and the mixing length has the same value as that of Newtonian fluid in the core region. The damping factor model for viscoelastic fluid of this study results in a velocity profile similar to that obtained by Seyer-Metzner's model at higher Reynolds numbers, but shows a

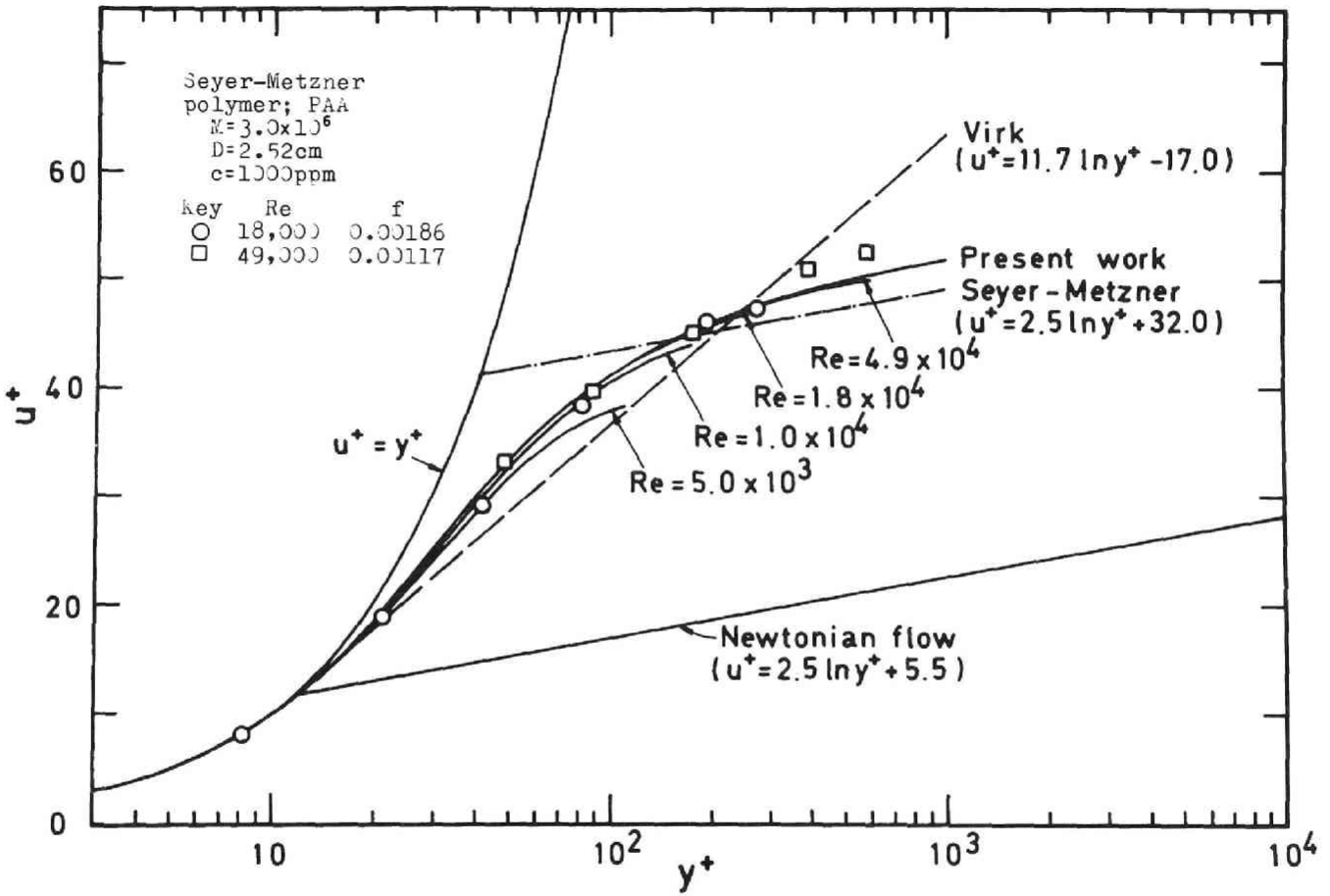

Fig. 2-10 Comparison of the present model with previous models in predicting the universal velocity profile at maximum reduction asymptote.

profile similar to that of Virk's model at lower Reynolds numbers. In the higher Reynolds number range, the damping factor becomes nearly unity and does not affect the velocity profile in the central part of the pipe. On the other hand, at lower Reynolds numbers, the damping effect of elasticity is very significant over the whole cross section of pipe, so the velocity profiles become similar to Virk's model. In Fig. 2-10 the experimental mean velocity profiles obtained by Seyer and Metzner (49), which are the only available experimental results at maximum drag reduction, are also represented. These velocity profiles obtained by means of the bubble tracer method agree very well with the present damping factor model for viscoelastic fluid. Summarizing the results mentioned above, it is concluded that in maximum drag reduction region the elastic sublayer reaches about $y^+ = 200$. Since the value of R^+ is larger than such a value as 200 at higher Reynolds numbers, there exists a turbulent core and since the value of R^+ becomes smaller than 200 at lower Reynolds numbers, the turbulent core disappears and the whole cross section consists of two regions, the laminar sublayer and the elastic sublayer.

It is convenient to adopt the Prandtl's co-ordinates for the comparison of the results of friction factor with those of previous works. Fig. 2-11 shows the present

experimental results and the curves predicted from the above-mentioned three models for maximum drag reduction. In the region of Reynolds numbers smaller than 10^5, both the present damping factor model and the elastic sublayer model predict nearly equal friction factor values at maximum drag reduction asymptote, and both are in good agreement with experimental results. The asymptote of Seyer-Metzner is valid only at higher Reynolds numbers because of the assumptions made for the derivation of this model. Thus the difference of these three models must be discussed at very high Reynolds numbers, which correspond to the region of $Re \cdot f^{1/2} > 2 \times 10^5$. But no friction factor results are available so far because experiments at higher Reynolds numbers are very difficult. The question of which model gives the most correct prediction for maximum drag reduction will be answered when friction factor data at higher Reynolds numbers or more precise measurements of turbulent characteristics for drag-reducing systems become available.

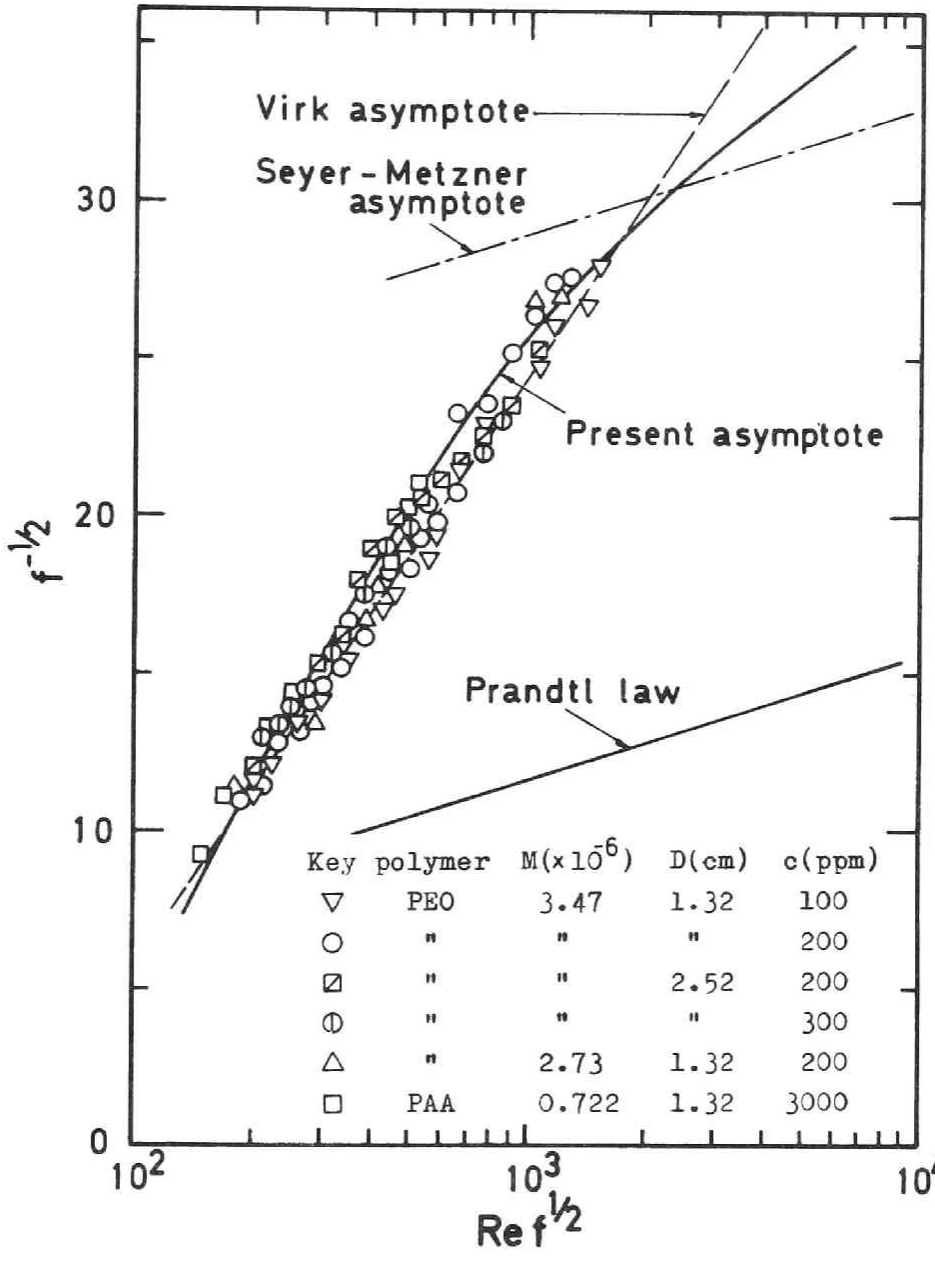

Fig. 2-11 Comparison of friction factor at maximum drag reduction with previous models.

2-4-3 Qualitative interpretation of maximum reduction.

In the preceding sections it was shown that the eddy diffusivity of viscoelastic fluid became smaller than that of Newtonian fluid in the drag-reducing systems, and that at maximum drag reduction asymptote the damping effect of elasticity ceased to increase. The value of α in Eq.(2-13) was taken as 60 at maximum reduction asymptote purely empirically from the results of pressure drop measurements. The question why the elasticity of polymer solutions decreases the eddy diffusivity of momentum transfer and why the effect of elasticity saturates will be discussed in this section.

For the convenience of analytical treatment, Denn model is employed as a constitutive equation of dilute polymer solutions. For the case of two dimensional flow of dilute polymer solutions which do not show non-Newtonian viscosity, Denn model may be given by next simplified formula,

$$\tau_{ij} = \mu B^{ij}_{(1)} - \lambda' B^{ij}_{(2)} \qquad (2\text{-}27)$$

, where $B^{ij}_{(1)}$ and $B^{ij}_{(2)}$ are the first order and the second order Rivlin-Ericksen accelaration tensors and they are

given for the case of imcompressible fluids as,

$$B^{ij}_{(1)} = g^{im} v^{j}_{,m} + g^{jm} v^{i}_{,m}$$

$$B^{ij}_{(2)} = \frac{\partial}{\partial t} B^{ij}_{(1)} + v^{m} B^{ij}_{(1),m} - v^{i}_{,m} B^{mj}_{(1)} - v^{j}_{,m} B^{im}_{(1)}$$

Navier-Stokes equation without the external forces is expressed as,

$$\rho \frac{du_i}{dt} = \frac{\partial}{\partial x_i} \{-p\delta_{ij} + \tau_{ij}\} \tag{2-30}$$

Substituting Eq.(2-27) into Eq.(2-30), one obtains the fundamental equation for viscoelastic fluid in rectangular co-ordinates;

$$\begin{aligned} \rho \frac{du_i}{dt} = & \frac{\partial p}{\partial x_i} + \mu \frac{\partial}{\partial x_i} \{\frac{\partial u_i}{\partial x_j} + \frac{\partial u_j}{\partial x_i}\} \\ & -\lambda' \frac{\partial}{\partial x_i} [\frac{\partial}{\partial t} \{\frac{\partial u_i}{\partial x_j} + \frac{\partial u_j}{\partial x_i}\} + u_k \frac{\partial}{\partial x_k} \{\frac{\partial u_j}{\partial x_i} + \frac{\partial u_i}{\partial x_j}\} \\ & - \frac{\partial u_i}{\partial x_k} \{\frac{\partial u_j}{\partial x_k} + \frac{\partial u_k}{\partial x_j}\} - \frac{\partial u_j}{\partial x_k} \{\frac{\partial u_i}{\partial x_k} + \frac{\partial u_k}{\partial x_i}\}] \end{aligned} \tag{2-31}$$

Then, employing the equation of continuity,

$$\frac{\partial u_i}{\partial x_i} = 0 \tag{2-32}$$

Eq.(2-31) is simplified as;

$$\begin{aligned} \rho \frac{du_i}{dt} = & -\frac{\partial p}{\partial x_i} + \mu \frac{\partial^2 u_i}{\partial x_j \partial x_j} - \lambda' \frac{\partial}{\partial x_i} [\frac{\partial}{\partial t} (\frac{\partial u_j}{\partial x_i}) \\ & + u_i \frac{\partial^2 u_j}{\partial x_i \partial x_i} + u_j \frac{\partial^2 u_i}{\partial x_j \partial x_j}] \end{aligned} \tag{2-33}$$

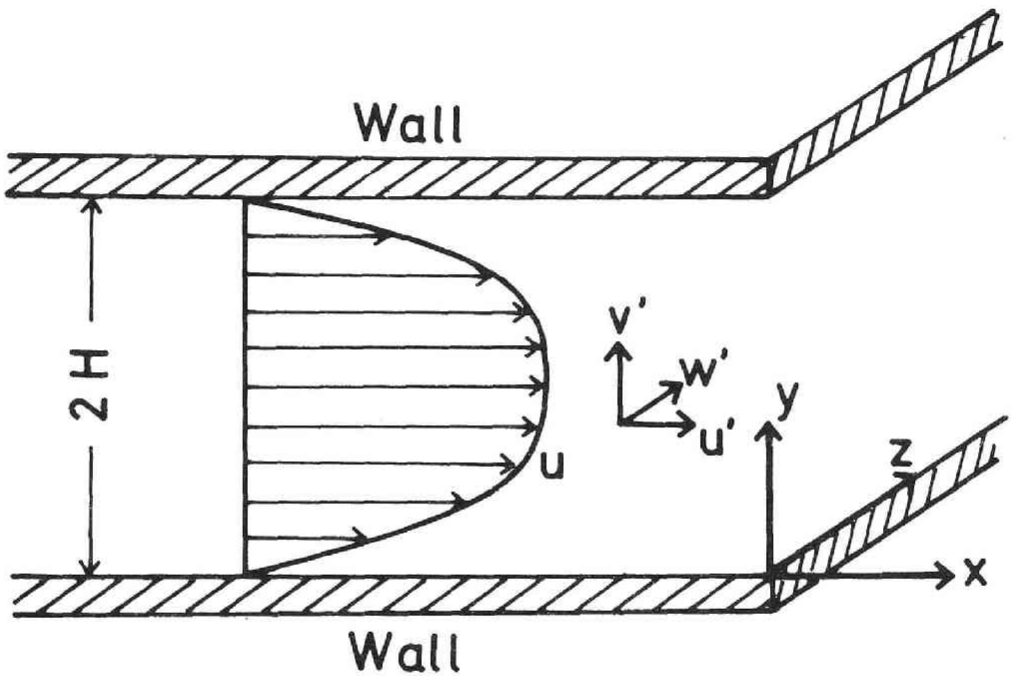

Fig. 2-12 Co-ordinate system.

Putting that

$$u_i = \bar{u}_i + u_i' \tag{2-34-a}$$

$$p = \bar{p} + p' \tag{2-34-b}$$

$$\rho = \bar{\rho} + \rho' \tag{2-34-c}$$

and after the time-smoothing procedure Eq.(2-32) becomes,

$$\bar{\rho}\frac{\partial \bar{u}_i}{\partial t} + \bar{\rho}\,\bar{u}_j\frac{\partial \bar{u}_i}{\partial x_j} + \bar{\rho}\,\overline{u_j'\frac{\partial u_i'}{\partial x_j}} = -\frac{\partial \bar{p}}{\partial x_i} + \mu\frac{\partial \bar{u}_i}{\partial x_i \partial x_j}$$
$$-\lambda'\frac{\partial}{\partial x_i}\left[\frac{\partial}{\partial t}\frac{\partial \bar{u}_j}{\partial x_i} + \bar{u}_i\frac{\partial^2 \bar{u}_j}{\partial x_i \partial x_i} + \bar{u}_j\frac{\partial^2 \bar{u}_i}{\partial x_j \partial x_j}\right.$$
$$\left. + \overline{u_i'\frac{\partial^2 u_j'}{\partial x_i \partial x_i}} + \overline{u_j'\frac{\partial^2 u_i'}{\partial x_j \partial x_j}}\right] \tag{2-35}$$

For the case of a steady and fully developed rectilinear flow between parallel flat plates shown in Fig.2-12, Eq.(3-34) is simplified by next conditions,

$$\bar{u}_1 = u\ ,\quad \bar{u}_2 = \bar{u}_3 = 0\ ,\quad u_1' = u'\ ,\quad \bar{u}_2 = v'\ ,$$
$$u_3' = w'\ ,\quad \bar{p} = p\ ,\quad \frac{\partial}{\partial t} = \frac{\partial}{\partial x} = \frac{\partial}{\partial z} = 0 \tag{2-36}$$

The final expression for x-component is,

$$-\frac{\partial p}{\partial x} = \frac{\partial}{\partial x}\left[-\mu\frac{\partial u}{\partial x} + \rho\overline{u'u'} + 2\lambda'\overline{u'\frac{\partial^2 u'}{\partial x^2}}\right]$$
$$+\frac{\partial}{\partial y}\left[-\mu\frac{\partial u}{\partial y} + \rho\overline{u'v'} + \lambda'\left(\overline{v'\frac{\partial^2 u'}{\partial y^2}} + \overline{u'\frac{\partial^2 v'}{\partial x^2}}\right)\right]$$
$$+\frac{\partial}{\partial z}\left[-\mu\frac{\partial u}{\partial z} + \rho\,\overline{u'w'} + \lambda'\left(\overline{u'\frac{\partial^2 w'}{\partial x^2}} + \overline{w'\frac{\partial^2 u'}{\partial z^2}}\right)\right] \tag{2-37}$$

Thus the total shear stress, $\tau_{xy|total}$ is given by the next expression,

$$\tau_{xy|total} = -\mu\frac{\partial u}{\partial y} + \rho\,\overline{u'v'} + \lambda'\left(\overline{v'\frac{\partial^2 u'}{\partial y^2}} + \overline{u'\frac{\partial^2 v'}{\partial x^2}}\right) \tag{2-38}$$

The first term of right hand of Eq.(2-37) means the momentum flux caused by viscosity, the second term means the momentum flux caused by turbulent eddy (i.e. Reynolds stress), and the last one is interpretted as the momentum flux caused by the elasticity of polymer solutions. The analysis in Section 2-2 shows that the turbulence is damped by elasticity. The decrease of fluctuation makes the values of u' and v' in Eq.(2-37) smaller. On the other hand the material constant λ' may become larger when Weissenberg number become larger. Thus the existence of maximum reduction asymptote is interpretted as the result of counter balance between the decrease of fluctuating velocities and the increase of viscoelastic property, λ'. The measurements of the fluctuating velocities in viscoelastic fluids are very difficult and the physical meaning of λ' used in turbulent flow is not clear. Thus the discussion given in this section is only a qualitative one.

2-5 Concluding remarks.

The damping factor model equation of viscoelastic fluids for momentum transfer was derived. The summary of this model is;

$$\frac{\varepsilon_M}{\nu} = fn(\, y^+,\, R^+ \,)^2 \, DF_M{}^2 \, \frac{d\, u^+}{d\, y^+}$$

$$DF_M = 1 - \exp\left(\frac{-y^+}{26} \left(- \alpha + \sqrt{\alpha^2 + 1} \right)^{1/2} \right)$$

where $\alpha = (2\lambda_t/\nu)\,(u^*/26)^2$

For unsaturated region:

$$\frac{\lambda_t}{\lambda_\ell} = 3.76 \times 10^8 \, We^{1.34}$$

For maximum reduction asymptote:

$$\alpha = 60$$

It was shown that this viscoelastic damping factor model gave a good prediction of the effects of various sources on drag reduction shown in Table 2-1.

From the analysis of this chapter, it was shown that the elasticity changed the turbulent structure of pipe flow and the elastic sublayer reached about $y^+=200$ at the maximum reduction asymptote.

CHAPTER 3

HEAT TRANSFER REDUCTION IN TURBULENT PIPE FLOW

3-1 Introduction.

3-1-1 Previous works.

Turbulent heat transfer of non-Newtonian fluids has been investigated mainly about purely viscous non-Newtonian fluids. The results of these investigations are listed in Table 3-1, and they give good predictions for practical applications.

Recently some investigators reported the severe reduction of heat transfer rate in dilute polymer solutions (9,46,65). In Table 3-2 the predicting equations for the Nusselt number of viscoelastic fluid in fully developed region are summarized. All of these predictions are based on the Reynolds-Prandtl's analogy. They give fairly good estimations when the friction factor is estimated correctly.

Table 3-1

Expressions for Nusselt number of purely viscous non-Newtonian fluids.

Metzner-Friend (37)

$$St = \frac{f/2}{1.2 + 11.8\sqrt{f/2}\,(Pr_w - 1)\,Pr_w^{-1/3}}$$

where $Pr_w = c_p \mu_w / k$

Mizushina-Kuriwaki (39)

$$Nu = 0.023\, n^2\, Re_p^{\frac{4(n+2)}{3(4n+1)}}\, Pr_p^{1/3}$$

where $Re_p = \frac{D^n \bar{u}^{2-n} \rho}{K}$, $Pr_p = \frac{c_p K}{k}\left(\frac{\bar{u}}{D}\right)^{n-1}$

Krantz-Wassan (31)

$$St = \frac{\sigma \frac{f}{2}}{1 + \sqrt{\frac{f}{2}} \int_0^{y_c^+} \frac{\frac{1}{\frac{\overline{u'v'}^+}{\frac{du^+}{dy^+}} + \frac{1}{\sigma \phi Pr}} - \frac{1}{\frac{\overline{u'v'}^+}{\frac{du^+}{dy^+}} + \left(\frac{du^+}{dy^+}\right)^{n-1}}}{} dy^+}$$

where $\phi = \left(\frac{f\,Re}{16}\right)^{\frac{n-1}{n}} / \left(\frac{3n+1}{4n}\right)$

Hartnett et al. (24)

$$Nu = \frac{0.0118}{n} Re'^{0.9}\, Pr'^{0.3}$$

where $Re' = \frac{\rho\, \bar{u}^{2-n} D^n}{K\, 8^{n-1}}$, $Pr' = \frac{c_p K\, 8^{n-1}}{k}\left(\frac{\bar{u}}{D}\right)^{n-1}$

Table 3-2

Expressions for Stanton number of

viscoelastic fluids.

Wells (65)

$$St = \frac{f/2}{1.02 \frac{u_L}{u^*} \sqrt{\frac{f}{2}} (Pr - 1) Pr^{-1/3} + 1.2}$$

, u_L : velocity at the edge of viscous sublayer.

Gupta-Metzner-Hartnett (22)

$$St = \frac{\frac{f}{2}(\frac{1}{\theta_m})}{\frac{1}{\phi_m} + \sqrt{\frac{f}{2}} (Pr_w \quad 1) I}$$

where $$I = \int_0^{y^+=R^+} \frac{(pr - 1)\, du^+}{(Pr_w - 1)(Pr_w \varepsilon_H/\nu + 1)}$$

$1/\Phi_m$; the ratio of the maximum to the mean velocity.

$1/\theta_m$; the ratio of the maximum to the mean temperature.

Poreh-Paz (45)

$$St = \frac{\sqrt{f/8}}{y_1^+ [\ln \{Pr - (Pr - 1) y_1^+/y_2^+\} + Pr - 1] + \sqrt{8/f}}$$

, y_1^+, y_2^+ : see Table 2-3.

For several years, it has been discussed (4,33) if the Colburn's analogy is valid in polymer solutions. The previous experimental results are only about the Nusselt number in fully developed region and there is no result of the temperature distribution measurements. The information about the mechanism of turbulent heat transfer of viscoelastic fluids is needed to answer the above-mentioned question.

3-1-2 Purpose and outline of this chapter.

The purpose of this chapter is to obtain the expression of eddy diffusivity for viscoelastic fluids. For this purpose the temperature distributions in fully developed turbulent pipe flow are measured. The damping factor model for viscoelastic fluid obtained in Chapter 2 is extended to the turbulent heat transfer of viscoelastic fluids. The extended damping factor model gives the eddy diffusivity of heat transfer and the Nusselt number of viscoelastic fluid in fully developed region. The predictions thus obtained are compared with the experimental results. The discussion about the mechanism of turbulent heat transfer of viscoelastic fluid in pipe flow will be given.

3-2 Extension of damping factor model to heat transfer reduction.

The basic equation of heat transfer in semi-infinite fluid on a flat plate is given as;

$$\frac{\partial T}{\partial t} = \frac{k}{\rho c_p} \frac{\partial^2 T}{\partial y^2} \tag{3-1}$$

B.C.

$$T(y,0) = 0 \qquad \text{at} \quad t = 0 \tag{3-2-a}$$

$$T(0,t) = T \cos \omega_H t \qquad \text{at} \quad y = 0 \tag{3-2-b}$$

$$T(\infty,t) = 0 \qquad \text{at} \quad y = \infty \tag{3-2-c}$$

By a similar procedure given in Chapter 2, the damping factor for heat transfer of Newtonian fluid is given from Eqs.(3-1) and (3-2) as;

$$DF_{Ho} = 1 - \exp\{-y^+ \sqrt{Pr}\ \sqrt{\omega_H \nu}\ /\sqrt{2}\ \ u^*\} \tag{3-3}$$

where ω_H is a quantity which is proportional to the representative frequency of temperature fluctuation in turbulent core, and is assumed to be the function of Prandtl number, as done by Na et al. (43) in the analysis of turbulent heat transfer of Newtonian fluid. After several computations, the best fit expression of ω_H for the available experimental results in wide range of Prandtl numbers

was obtained as,

$$\frac{\sqrt{2}\ u^*}{\sqrt{\omega_H\ \nu}\ \sqrt{Pr}} = a_0 + a_1\ /\sqrt{Pr} \qquad (3\text{-}4)$$

Thus the damping factor for heat transfer becomes,

$$DF_{Ho} = 1 - \exp\{-y^+/(a_0 + a_1/\sqrt{Pr})\} \qquad (3\text{-}5)$$

, where a_o and a_1 must be determined from the experimental results.

Many investigators (41) showed that the ratio of eddy diffusivities, $\varepsilon_{Ho}/\varepsilon_{Mo}$ approached to a value, 1.5, in the turbulent core of Newtonian pipe flow, where both DF_{Mo} and DF_{Ho} became unity. Since the eddy diffusivity of momentum and heat transfer are expressed as,

$$\frac{\varepsilon_{Mo}}{\nu} = \ell_{Mo}^{+2}\ \frac{du^+}{dy^+} \qquad (3\text{-}6)$$

$$\frac{\varepsilon_{Ho}}{\nu} = \ell_{Mo}^{+}\ \ell_{Ho}^{+}\ \frac{du^+}{dy^+} \qquad (3\text{-}7)$$

, we obtain the following relation in the turbulent core,

$$\ell_{Ho}^{+} = 1.5\ \ell_{Mo}^{+} \qquad (3\text{-}8)$$

Thus the mixing length for heat transfer in the wall region may be expressed as,

$$\ell_H^{+} = 1.5\ fn(y^+, R^+)\ DF_{Ho} \qquad (3\text{-}9)$$

Substituting Eqs.(2-22) and (3-9) into Eq.(3-7) we obtain,

$$\frac{\varepsilon_{Ho}}{\nu} = 1.5\ fn(y^+,R^+)^2\ DF_{Mo}\ DF_{Ho}\ \frac{d\ u^+}{d\ y^+} \qquad (3\text{-}10)$$

, and the ratio of eddy diffusivities, σ is given from Eqs.(2-21) and (3-10) as,

$$\sigma = \frac{\varepsilon_{Ho}}{\varepsilon_{Mo}} = 1.5\ DF_{Ho}/DF_{Mo} \qquad (3\text{-}11)$$

There seems to be no direct effect of elasticity on heat transfer and the elasticity only affects on the flow characteristics, so the expression of σ given by Eq.(3-11) may be approximately applicable to the turbulent heat transfer of viscoelastic fluids, although the structure of turbulence may be different to some extent. Thus the eddy diffusivity of viscoelastic fluid for heat transfer is obtained as;

$$\frac{\varepsilon_H}{\nu} = \sigma\ |(\ \varepsilon_M/\nu\ )$$

$$= 1.5\ fn(y^+,R^+)^2\ DF_M{}^2\ (DF_{Ho}/DF_{Mo})\ \frac{d\ u^+}{d\ y^+} \qquad (3\text{-}12)$$

3-3 Nusselt number in fully developed flow with constant heat flux.

The co-ordinate system shown in Fig. 3-1 is taken for the analysis of heat transfer in fully developed turbulent pipe flow. the basic equation of heat transfer and boundary conditions (fully developed and constant heat flux) in this co-ordinate system are,

$$u^+\frac{\partial T^+}{\partial x^+} = \frac{1}{r^+}\frac{\partial}{\partial r^+}\{(\frac{1}{Pr} + \frac{\varepsilon_H}{\nu})\ r^+\ \frac{\partial T^+}{\partial r^+}\} \qquad (3\text{-}13)$$

B.C. $$\frac{\partial T^+}{\partial r^+} = 0 \qquad \text{at} \qquad r^+ = 0 \qquad (3\text{-}14\text{-}a)$$

$$\frac{\partial T^+}{\partial r^+} = Pr \qquad \text{at} \qquad r^+ = R^+ \qquad (3\text{-}14\text{-}b)$$

$$T^+ = 0 \qquad \text{at} \qquad x^+ = 0 \qquad (3\text{-}14\text{-}c)$$

where u,x,r are nondimensionalized by the wall parameters and T^+ is given by, $T^+ = \rho\, c_p\, u^*\, (T - T_o)/(-q_w)$ and T_o is the inlet uniform temperature at $x^+ = 0$.

Assuming that,

$$T^+ = C_o x^+ + \textcircled{H}(r^+) \qquad (3\text{-}15)$$

, and substituting Eq.(3-15) into Eq.(3-13) one can obtain the nondimensinal temperature gradient,

$$\frac{d\,\textcircled{H}}{dr^+} = \frac{C_o}{(\frac{1}{Pr} + \frac{\varepsilon_H}{\nu})\ r^+}\int_0^{r^+} u^+\ r^+\ dr^+ \qquad (3\text{-}16)$$

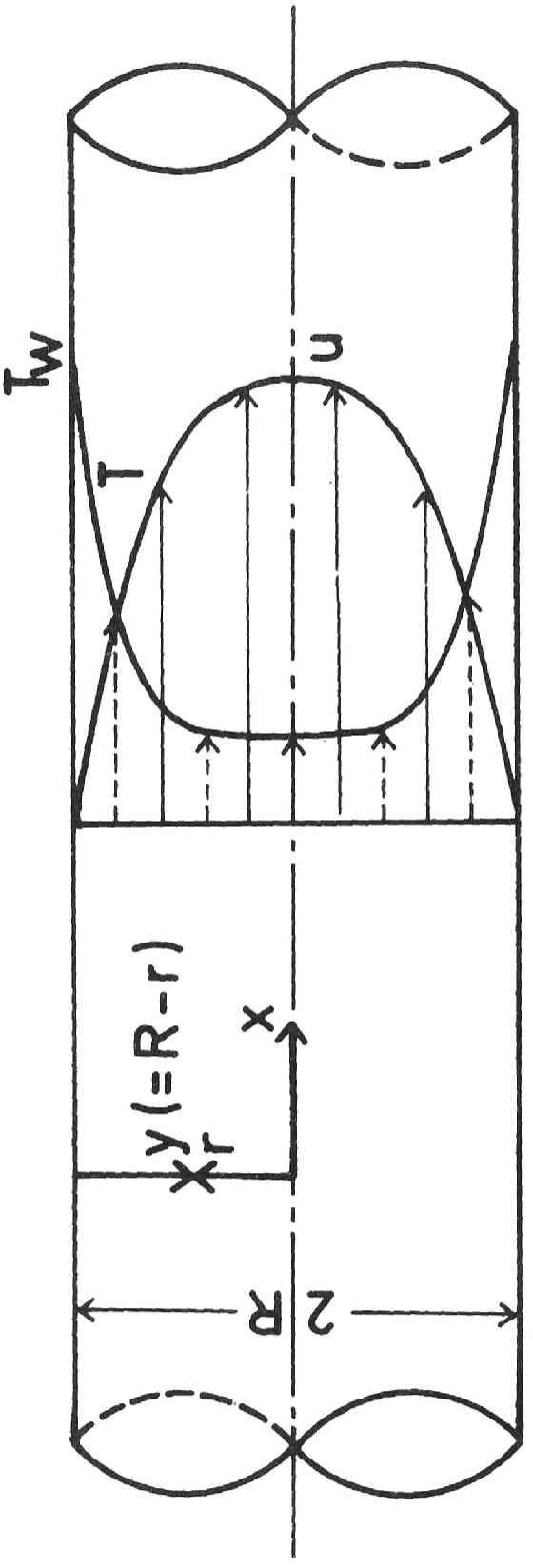

Fig. 3-1 Co-ordnate system.

From Eqs.(3-13),(3-14-c) and (3-15), C_o is expressed as,

$$C_o = \sqrt{2f} \,/\, R^+ \tag{3-17}$$

Substituting Eq.(3-17) into Eq.(3-16), one can integrate Eq.(3-16) to obtain,

$$\textcircled{H} - \textcircled{H}\big|_{r^+=0} = \frac{\sqrt{2f}}{R^+} \int_0^{r^+} \left\{ \frac{1}{\left(\frac{1}{Pr} + \frac{\varepsilon_H}{\nu}\right) r^+} \int_0^{r^+} u^+ r^+ dr^+ \right\} dr^+ \tag{3-18}$$

The bulk temperature is defined as,

$$\textcircled{H}_b = \int_0^{R^+} u^+ \textcircled{H}\, r^+ \, dr^+ \,/\, \int_0^{R^+} u^+ \, r^+ \, dr^+ \tag{3-19}$$

,and the Nusselt number in fully developed region is given as,

$$Nu = 2 \, Pr \, R^+ \,/\, \left(\textcircled{H}_b - \textcircled{H}\big|_{r^+=R^+} \right) \tag{3-20}$$

3-4 Experimental apparatus and procedure.

A simplified diagram of test equipment is shown in Fig. 3-2. The experimental apparatus is same as that of Chapter 2 except the test section. The test section was

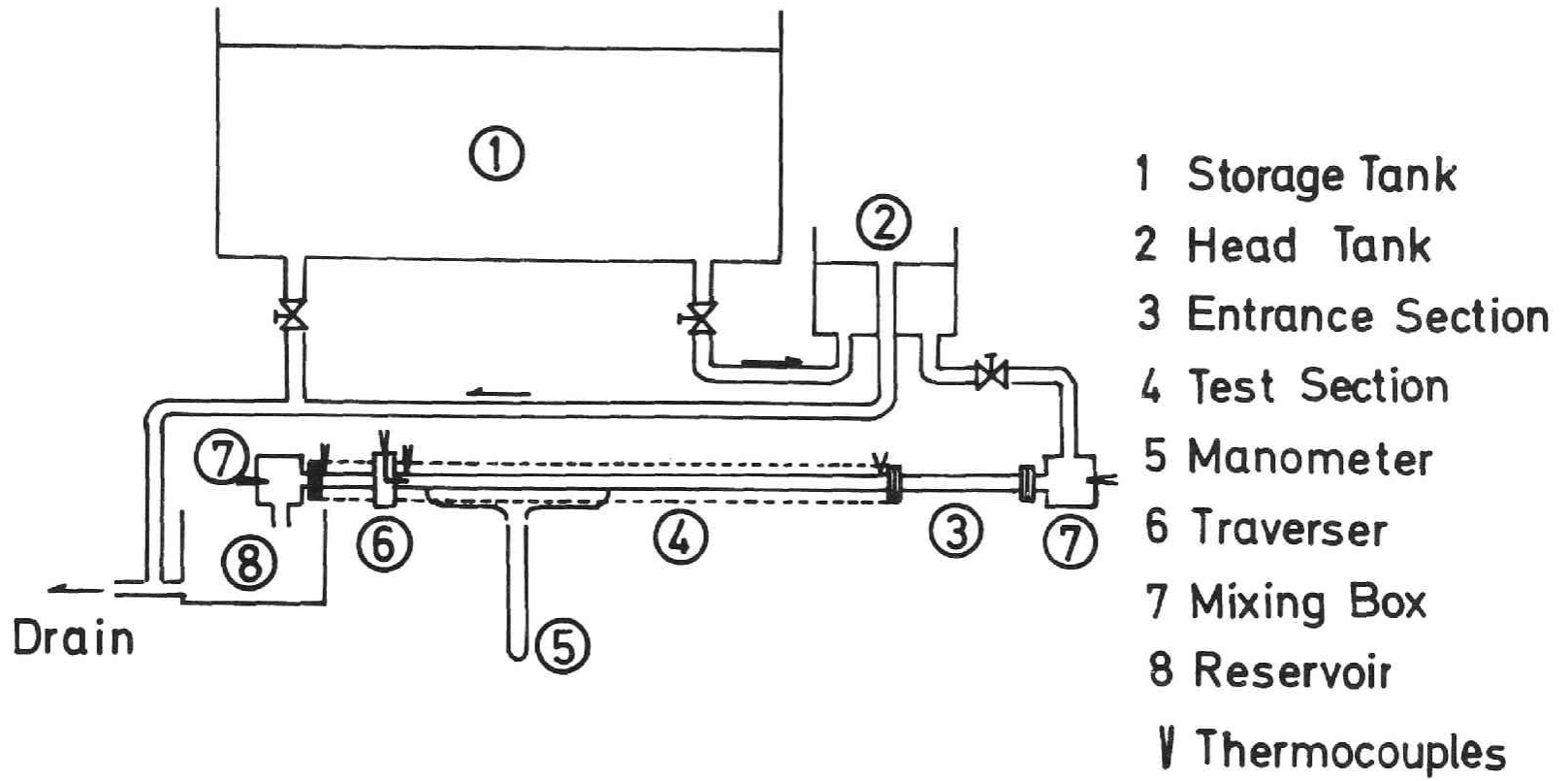

Fig. 3-2 Experimental apparatus

a circular tube of copper of 2.6 cm i.d. and 4.2 m long with smooth wall. The test section was heated with alternating current through the nickrom wire which was uniformly rolled around the tube. The temperature of the outer surface of the tube was measured by copper-constantan thermocouples. The temperature of inner surface of the tube was calculated from the outer wall temperature, the thermal conductivity of copper and the heat flux which was given by electrical energy dissipation. The thermal conductivity of copper used in this apparatus was determined experimentally to be 302 (kcal/m hr ^{o}C). Temperature distribution of fully developed region and the cup mixed temperature of inlet and outlet sections were also measured by thermocouples. Pressure drop in the test section was measured with the U tube manometer of CCl_4. The distance between pressure taps was 150 cm.

Polymer species used in this study was polyethylene oxide. The solvent of test liquids was water. The intrinsic viscosity of polymer solution was determined as 13.5 (dl/g), and molecular weight was determined by Eq.(2-22) as 3.64×10^6. None of the dilute polymer solutions uesd in this study showed a non-Newtonian viscosity. Since the temperature difference between bulk and wall temperatures was less than 20 ^{o}C in this experiments, the dependency of viscosity on temperature was not considered.

Thermal conductivity of the test liquids was assumed to be equal to that of water, because of the diluteness of the polymer solutions.

3-5 Results and discussions.

As the first step of this study, the friction factor results were compared with the predictions given by the damping factor model of Chapter 2. This comparison is shown in Fig. 3-3. This diagram shows the concentration and saturation effects of Toms phenomenon. The agreement between the predictions and the measurements is good. Thus the velocity distributions predicted by Eq.(2-17), which were necessary to calculate the eddy diffusivity of heat transfer or Nusselt number, were used for the integration of Eqs.(3-18) and (3-21).

The question about the availability of Colburn's analogy in viscoelastic fluids which was pointed out in the introduction of this chapter was tested by the results of this experiments. The experimental results of Colburn's j-factor are plotted with the predicted friction factor in Fig. 3-4. It is clear that the reduction of heat

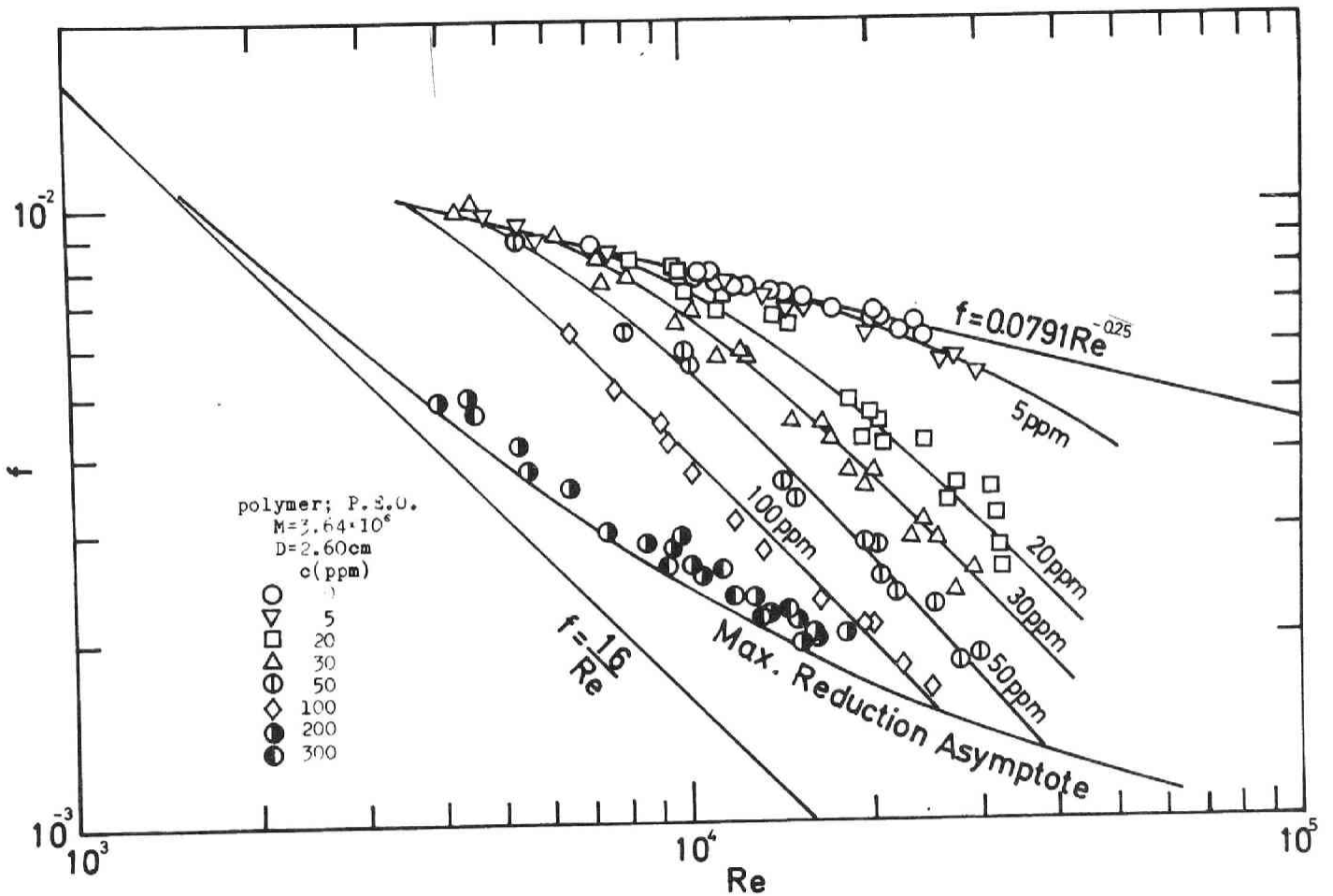

Fig. 3-3 The dependence of friction factor on polymer concentration.

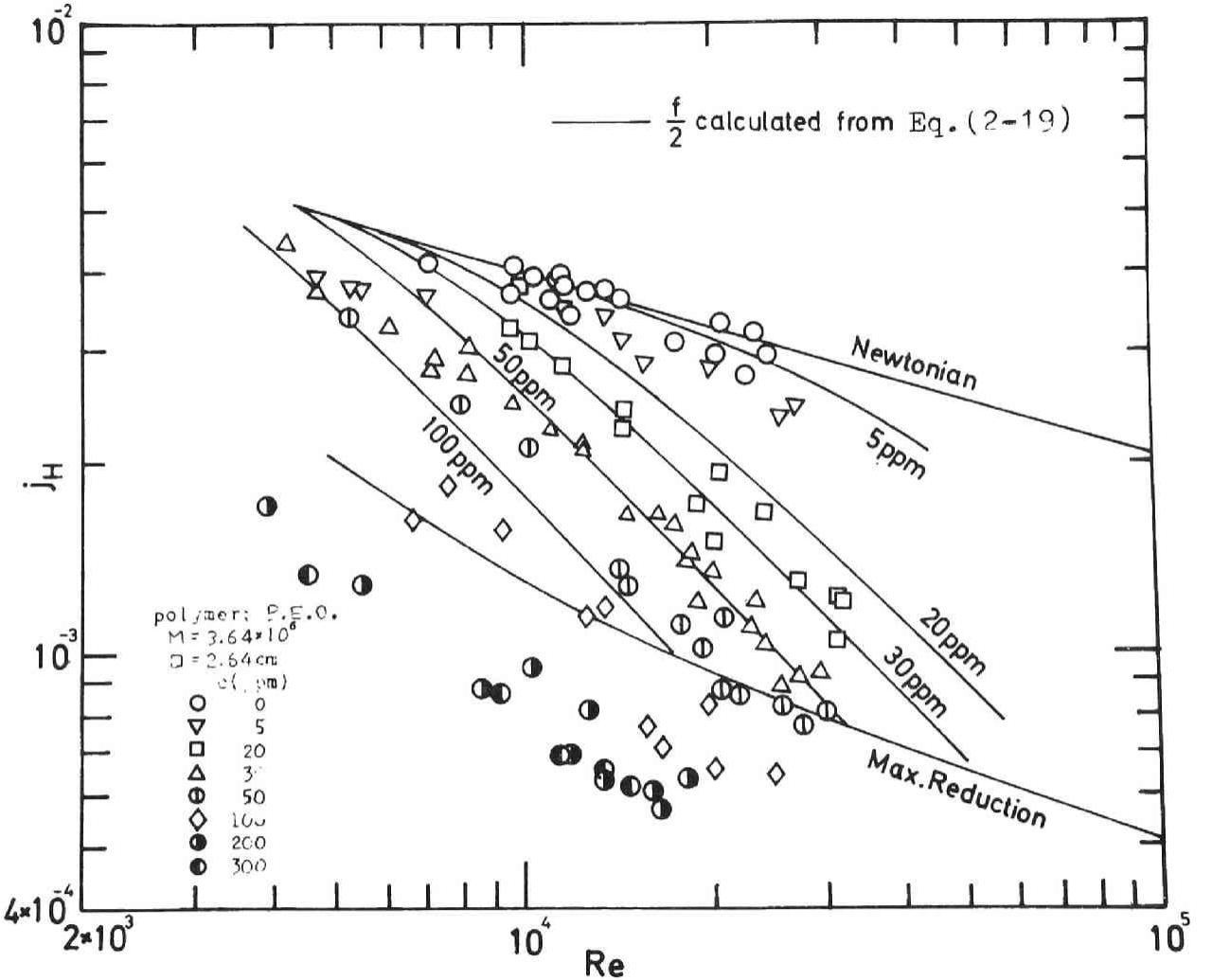

Fig. 3-4 Comparison of j_H with f/2 .

transfer rate is greater than that of momentum transfer rate. The deviations of the both reductions become larger as the reduction rate becomes larger. This result coincides with the results obtained by Marrucci-Astarita (33). It was shown in Chapter 2 that the damping effect caused by the elasticity of polymer solutions reached the central part of turbulent pipe flow when the Reynolds number is small. In such a condition, the Colburn's analogy should no longer hold. Thus the quantitative discussions to predict the reduction of Nusselt number will be done in the following section of this chapter.

From the Eq.(3-16), the eddy diffusivity for heat transfer is calculated as;

$$\frac{\varepsilon_H}{\nu} = \frac{\sqrt{2f}}{r^+R^+\frac{\partial T^+}{\partial r^+}} \int_0^{r^+} u^+ r^+ dr^+ - \frac{1}{Pr} \qquad (3\text{-}21)$$

The experimental results of the temperature distributions and the predicted velocity profiles given in Chapter 2, were used to calculate the eddy diffusivity for heat transfer of viscoelastic fluid. The profiles of ε_H/ν of Newtonian and viscoelastic fluids are shown in Fig. 3-5 and Fig. 3-6. Fig. 3-5 shows the results of Newtonian fluid and those of viscoelastic fluids at maximum reduction region. Fig.3-6 shows the results of unsaturated region of viscoelastic fluid.

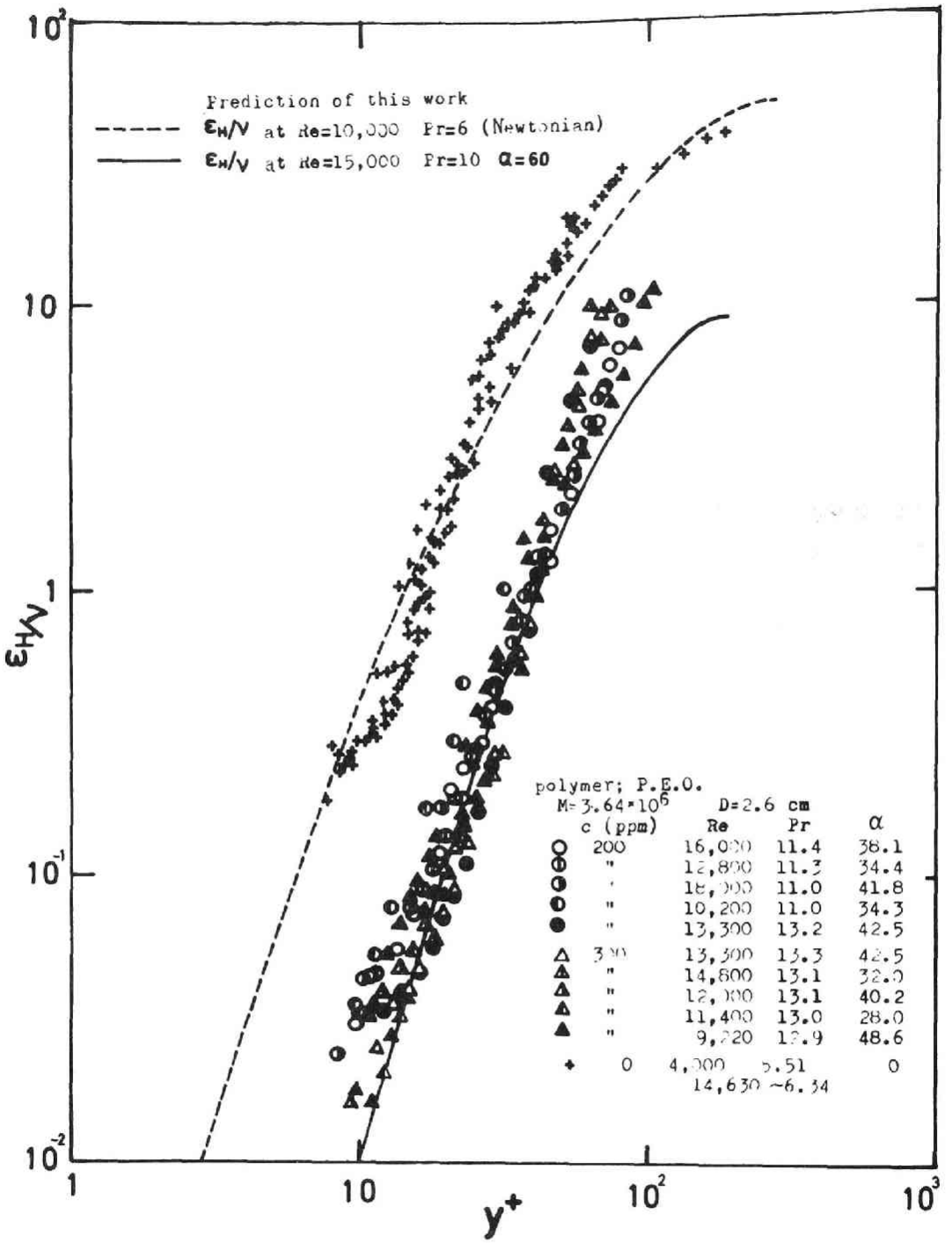

Fig. 3-5 Eddy diffusivity of heat in Newtonian and viscoelastic fluid.

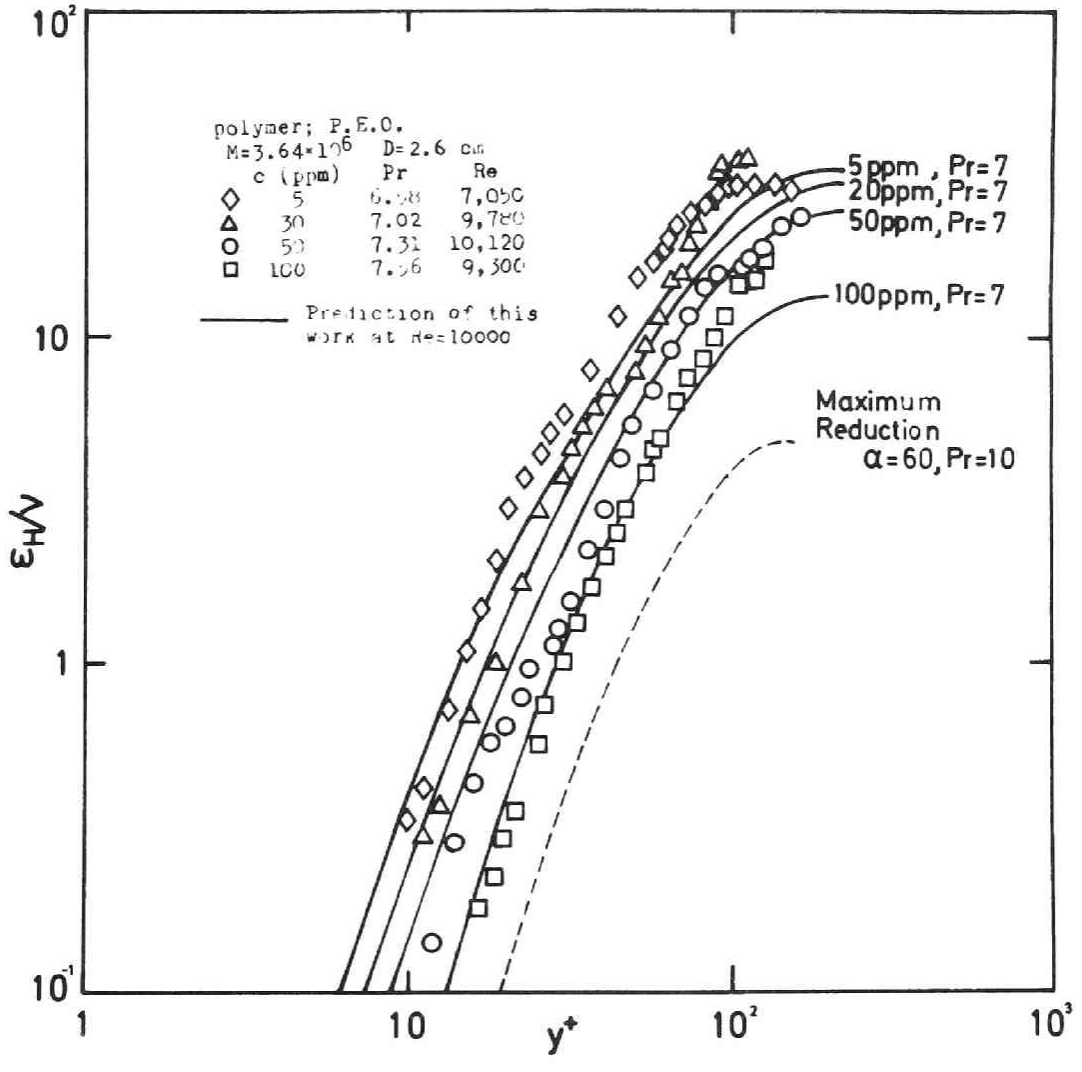

Fig. 3-6 Eddy diffusivity of heat in viscoelastic fluid (unsaturated region) .

The constants a_o and a_1 in Eq.(3-5) can now be determined as $a_o = 42$ and $a_1 = 120$ from the conditions that ε_H/ν becomes equal to ε_M/ν near the wall at $Pr \to \infty$, and Eq.(3-10) fits the experimental result of Newtonian fluid at $y^+=20$. Thus from Eq.(3-12), the eddy diffusivity of viscoelastic fluid is finally given as;

$$\frac{\varepsilon_H}{\nu} = 1.5\, f_n(y^+, R^+)^2 \left[\left\{1 - \exp\left(\frac{-y^+}{42 + \frac{120}{\sqrt{Pr}}}\right)\right\} \Big/ \left\{1 - \exp\left(\frac{-y^+}{26}\right)\right\}\right] \times \left\{1 - \exp\left(\frac{-y^+}{26}\sqrt{-\alpha + \sqrt{\alpha^2+1}}\right)\right\}^2 \times \frac{du^+}{dy^+} \qquad (3\text{-}23)$$

The profiles of ε_H/ν of Newtonian fluid calculated for various Prandtl numbers are shown in Fig. 3-7, being compared with the previous models and measurements. The prediction of this study shows fairly good agreement with the other's in the high Prandtl number range. The comparison of the eddy diffusivity ratio at $y^+/R^+=0.5$ with previous works for Newtonian fluid is done in Fig. 3-8. It is shown from this diagram that the prediction of this study can explain the experimental results nearly quantitatively even at the very low Prandtl number range.

Let us return again to the discussion about the viscoelastic fluids. The eddy diffusivity for heat transfer of viscoelastic fluids is calculated by Eq.(3-22) and shown in Fig.3-5 and Fig. 3-6. The value of α given in Chapter 2 was used in this calculation. The eddy diffu-

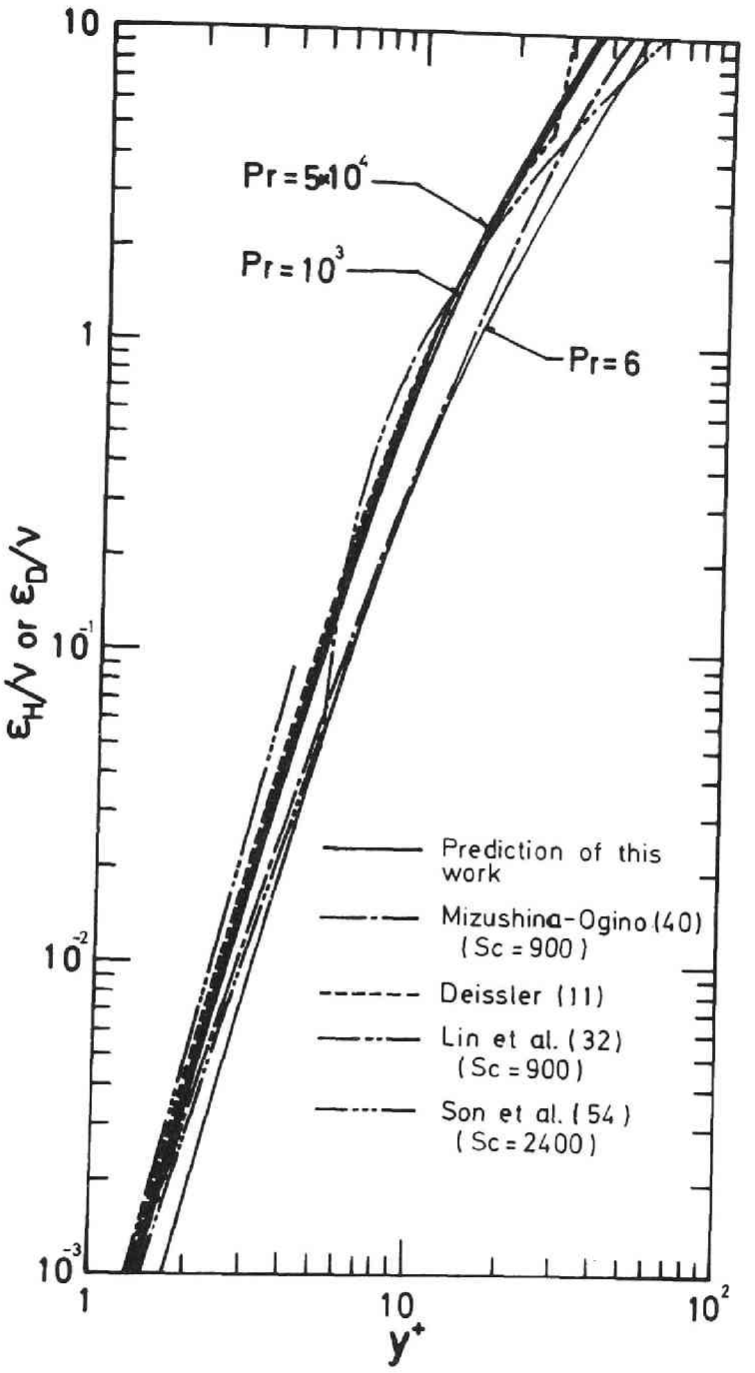

Fig. 3-7 Comparison of eddy diffusivity of heat with the previous works for the case of Newtonian fluid.

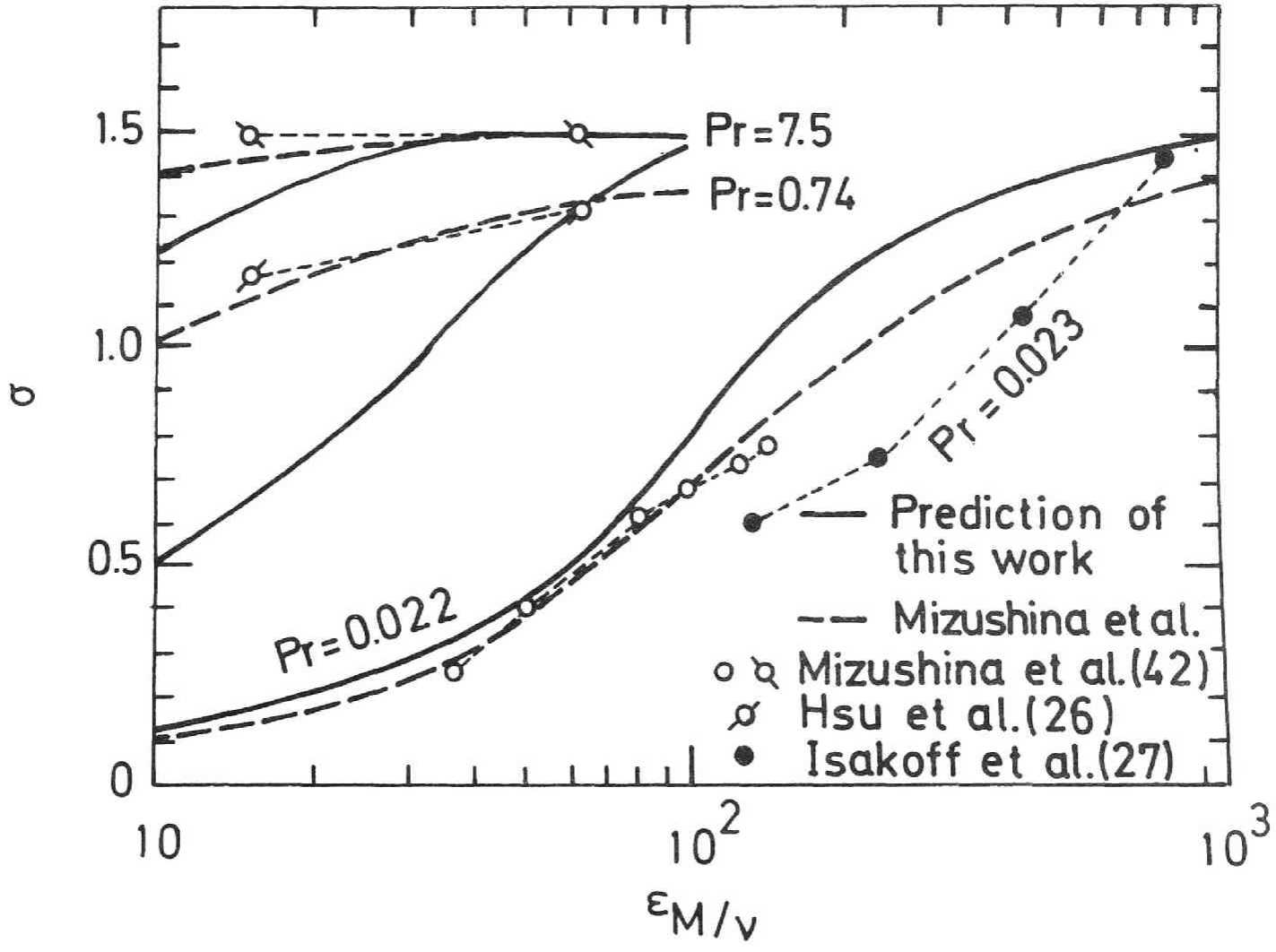

Fig. 3-8 Ratio of eddy diffusivity of heat to that of momentum in various fluids (at $y^+/R^+=0.5$).

sivity thus obtained agrees quantitatively with experimental results. Moreover the experimental results of Fig. 3-5 show that there exists an universal distribution of $^{\varepsilon}H/\nu$ within the experimental errors at maximum reduction region. This confirms that at maximum reduction asymptote the flow system of viscoelastic fluids reaches a certain equiliblium state which is independent of the concentration, molecular weight of polymers, Reynolds number, etc.. The damping effect caused by the elasticity of polymer solutions seems to cease to increase at this point. The distribution of $^{\varepsilon}H/\nu$ in unsaturated region are shown in Fig. 3-6. This diagram shows the concentration effect at Re=10000. It is clear from this diagram that the damping factor model for viscoelastic fluid can predict the correct distribution of eddy diffusivity of polymer polymer solution in the unsaturated region.

The generalized temperature distribution was calculated from Eqs.(3-18) and (3-22) and shown in Fig. 3-9. In this diagram the difference from the wall temperature is nondimensionalized. The line of α=60 is the temperature distribution at maximum reduction asymptote. The region in which T^+ is equal to y^+ becomes larger in viscoelastic fluid and reaches to y^+=15 when the value of α is equal to 60. This profile of α=60 at Pr=10 is found to be similar to that of Newtonian fluid at Pr=1.0. Thus

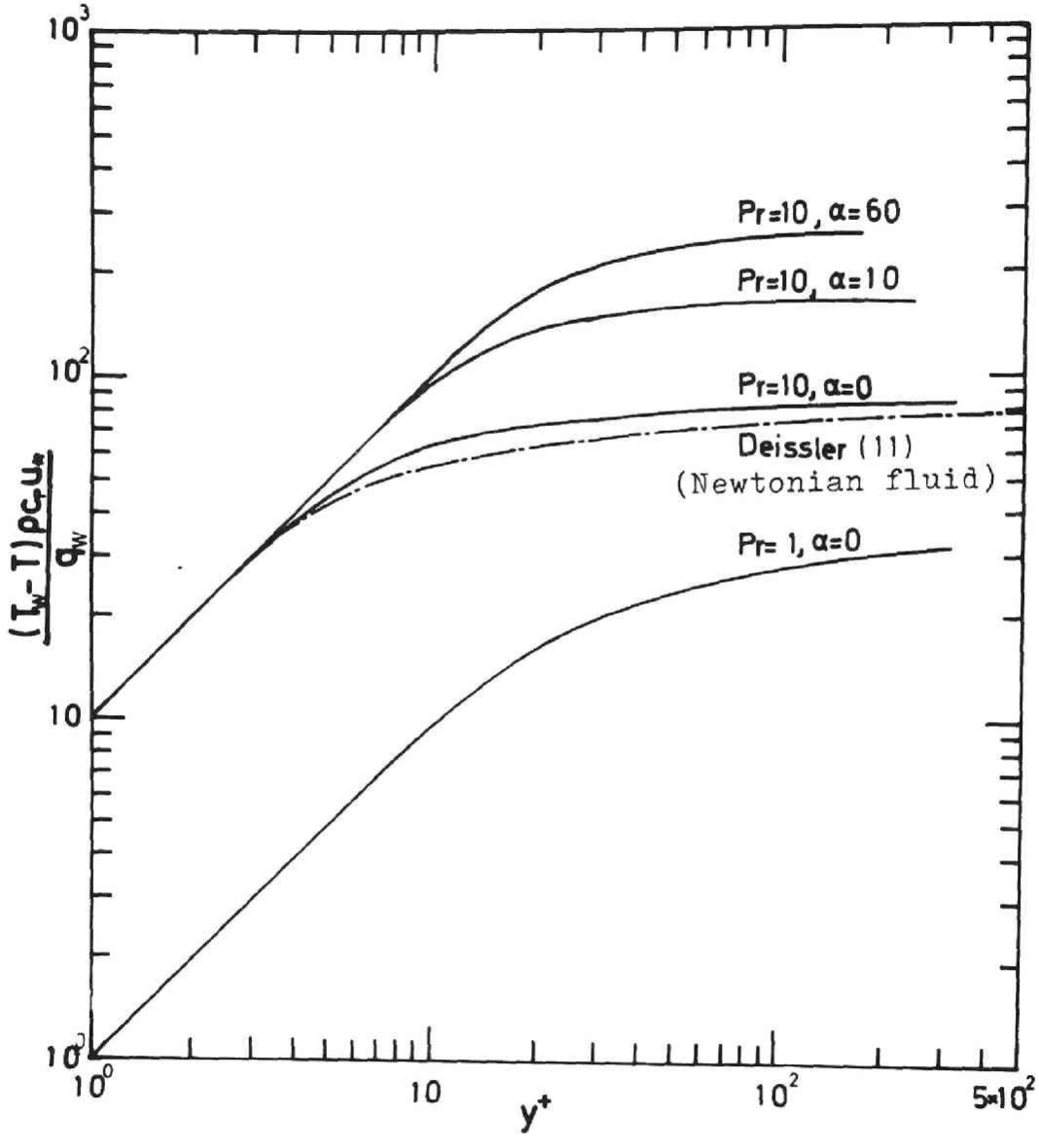

Fig. 3-9 Generalized temperature distribution for Newtonian and viscoelastic fluids.

the laminar sublayer is thickened very much in case of viscoelastic fluid. It is found from this diagram that the buffer region reaches to $y^+=10^2$ at maximum reduction asymptote.

The Nusselt number in fully developed region was calculated from Eqs.(3-18),(3-20) and (3-22), and shown in Fig. 3-10. All of the previous works are those of Newtonian fluid. The line of $\alpha=60$ shows the lower limit of heat transfer reduction of viscoelastic fluid. As expected from the calculation of eddy diffusivity of heat and temperature distributions, the reduction of heat transfer coefficient is very large. The dependency of Nusselt number on Prandtl number was determined as; $Nu \propto Pr^{1/3}$, also in the viscoelastic fluid from this diagram. Thus in Fig. 3-11, the co-ordinates were taken as $Nu/Pr^{1/3}$ and Re for the comparison of the predictions of this study with experimental results. In Fig. 3-11, the curves are the predictions given by the damping factor model of this work. The agreement between the prediction and experimental results is good. Moreover it must be pointed out that there exists a region where Nusselt number is constant over a wide range of Reynolds number. Since the relaxation time of simple shear flow; λ_ℓ is constant along the equi-concentration line in Fig. 3-11, the damp-

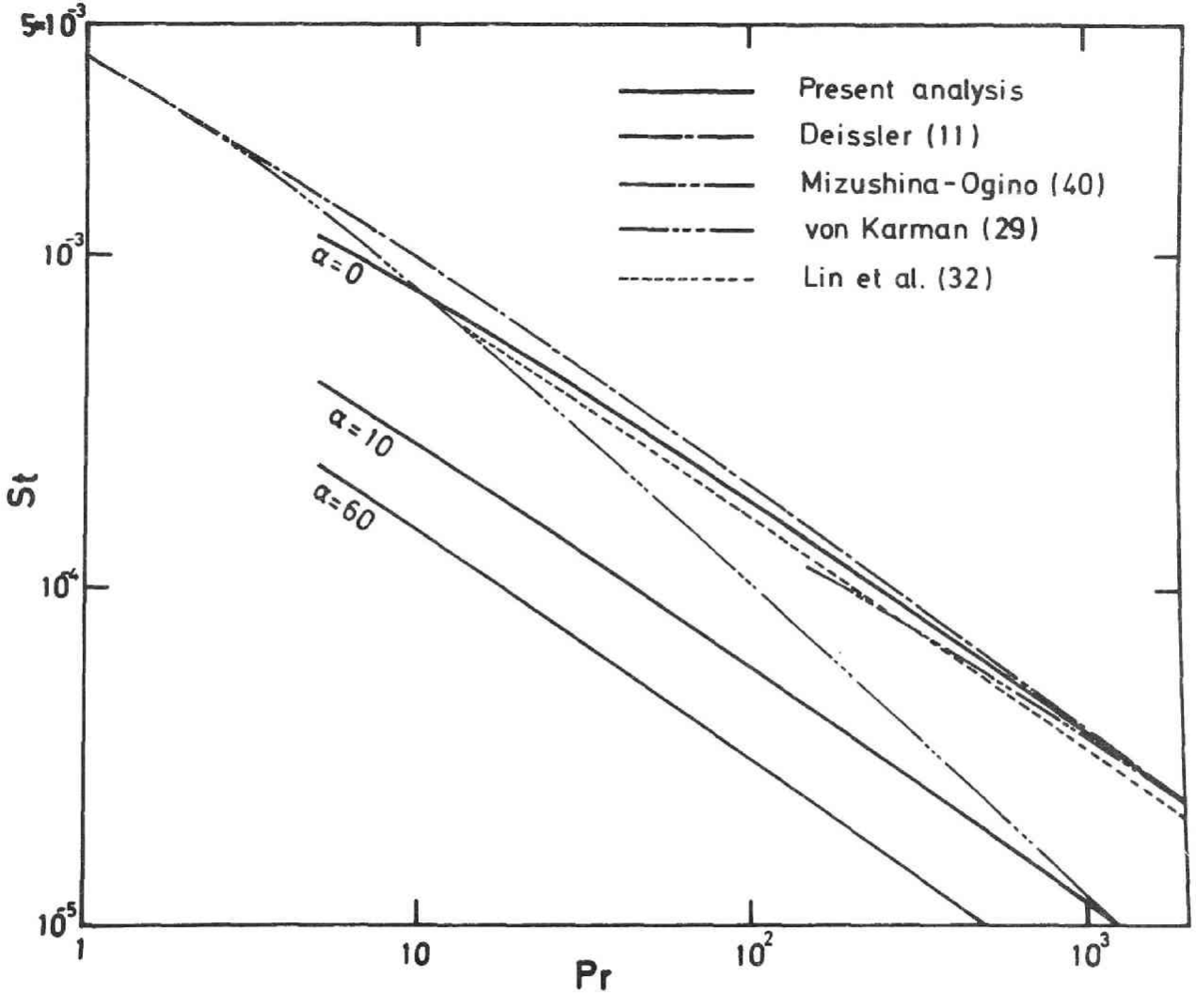

Fig. 3-10 Stanton number in fully developed region for Newtonian and viscoelastic fluids.(at $Re=10^4$)

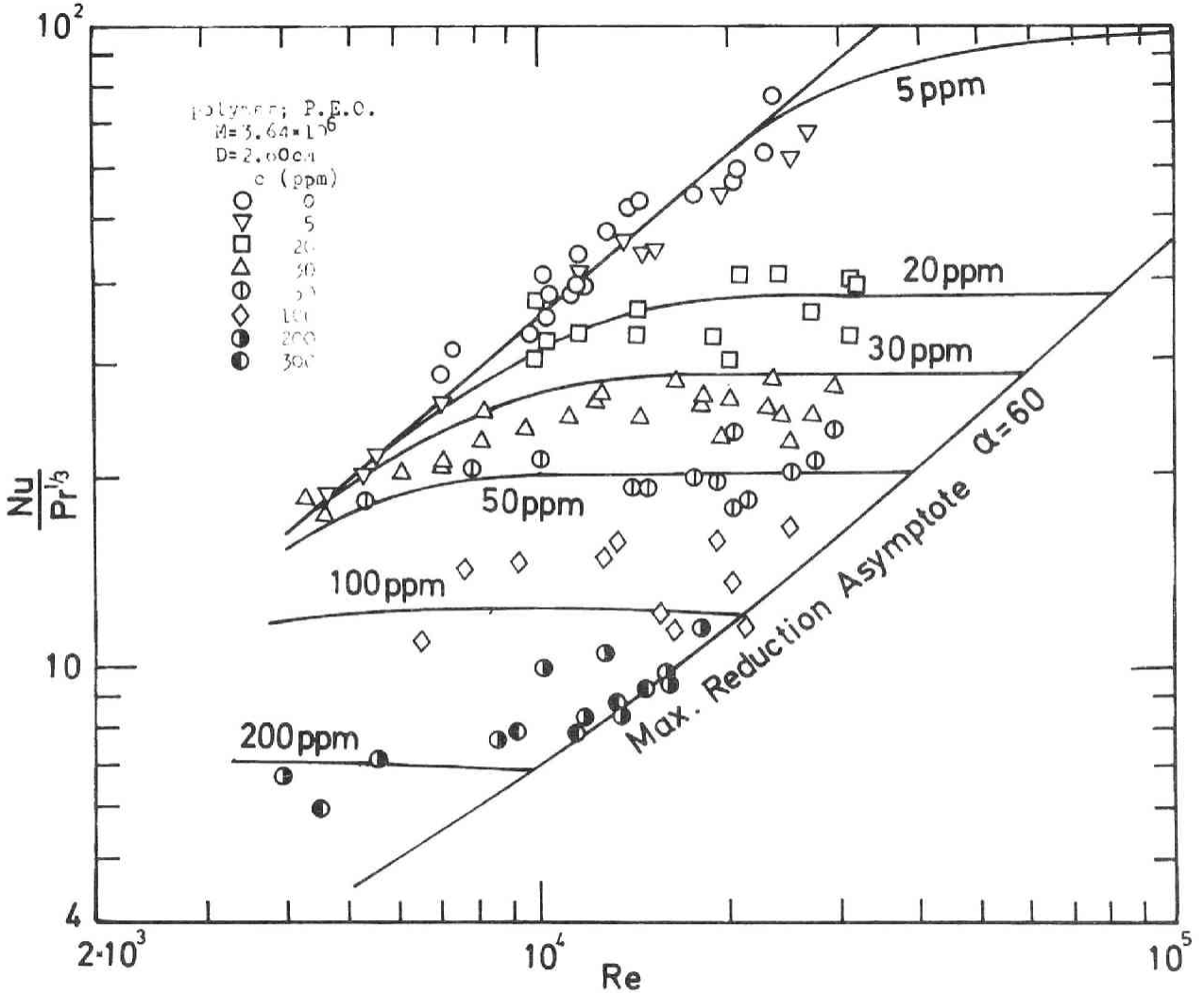

Fig. 3-11 Nusselt number for various concentration of P.E.O..

ing effect caused by the elasticity of polymer solutions becomes larger as the averaged velocity increases, i.e. as the Weissenberg number increases. So the existence of constant Nusselt number range is interpretted as the result of the counterbalance between the effect of Reynolds number increase and of Weissenberg number increase.

Finally the comparison of calculated Nusselt number of this study with the experimental results is shown in Fig. 3-12. They agree each other within $\pm$20%.

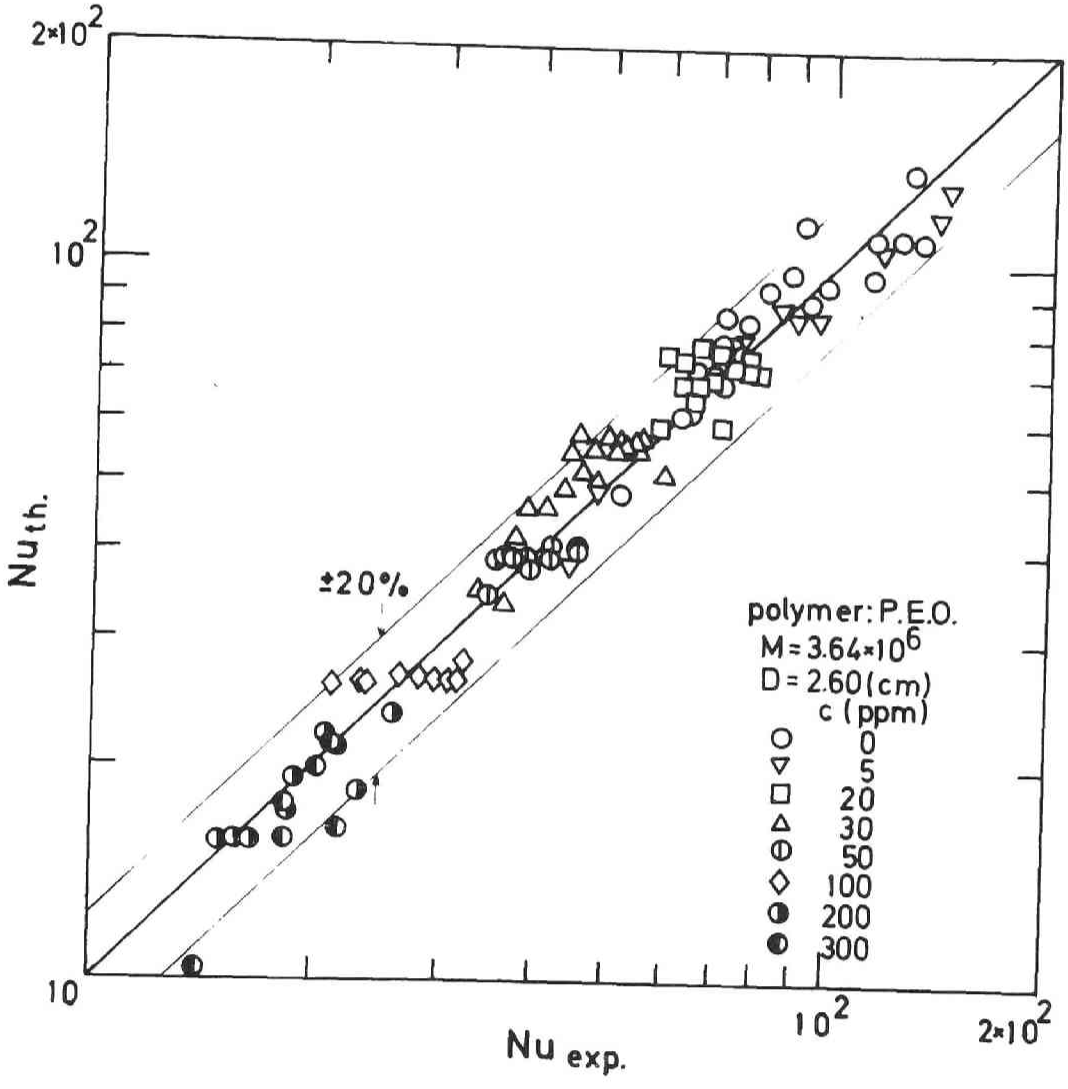

Fig. 3-12 Comparison of calculated Nusselt number with measurements.

3-6 Concluding remarks.

The damping factor model for momentum transfer of viscoelastic fluid was extended to the turbulent heat transfer in pipe flow. The final result of the eddy diffusivity of viscoelastic fluid for heat transfer was given by,

$$\frac{\varepsilon_H}{\nu} = 1.5\, f_n(y^+, R^+)^2 [\{1 - \exp(\frac{-y^+}{42 + \frac{120}{\sqrt{Pr}}})\} / \{1 - \exp(\frac{-y^+}{26})\}] \times \{1 - \exp(\frac{-y^+}{26}\sqrt{-\alpha + \sqrt{\alpha^2+1}})\}^2 \frac{du^+}{dy^+}$$

Combining the above expression with the damping factor model for momentum transfer given in Chapter 2, the reduction of heat transfer rate was able to be predicted, and it was explained that the reduction of heat transfer rate was larger than the reduction of momentum transfer rate, which was not explained by the Colburn's analogy.

From the experimental results of eddy diffusivity for heat transfer of viscoelastic fluids, the existence of maximum reduction asymptote was confirmed.

CHAPTER 4

VELOCITY MEASUREMENT OF VISCOELASTIC FLUIDS WITH LASER DOPPLER METER.

4-1 Introduction.

4-1-1 Summary of previous works.

The Doppler effect is named after Christian Doppler who gave an explanation in 1842 for the higher frequency of a train whistle as it approached to an observer and lower frequency as the train went away from an observer. During the Second World War this effect was applied successfully to the measurement of flying velocity of a plane. This measurement made use of the interference of electric wave with a single frequency which reflected from the earth. From this stage, the practical use of optical method with the Doppler effect has been suggested , but a difficulty to obtain an appropriate light source prevented it from practical applications before the appearance of laser beam.

The first measurement of velocity profiles in fluid by an optical Doppler technique was done by Yeh and Cummis

(67) in 1964. They used a He-Ne gas laser as a light source of this measurement. This optical Doppler technique has been called as Laser Doppler anemometry. Shortly after Yeh and Cummis, the laminar velocity profile were measured by Barman and Santos (6) and by Goldstein and Kreid (21). Recently this technique was extended to the measurement of turbulence by Goldstein, Adrian and Kreid (20) and Donohue, McLaughlin and Tiederman (15). Recent works in these areas were summarized by Durst, Melling and Whitelaw (17).

One of the main advantages of Laser Doppler anemometry is that it does not need any probe submerged in the test fluid. Thus this optical technique is superior to the other techniques which use some probes for the measurement of velocity profile of viscoelastic fluids. The measurement of viscoelastic fluid with Laser Doppler meter was done by Rudd (48) for the case of fully developed turbulent pipe flow of dilute polymer solutions. But the available results obtained by Laser Doppler meter in this area are very scarce. More accumulation of experimental results is expected.

4-1-1 Purpose and outline of this chapter.

The purpose of this chapter is to describe the result of the Laser Doppler anemometry for the case of fully developed turbulent flow of highly elastic fluids. As described in Chapter 2, the velocity profiles of turbulent pipe flow at low reduction region were measured by pitot tube method. But at maximum reduction region the experimental results were not obtained because of the anomalous behavior of pitot tube measurements caused by elasticity. Thus in this chapter the results at maximum reduction asymptote obtained by Laser Doppler meter will be compared with the damping factor model given in Chapter 2.

4-2 Principle of Laser Doppler anemometry.

An observer on a particle moving away from a fixed source of light would see the light with a lower frequency than the source, and the scattered light would show a different frequency from that of the source if it is detected by a stationary observer. Let us consider the geometry shown in Fig. 4-1. For an observer on the particle, the incident wave is expressed by,

$$\lambda_i \nu_p = C - k_i \cdot V \qquad (4\text{-}1)$$

, and the scattered wave is expressed by,

$$\lambda_s \nu_p = C - k_s \cdot V \qquad (4\text{-}2)$$

Where, C is the velocity of light, ν_p is the frequency observed by the particle, and λ_i and λ_s are the wave lengthes of the incident and scattered beam respectively. Thus the ratio of λ_i and λ_s is given by,

$$\frac{\lambda_i}{\lambda_s} = \frac{C - k_i V}{C - k_s V} \qquad (4\text{-}3)$$

By using the relation that; $C = \lambda_o \nu_o$, and solving for the Doppler beat frequency; $\Delta\nu$ ($= \nu_s - \nu_i$), we obtain,

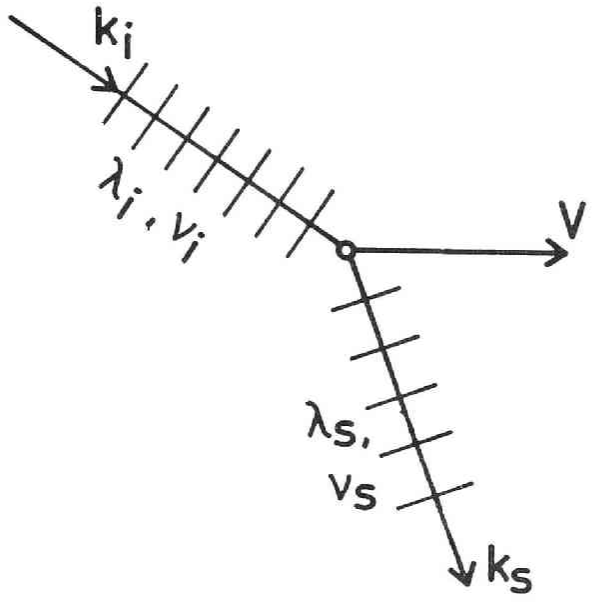

Fig. 4-1 Scattering geometry.

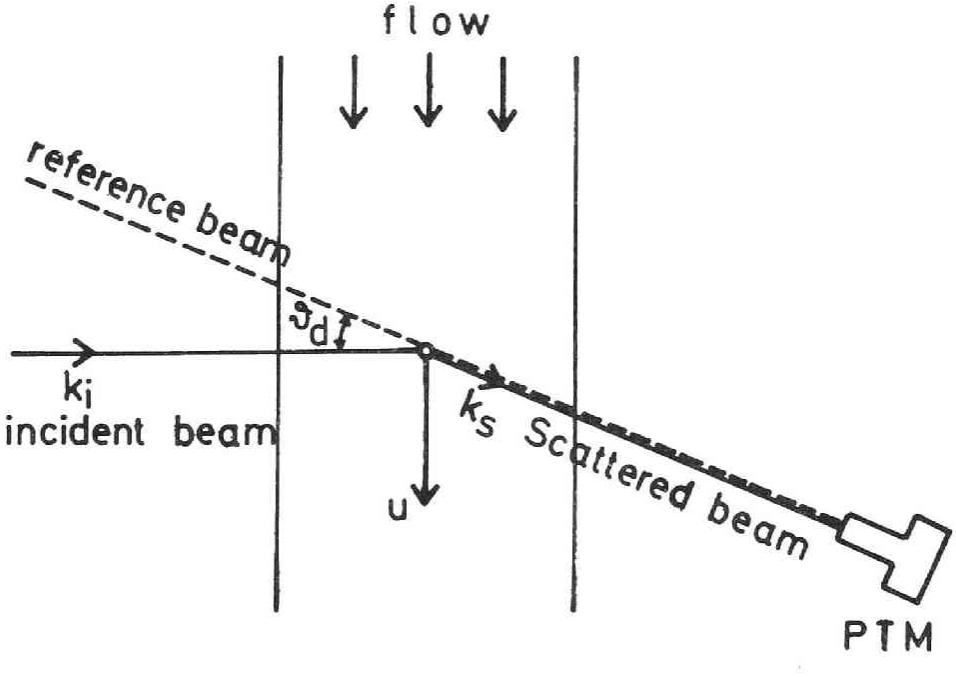

Fig. 4-2 Optical arrengement of this experiment.

$$\Delta\nu = \frac{\nu_i \, V \, (\, k_s - k_i \,)}{C \, (\, 1 - k_s \cdot V/C \,)} \qquad (4\text{-}4)$$

Since $k_s \cdot V/C \fallingdotseq 0$,

$$\Delta\nu = \frac{\nu_i}{C} \, V \, (\, k_s - k_i \,) = \frac{V \, (\, k_s - k_i \,)}{\lambda_i} \qquad (4\text{-}5)$$

In terms of the vacuum wavelength, λ_o , and the index of refraction, n_r , we obtain,

$$\Delta\nu = \frac{n_r}{\lambda_o} \, V \, (\, k_s - k_i \,) \qquad (4\text{-}6)$$

In this study the scattering geometry was taken as that shown in Fig. 4-2. The incident beam fell at right angles with the averaged velocity vector to minimize the effect of strong reflection of incident beam from the optical glass of test section. In this case the product of V and k_i becomes zero and the Doppler beat frequency is finally given by,

$$\Delta\nu = \frac{n_r}{\lambda_0} \, u \, \cos(\frac{\pi}{2} - \theta_d) = \frac{n_r}{\lambda_0} \, u \sin \theta_d \qquad (4\text{-}7)$$

4-3 Experimental apparatus and procedure.

The Laser Doppler meter employed in this study is one of the so-called reference beam mode. In this study the beam from a He-Ne gas laser was split into two beams. The wave length of laser beam was 6328 $\mathring{A}$. The scattered beam was mixed with the reference beam, and the beat signal obtained by the interference of these two beams was detected by photomultiplier. A diagram of the apparatus is shown in Fig. 4-3. The scattering angle, θ_d , was about 7 degrees. The diameter of laser beam was 0.3 mm at the measuring point.

The flow system of test equipment was almost same as that of Chapter 2. Only the test section was changed to a rectangular duct having an aspect ratio (=2H/W) of 1/10. A rectangular duct was chosen to prevent the refraction effect of laser beam near the wall. The length of test duct was 4 m and equivalent diameter was 1.687 cm with a cross section of 10.11x0.92 cm. The length between the inlet and measuring point was 170 times of equivalent diameter, so the condition of fully developed flow region was satisfied. It was difficult to traverse a laser beam , so the test section was forced to move slightly up and down to measure a velocity distribution.

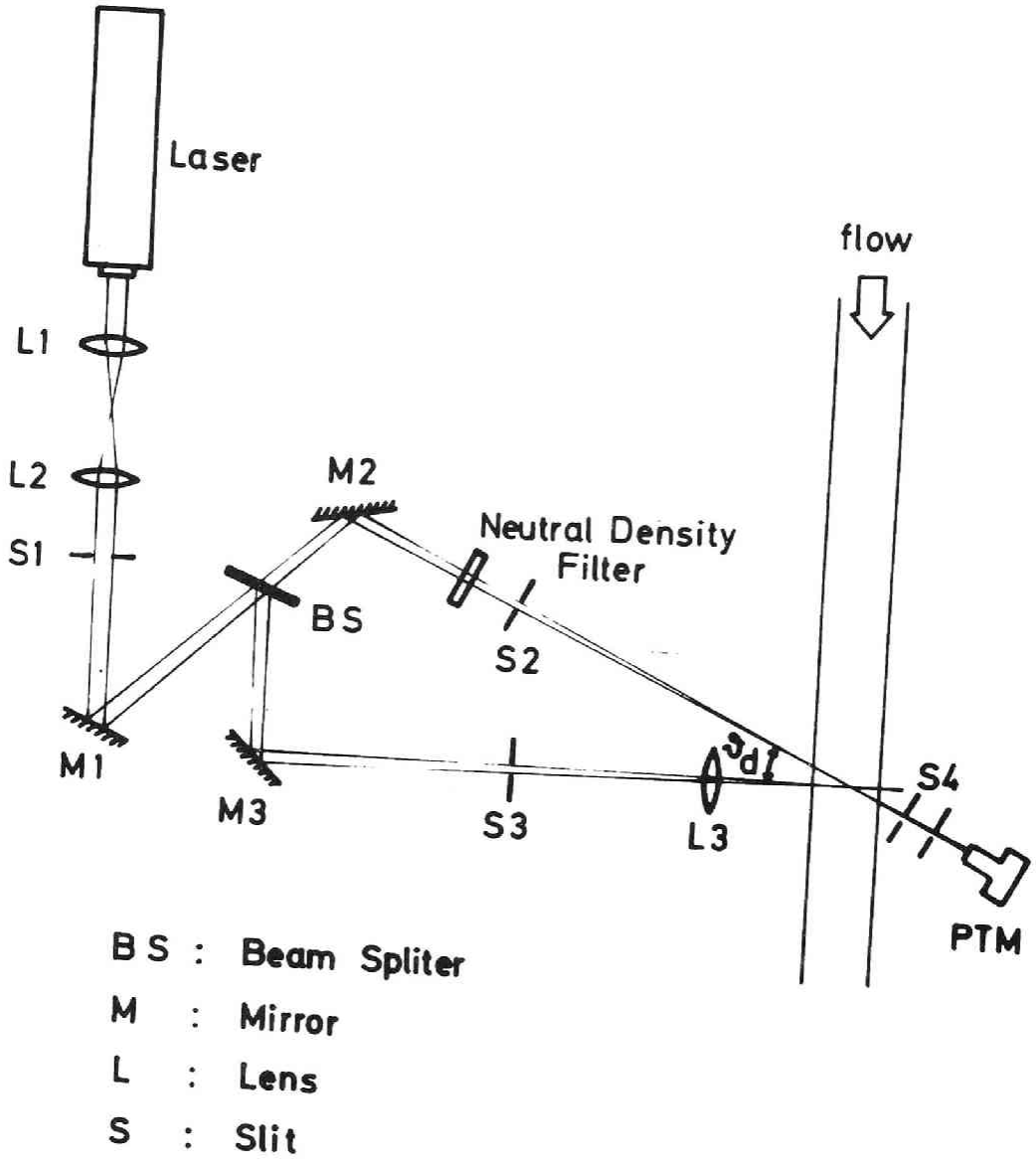

Fig. 4-3 Optical system of the experiment.

The doppler beat frequency detected by photomultiplier must be counted by means of an appropriate data acquistion system. The data analyzing methods most commonly used by many investigators are following three methods, i.e. one is to ues a frequency analyzer and the second is to use a autocorrelation of beat signal and the last is to use frequency-voltage converter. The methods by frequency analyzer or autocorrelation are simple to measure an averaged velocity, but difficult to measure a fluctuating velocity. So the third method with F.-V. (frequency-voltage) converter was employed in this study. But for the measurement of very low laminar velocity profile, the phase locking range of F.-V. converter becomes very narrow. So three or four kinds of reference frequency of the phase locking loop were needed even to obtain one velocity profile of a given Reynolds number. Thus a simple method to use a comparator was developed. The data acquistion system by comparator is shown in Fig. 4-4 -a. A comparator converts a beat signal to pulse signal cutting off the ambiguous signal at low amplitude. The time interval of two succeeding pulses was counted. The data acquistion system by F.-V. converter is shown in Fig. 4-4-b. This method was mainly used for the measurement of turbulent flow. In the measurement of turbulent flow, it was anavoidable to suppress the noise of low

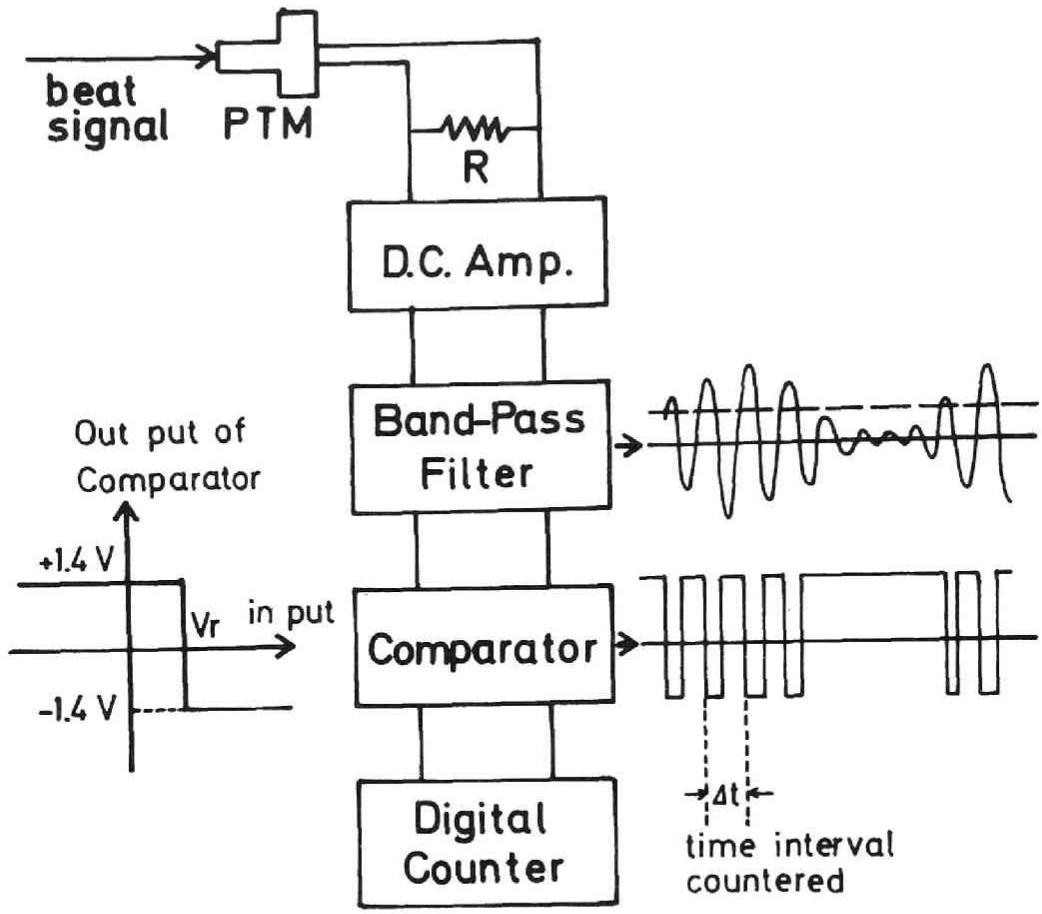

Fig. 4-4-a Data acquisition system
(for low velocity measurement).

frequency caused by the fluctuation of scattered beam. This fluctuation seems to be caused by the concentration fluctuation of scattering particles dispersed in the test fluids. So a band-pass filter was indispensable in the measurement of turbulent flow. The out put of F.-V. converter gave a instantaneous velocity of turbulent flow and it was recorded to be analyzed.

The test fluids in this study were water solution of P.E.O.. The concentration range of P.E.O. was 0 to 300 ppm. The polymer species used in this study was same as that used in the experiments of Chapter 3, so the rheological parameters were determined as $[\eta] = 13.5$ (dl/g) and $M = 3.64 \times 10^6$. It was desirable to disperse some scattering particles to intensify the out put signal. A solution of milk with about 300 ppm was found to be most suitable for this purpose.

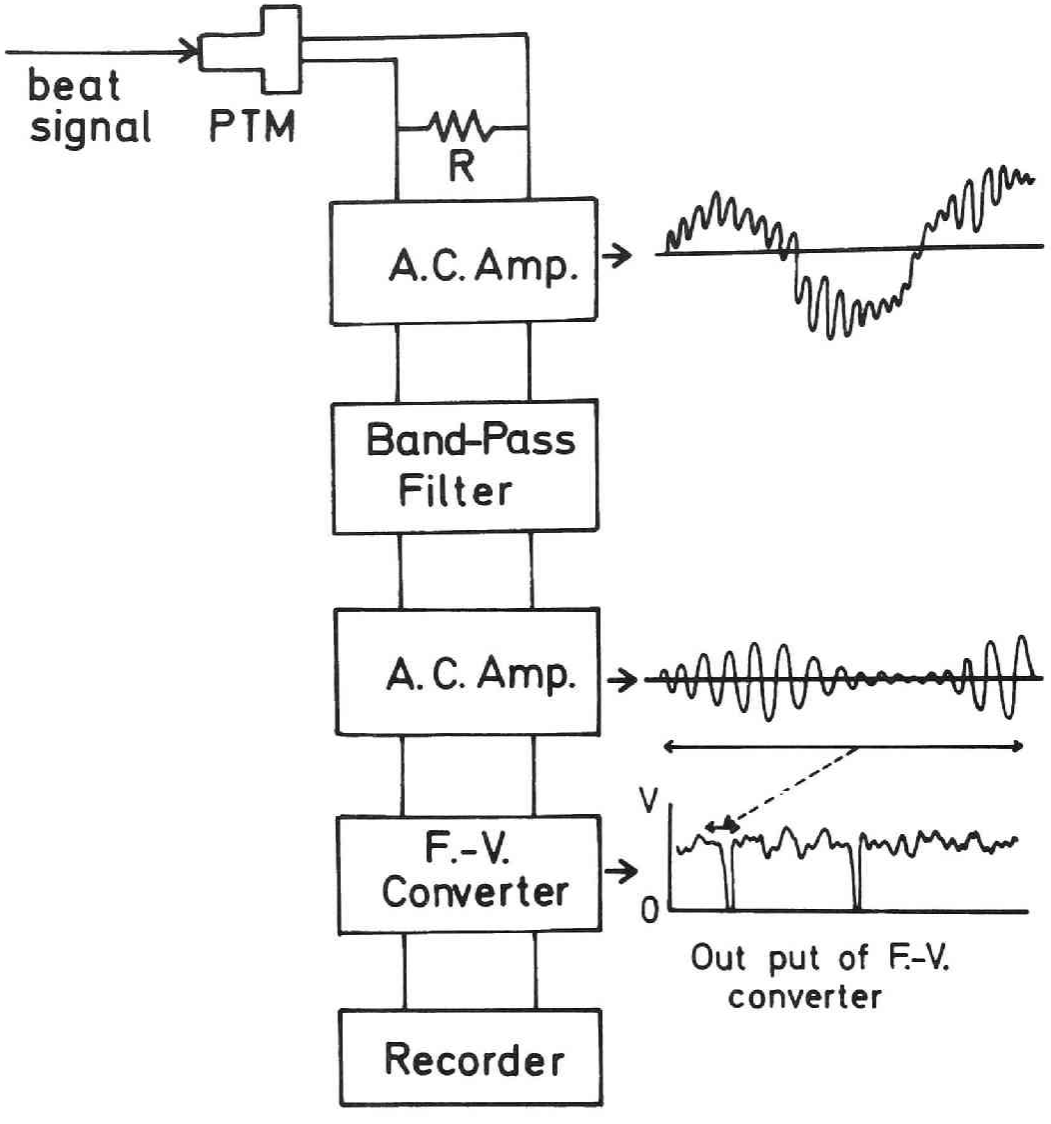

Fig. 4-4-b Data acquisition system
(for high velocity measurement).

4-4 Results and discussions.

4-4-1 Laminar flow.

The observation of out put signal are shown in Fig. 4-5. The reference beam shows nearly constant intencity (see Fig. 4-5-a), and the scattered beam shows a weak fluctuation of low ferquency. When these two beams are mixed, the Doppler beat signal appears (see Fig. 4-5-c) . A comparator was used for the purpose of counting the frequency of this beat signal, and the out put of a comparator is shown in Fig. 4-5-d. The time intervals counted by digital counter had a slight dispersion because of the single time intervals were counted. Thus the averaged value of twenty individual time intervals were used for calculating the velocity.

The results thus obtained by means of a comparator are shown in Fig. 4-6. This diagram shows the results of Newtonian fluid flow in a Reynolds number range of 29 to 279. The measured velocity varied 3.19×10^{-2} to 3.07 cm/sec. The line shown in Fig. 4-6 is the prediction of approximate solution given by Han (23). The results of this experimenta agree well with the theoretical calculation. It can be concluded that the method of this study is effective to measure a very low velocity.

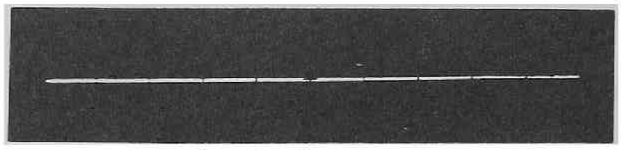

3 m sec

Fig. 4-5-a The signal of Reference beam

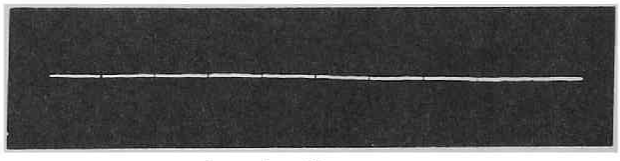

3 m sec

Fig. 4-5-b The signal of Scattered beam

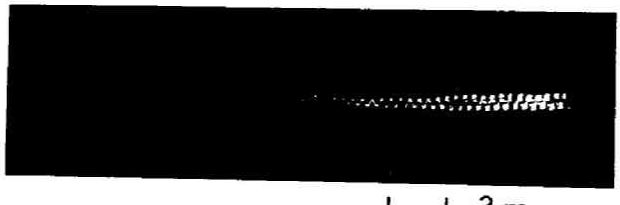

3 m sec

Fig. 4-5-c The signal of Doppler beat

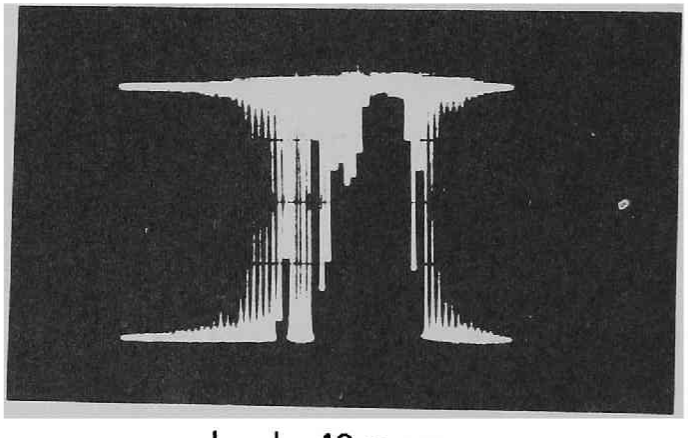

10 m sec

Fig. 4-5-d The signal of Doppler beat after Comparator

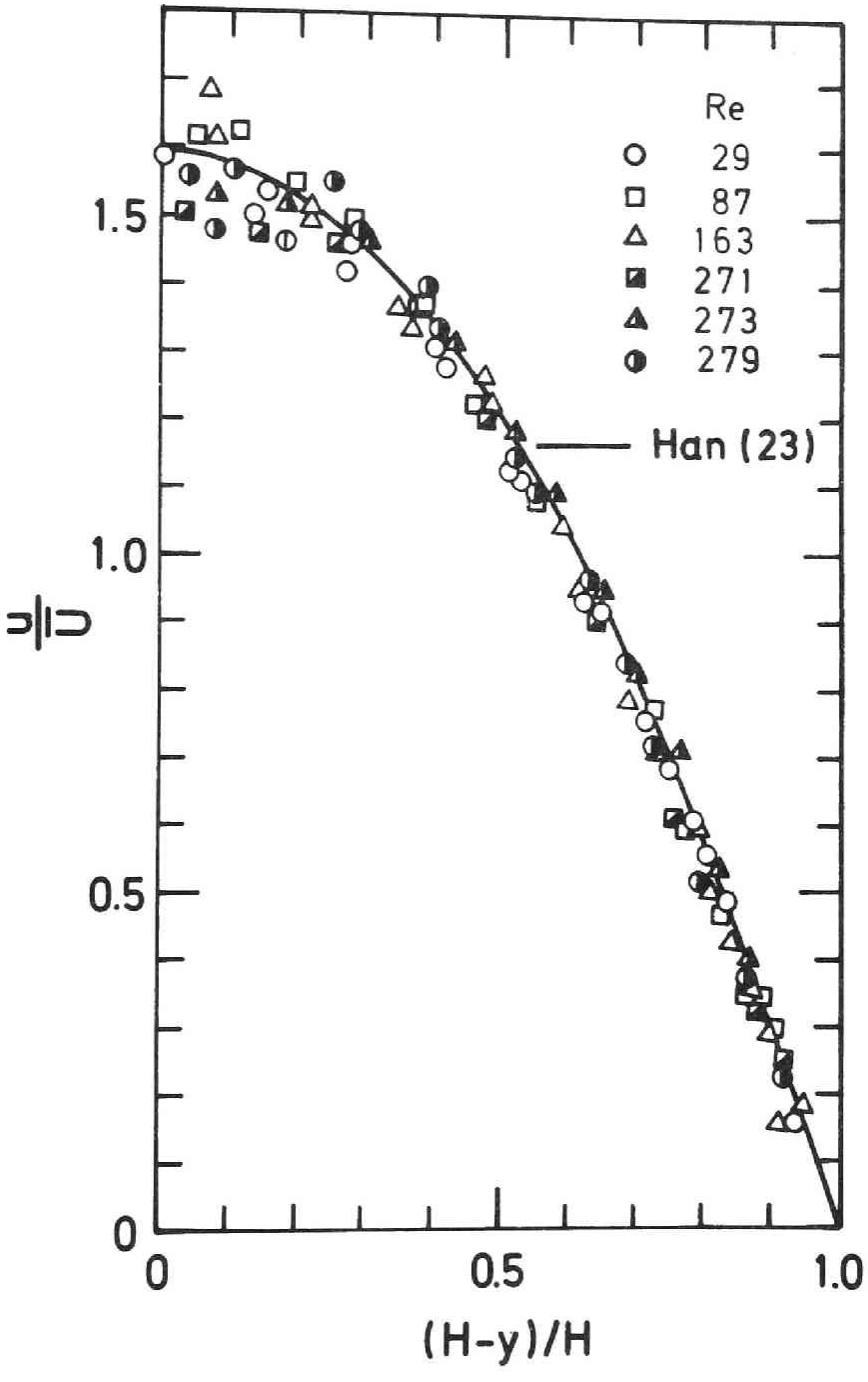

Fig. 4-6 Laminar velocity distribution of Newtonian fluid in rectangular channel.

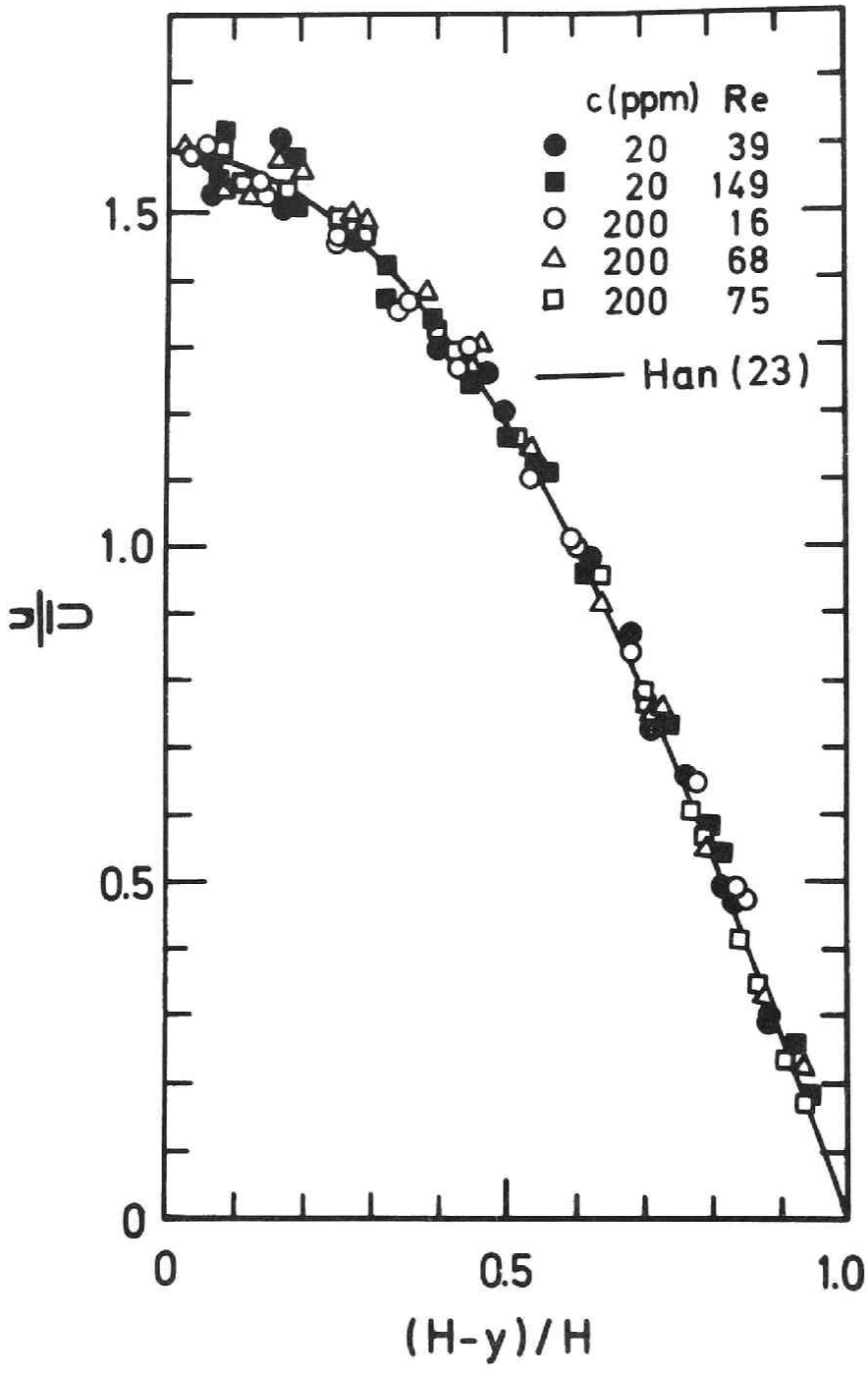

Fig. 4-7 Laminar velocity distribution of viscoelastic fluid in rectangular channel.

The results of viscoelastic fluid in laminar flow region are shown in Fig. 4-7. It is generally accepted that there is no effect of elasticity on a steady laminar flow of viscoelastic fluids in straight channel of constant cross section. The results given in Fig. 4-7 also show no deviation from that of Newtonian fluid.

The response of the comparator used in this study was about 0.05 msec, so the upper limit of measureable beat frequency obtained in this experiment was about 10 kHz which corresponded to $u_{max.} \fallingdotseq 6$ (cm/sec). For the measurements of higher velocity, the method by F.-V. converter is needed which will be discribed in the next section.

4-4-2 Turbulent flow.

The friction factor correlation of turbulent viscoelastic fluid flow given in Chapter 2 was for the case of circular pipe flow. Weissenberg number defined by $\lambda_\ell \bar{u}/D$ was introduced for explaining the pipe diameter effect of Toms phenomenon, and Eq.(2-25) predicted successfully the drag reduction of polymer solutions in unsaturated region . In the discussions given in previous chapters, it was suggested that the scale of turbulent eddy became larger because of the damping effect of elasticity. When the scale of eddy becomes larger the shape of channel may

affect to the growth of large eddy. Thus the friction factor of rectangular duct was measured. The results of this measurements are shown in Fig. 4-8. The broken line in Fig. 4-8 is the maximum reduction asymptote of pipe flow given in Chapter 2. It is clear that the effectiveness of damping in rectangular duct flow is significantly different from that in circular tube flow. The aspect ratio of test section is thought to be the parameter of reduction rate. It seems to be important to discuss this effect in the relation with the deformation of turbulent eddy. But the author can have only the results of one aspect ratio such as 1/10. So, at present stage, the correlation of turbulent relaxation time for the rectangular duct of an aspect ratio of 1/10 was obtained from the results of friction factor measurements shown in Fig. 4-8.

For the case of a steady and fully developed rectilinear flow between parallel flat plates, the co-ordinate system was shown in Fig. 2-12. In this case, the damping factor of viscoelastic fluid may be given by,

$$DF_M = 1 \quad \exp\left(-\frac{y^+}{26}\sqrt{-\alpha + \sqrt{\alpha^2 + 1}}\right) \tag{4-8}$$

where

$$\alpha = \frac{2\lambda}{\nu}\left(\frac{u^*}{26}\right)^2 \tag{4-9}$$

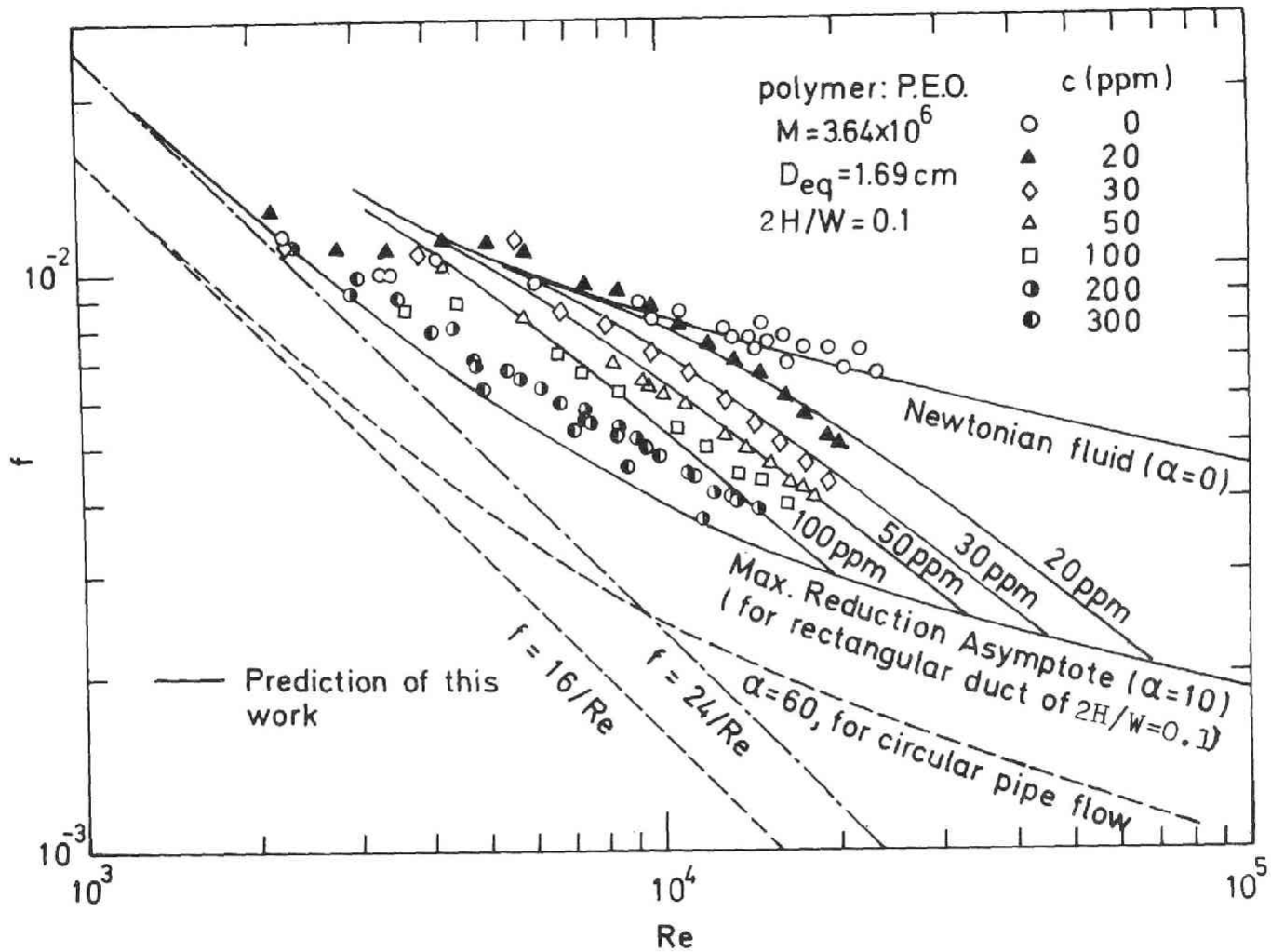

Fig. 4-8 Drag reduction in rectangular channel flow (2H/W = 0.1)

The friction factor and the velocity distribution of fully developed rectilinear flow are given by,

$$f = 2 \{H^+ / \int_0^{H^+} u^+ \, dy^+\}^2 \tag{4-10}$$

and

$$u^+ = \int_0^{y^+} \frac{2(1 - y^+/H^+)dy^+}{1 + \sqrt{1+4 \, f_n(y^+,H^+)^2 DF_M^2 (1 - y^+/H^+)}} \tag{4-11}$$

, where

$$f_n(y^+,H^+) = 0.4y^+ - 0.44\frac{y^{+2}}{H^+} + 0.24\frac{y^{+3}}{H^{+2}} - 0.06\frac{y^{+4}}{H^{+3}} \tag{4-12}$$

The correlation of turbulent relaxation time calculated from results of friction factor measurements with Eqs.(4-8), (4-10) and (4-11) was given for unsaturated region,

$$\frac{\lambda_t}{\lambda_\ell} = 3.40 \times 10^5 \, We^{0.61} \tag{4-13}$$

, and for maximum reduction asymptote,

$$\alpha = 10 \tag{4-14}$$

The prediction of friction factor obtained from Eqs.(4-8), (4-10), (4-11), (4-13) and (4-14) are shown in Fig. 4-8. They can predict well the friction factor of polymer solutions' flow in a rectangular duct of the aspect ratio of 1/10.

The power index of Weissenberg number in Eq.(4-13) is different from that of Eq.(2-25). In both cases, i.e. in

circular pipe flow and in rectangular duct flow, the ratio of λ_t and λ_ℓ was nearly same order and the nondimensional parameter α which appeared in the damping factor became larger as the reduction rate became larger. In this experiment, a duct of only one equivalent diameter with one aspect ratio was used. Moreover only one polymer species of $M = 3.64 \times 10^6$ was tested. So the molecular weight effect and pipe diameter effect shown in Chapter 2 were not tested in this experiment. Thus only the concentration effect was evaluated in Fig. 4-8. In this case the increase of Reynolds number results in the increase of both α and u^*. But there is a relationship between α and λ_t and u^*, such as

$$\alpha/\lambda_t u^{*2} = \text{const.}$$

And the rate of increase of α was smaller than that of pipe flow, and the rate of increase of u^* was larger than that of pipe flow. This means that the rate of decrease of friction factor in rectangular duct is more gradual than that in pipe flow. As a result, the rate of increase of λ_t became smaller and the smaller power index of Weissenberg number in Eq.(4-13) was obtained.

There seems to be very important problem in discussing the growth of turbulent eddy in the flow in rectangular ducts of various aspect ratios. But the author has

not yet obtained the experimental results except one aspect ratio, so in the following discussion about the velocity distribution of highly viscoelastic fluids, the predictions given by Eqs.(4-8), (4-10), (4-11), (4-13) and (4-14) will be compared with the experimental results obtained by Laser Doppler meter.

The results obtained by Laser Doppler meter are shown in Fig. 4-9. This results were obtained by F.-V. converter method shown in Fig. 4-4-b. The range of band pass filter was 0 to 200 kHz, so the upper limit of measurerable velocity was about 1 m/sec in this study. In the measurements of fluctuating velocity, it was necessary that we have perfectly continuous Doppler signal to obtain the continuous out put of F.-V. converter. A relatively continuous signal was achieved by adding a large number of small scattering particles (in this study, milk was added at the concentration of 300 ppm). But even in this condition, the Doppler signal sometimes faded instantaneously, and the phase locking of F.-V. convertor was broken at this moment. This phenomenon inevitable in the measurements of turbulence by means of Laser Doppler technique has been commonly called as signal "drop-out" , and many efforts to avoid this phenomenon have been made by previous investigators (15). But so far, an effective method to overcome this disadvantage has not been found. In this

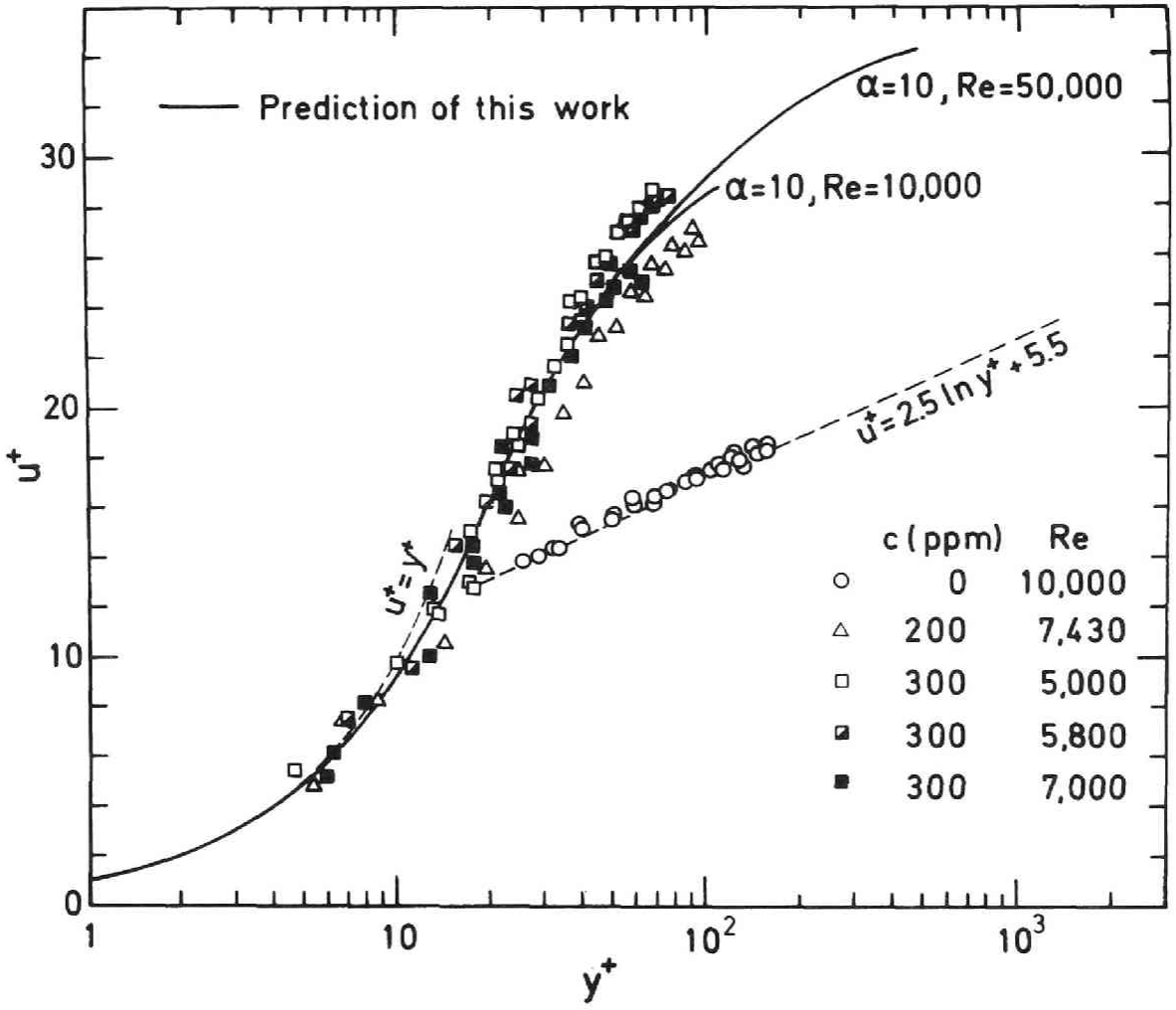

Fig. 4-9 Universal velocity profile of viscoelastic fluids at maximum reduction asymptote.

study, the signal "drop-Out" occured at intervals of about 1 msec, so the averaged out put of F.-V. converter gave almost correct velocity profiles, but the fluctuating velocity was not measured.

Hence in this study the averaged velocity profiles of Newtonian and viscoelastic turbulent flow were measured. The results shown in Fig. 4-9 are those of Newtonian fluid and viscoelastic fluid at maximum drag reduction asymptote . It is clear from this diagram that the velocity profile at maximum reduction asymptote is predicted successfully by the damping factor model of this study. It was not detected by pitot tube method that there is a certain equilibium state at maximum reduction asymptote of viscoelastic fluid, and this was indirectly detected by the measurements of eddy diffusivity of heat given in Chapter 3. Now, the existence of an universal velocity profile of viscoelastic fluids at maximum reduction asymptote was ascertained.

4-5 Concluding remarks.

The Laser Doppler technique was employed for the measurements of the velocity distribution of viscoelastic fluids in rectangular duct flow. The range of measurable velocity of this experimental apparatus was 3×10^{-2} to 10^{2} cm/sec.

The existence of an universal velocity profile of highly viscoelastic fluid was acertained at maximum reduction asymptote.

There is a significant difference of the damping effect between the rectangular duct flow and the circular pipe flow of viscoelastic fluids. The correlation of relaxation time in turbulent flow of viscoelastic fluids in a rectangular duct of an aspect ratio of 1/10 was obtained for unsaturated region as,

$$\frac{\lambda_t}{\lambda_\ell} = 3.40\times10^{5}\ We^{0.61}$$

and for maximum reduction asymptote, we obtained,

$$\alpha = 10$$

More detailed study about the relationship between the drag reduction and the shape of test tube is still needed.

CHAPTER 5

TRANSPORT PHENOMENA OF VISCOELASTIC FLUID IN CROSS FLOW AROUND A CIRCULAR CYLINDER.

5-1 Introduction.

5-1-1 Summary of previous works.

The previous works about the transport phenomena of non-Newtonian fluid flow across a blunt body are briefly summarized in Table 5-1. For purely viscous non-Newtonian fluids, there exist theoretical works over the wide range of Reynolds number. But the detailed experimental study is still needed.

In contrast, the works about the viscoelastic fluids are very scarce. Only the analysis of Ultman and Denn (61) and the experiments of James et al. (28) and Smith et al. (52) are found. Recently the anomalous behavior of hot wire measurements in drag reducing fluids has been discussed by some authors (52),(60). This is just the problem of this chapter. James et al. measured the heat

Table 5-1

Summary of previous works about the non-Newtonian fluid cross flow across a blunt body.

(A) Low Reynolds number, $Re < 1.0$

Ostwald-de Waele model : Wasserman-Slattery (64) (Theoretical)

extended Williamson model : Yoshioka-Adachi (68) (Theoretical)

Maxwell model : Ultman-Denn (61) (Theoretical)

(B) Middle Reynolds number, $1.0 < Re < 1000$

extended Williamson model : Yoshioka-Adachi (68) (Theoretical)

viscoelastic fluid : James-Acosta (28) (Experimental)

viscoelastic fluid : Smith et al. (52) (Experimental)

(C) High Reynolds number, $Re > 1000$

Ostwald-de Waele model : Shah-Petterson-Acrivos (50) (Experimental and Theoretical)

Ostwald-de Waele model : Bizzel-Slattery (7) (Theoretical)

Ostwald-de Waele model
Prandtl Eyring model : Mizushina-Usui (42) (Experimental and Theoretical)

transfer reduction of dilute polymer solutions in cross flow. The condition of high Weissenberg number keeps the Reynolds number small, i.e. $0.1 < Re < 100$. Because of the necessity to avoid the effect of natural convection, the Reynolds number range of forced convection heat transfer results obtained by James et al. was restricted within $1 < Re < 100$. No reliable results of drag coefficient is available and only the flow pattern were observed by some investigators (28),(61). Ultman and Denn used Maxwell model and discussed the viscoelastic fluid flow around a circular cylinder by means of Oseen approximation at $Re = 0.1$ and $We = 0.5$. They discussed qualitatively about the change of flow pattern in viscoelastic fluid. For the quantitative discussion on the available results of heat transfer reduction, the analysis of viscoelastic fluids in middle Reynolds number range is needed.

5-2 Purpose and outline of this chapter.

The purpose of this chapter is to analyze the transport phenomena of viscoelastic fluid in middle Reynolds number range, and to explain the anomalous behavior of hot wire measurements in polymer solutions. For this purpose the Navier-Stokes equation is solved numerically. The distribution of local Nusselt number

and averaged Nusselt number are calculated from the results of surface vorticity for the case of $Pr \to \infty$, and compared with the experimental results of mass transfer obtained by electrochemical method.

5-2 Numerical solution of Navier-Stokes equation with generalized Maxwell model.

The flow configulation is shown in Fig. 5-1. The viscoelastic fluid flow across a circular cylinder at uniform velocity U. The steady state equation of motion of incompressible fluid are,

$$\rho\left(v_r\frac{\partial v_r}{\partial r} + \frac{v_\theta}{r}\frac{\partial v_r}{\partial \theta} - \frac{\partial v_\theta^{\,2}}{r}\right) = -\frac{\partial p}{\partial r}$$

$$+ \left[\frac{1}{r}\frac{\partial}{\partial r}(r\,\tau_{rr}) + \frac{1}{r}\frac{\partial \tau_{r\theta}}{\partial \theta} - \frac{\tau_{\theta\theta}}{r}\right] \qquad (5\text{-}1)$$

$$\rho\left(v_r\frac{\partial v_\theta}{\partial r} + \frac{v_\theta}{r}\frac{\partial v_\theta}{\partial \theta} + \frac{v_r v_\theta}{r}\right) = -\frac{1}{r}\frac{\partial p}{\partial \theta}$$

$$+ \left[\frac{1}{r^2}\frac{\partial}{\partial r}(r^2\tau_{r\theta}) + \frac{1}{r}\frac{\partial \tau_{\theta\theta}}{\partial \theta}\right] \qquad (5\text{-}2)$$

The equation of continuity is

$$\frac{1}{r}\frac{\partial}{\partial r}(r\,v_r) + \frac{1}{r}\frac{\partial v_\theta}{\partial \theta} = 0 \qquad (5\text{-}3)$$

Generalized Maxwell model is taken as the constitutive equation of this analysis;

$$\tau + \lambda\frac{\delta \tau}{\delta t} = \mu\Delta \qquad (5\text{-}4)$$

Two assumptions are made for the practical calculation.

Assumption 1 : The value λ and μ of simple shear flow can be used.

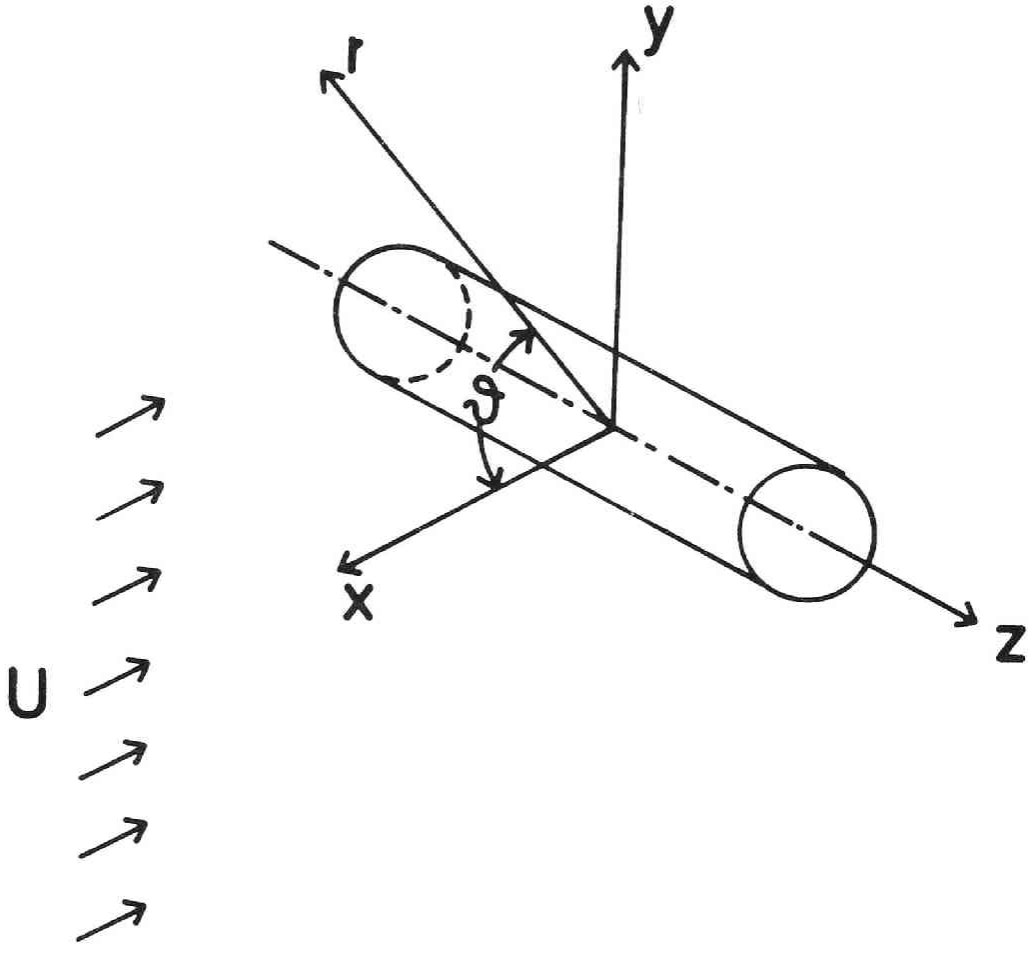

Fig. 5-1 Co-ordinate system.

Assumption 2 : The deformations are small, and the convected derivative is linearized as:

$$\frac{\delta}{\delta t} = \frac{U}{r}\frac{\partial}{\partial \theta} \tag{5-5}$$

According to the above assumptions, Maxwell model is expressed as,

$$\tau_{rr} + \frac{\lambda U}{r}\frac{\partial \tau_{rr}}{\partial \theta} = 2\mu\frac{\partial v_r}{\partial r} \tag{5-6-a}$$

$$\tau_{r\theta} + \frac{\lambda U}{r}\frac{\partial \tau_{r\theta}}{\partial \theta} = \mu\left\{r\frac{\partial}{\partial r}\left(\frac{v_\theta}{r}\right) + \frac{1}{r}\frac{\partial v_r}{\partial \theta}\right\} \tag{5-6-b}$$

$$\tau_{\theta\theta} + \frac{\lambda U}{r}\frac{\partial \tau_{\theta\theta}}{\partial \theta} = 2\mu\left(\frac{1}{r}\frac{\partial v_\theta}{\partial \theta} + \frac{v_r}{r}\right) \tag{5-6-c}$$

Substituting Eqs.(5-6-a,b,c) in Eqs.(5-1) and (5-2), and nondimensionalizing by next expressions,

$$\frac{r}{R} \rightarrow r\ , \quad \frac{v_i}{U} \rightarrow v_i\ , \quad \frac{p}{\frac{1}{2}\rho U^2} \rightarrow p\ ,$$

$$Re = \frac{2RU}{\nu}\ , \quad We = \frac{\lambda U}{2R}\ ,$$

basic equations become,

$$\left(1 + \frac{2\ We}{r}\frac{\partial}{\partial \theta}\right)\left\{v_r\frac{\partial v_r}{\partial r} + \frac{v_\theta}{r}\frac{\partial v_r}{\partial \theta} - \frac{v_\theta^2}{r}\right\} = -\frac{1}{2}\frac{\partial p}{\partial r}$$

$$-\frac{We}{2r}\frac{\partial^2 p}{\partial r \partial \theta} + \frac{2}{Re}\left[\frac{\partial}{\partial r}\left(\frac{1}{r}\frac{\partial (r v_r)}{\partial r}\right) + \frac{1}{r^2}\frac{\partial^2 v_r}{\partial \theta^2} - \frac{2}{r^2}\frac{\partial v_\theta}{\partial \theta}\right] \tag{5-7}$$

$$(1 + \frac{2We}{r}\frac{\partial}{\partial\theta})\{v_r\frac{\partial v_\theta}{\partial r} + \frac{v_\theta}{r}\frac{\partial v_\theta}{\partial\theta} + \frac{v_r v_\theta}{r}\} = -\frac{1}{2r}\frac{\partial p}{\partial\theta}$$

$$- \frac{We}{2r^2}\frac{\partial^2 p}{\partial\theta^2} + \frac{2}{Re}[\frac{\partial}{\partial r}(\frac{1}{r}\frac{\partial(rv_\theta)}{\partial r}) + \frac{1}{r^2}\frac{\partial^2 v_\theta}{\partial\theta^2} + \frac{2}{r^2}\frac{\partial v_r}{\partial\theta}] \tag{5-8}$$

Stream function and vorticity are defined as,

$$v_r = \frac{1}{r}\frac{\partial\psi}{\partial\theta} \quad , \quad v_\theta = -\frac{\partial\psi}{\partial r} \tag{5-9}$$

, and $$\zeta = \frac{\partial^2\psi}{\partial r^2} + \frac{1}{r}\frac{\partial\psi}{\partial r} + \frac{1}{r^2}\frac{\partial^2\psi}{\partial\theta^2} \tag{5-10}$$

From Eqs.(5-7),(5-8),(5-9) and (5-10), the vorticity transport equation is obtained as,

$$(1 + \frac{2\ We}{r}\frac{\partial}{\partial\theta})\ \{\frac{\partial\psi}{\partial\theta}\frac{\partial\zeta}{\partial r} - \frac{\partial\psi}{\partial r}\frac{\partial\zeta}{\partial\theta}\}$$

$$= \frac{2}{Re}\ \{r\frac{\partial^2\zeta}{\partial r^2} + \frac{\partial\zeta}{\partial r} + \frac{1}{r}\frac{\partial^2\zeta}{\partial\theta^2}\} \tag{5-11}$$

Boundary conditions are

$$\psi = \frac{\partial\psi}{\partial r} = 0 \qquad \text{at} \qquad r = 1$$

$$\zeta = 0 \quad \psi = r\sin\theta \qquad \text{at} \qquad r \to \infty \tag{5-12}$$

$$\psi = \xi = 0 \qquad \text{at} \qquad \theta = 0\ ,\ \pi$$

Since it is desirable to have a finer mesh near the cylinder, the following transformation has been made;

$$r = e^{\pi\xi} \quad , \qquad \eta = \theta/\pi$$

Then we obtain,

$$(1 + \frac{2\ We}{E}\frac{\partial}{\partial\eta})(\frac{\partial\psi}{\partial\eta}\frac{\partial\zeta}{\partial\xi} - \frac{\partial\psi}{\partial\xi}\frac{\partial\zeta}{\partial\eta}) = \frac{2}{Re}\{\frac{\partial^2\zeta}{\partial\eta^2} + \frac{\partial^2\zeta}{\partial\xi^2}\} \tag{5-13}$$

$$E^2\zeta = \frac{\partial^2\psi}{\partial\eta^2} + \frac{\partial^2\psi}{\partial\xi^2} \tag{5-14}$$

$$\text{B.C.} \quad \psi = \frac{\partial\psi}{\partial\xi} = 0 \qquad \text{at} \qquad \xi = 0$$

$$\zeta = 0 \quad \psi = e^{\pi\xi}\sin\pi\eta \quad \text{at} \qquad \xi \to \infty \tag{5-15}$$

$$\psi = \zeta = 0 \qquad \text{at} \qquad \eta = 0.1$$

where $E = \pi e^{\pi\xi}$.

In the numerical calculation, five-point approximation was taken for the successive finite difference procedure. By considering the lattice spacing shown in Fig. 5-2, Eqs.(5-13) and (5-14) may be written in finite-difference form as,

$$\zeta_{ij} = (\zeta_{i,j+1} + \zeta_{i,j-1})\ F1 + (\zeta_{i+1,j} + \zeta_{i-1,j})\ F2$$

$$-\frac{Re}{2FO}\{(\frac{\psi_{i+1,j}-\psi_{i-1,j}}{2b})(\frac{\zeta_{i,j+1}-\zeta_{i,j-1}}{2a}) - (\frac{\psi_{i,j+1}-\psi_{i,j-1}}{2a})$$

$$\times(\frac{\zeta_{i+1,j}-\zeta_{i-1,j}}{2b})\} - \frac{Re\ We}{FO\ E}\{(\frac{\psi_{i+1,j}-2\psi_{i,j}+\psi_{i-1,j}}{b^2})$$

$$\times(\frac{\zeta_{i,j+1}-\zeta_{i,j-1}}{2a}) + (\frac{\psi_{i+1,j}-\psi_{i-1,j}}{2b})$$

$$\times(\frac{\zeta_{i+1,j+1}-\zeta_{i-1,j+1}-\zeta_{i+1,j-1}+\zeta_{i-1,j-1}}{4ab})$$

$$-\left(\frac{\psi_{i+1,j+1}-\psi_{i-1,j+1}-\psi_{i+1,j-1}+\psi_{i-1,j-1}}{4ab}\right)\left(\frac{\zeta_{i+1,j}-\zeta_{i-1,j}}{2b}\right)$$

$$-\left(\frac{\psi_{i,j+1}-\psi_{i,j-1}}{2a}\right)\left(\frac{\zeta_{i+1,j}-2\zeta_{i,j}+\zeta_{i-1,j}}{b^2}\right)\} \qquad (5\text{-}16)$$

$$\psi_{i,j} = (\psi_{i,j+1} + \psi_{i,j-1})\ F1 + (\psi_{i+1,j} + \psi_{i-1,j})\ F2$$

$$E^2\zeta_{i,j}\ FO \qquad (5\text{-}17)$$

where $FO = \frac{2}{a^2} + \frac{2}{b^2}$, $F1 = \frac{1}{a\ FO}$ and $F2 = \frac{1}{b\ FO}$.

The value of ψ at the outer edge of grid was calculated from the following equation,

$$\psi_{i,J+1} = e^{\pi aJ} \sin \pi\eta \qquad (5\text{-}18)$$

The distribution of surface vorticity was obtained from the values of ψ near the wall as follows. The Tayler series expansions for the stream function at points, (i,2) and (i,3) in Fig. 5-2 are

$$\psi_{i,2} = \psi_{i,1} + a\left(\frac{\partial\psi}{\partial\xi}\right)_{i,1} + \frac{a^2}{2}\left(\frac{\partial^2\psi}{\partial\xi^2}\right)_{i,1} + \ldots \qquad (5\text{-}19)$$

$$\psi_{i,3} = \psi_{i,1} + 2a\left(\frac{\partial\psi}{\partial\xi}\right)_{i,1} + \frac{(2a)^2}{2}\left(\frac{\partial^2\psi}{\partial\xi^2}\right)_{i,1} + \ldots \qquad (5\text{-}20)$$

Eqs.(5-14),(5-19) and (5-20), together with the next boundary condition,

$$\frac{\partial^2\psi}{\partial\eta^2} = 0 \qquad \text{at} \qquad \xi = 0$$

give the distribution of surface vorticity as,

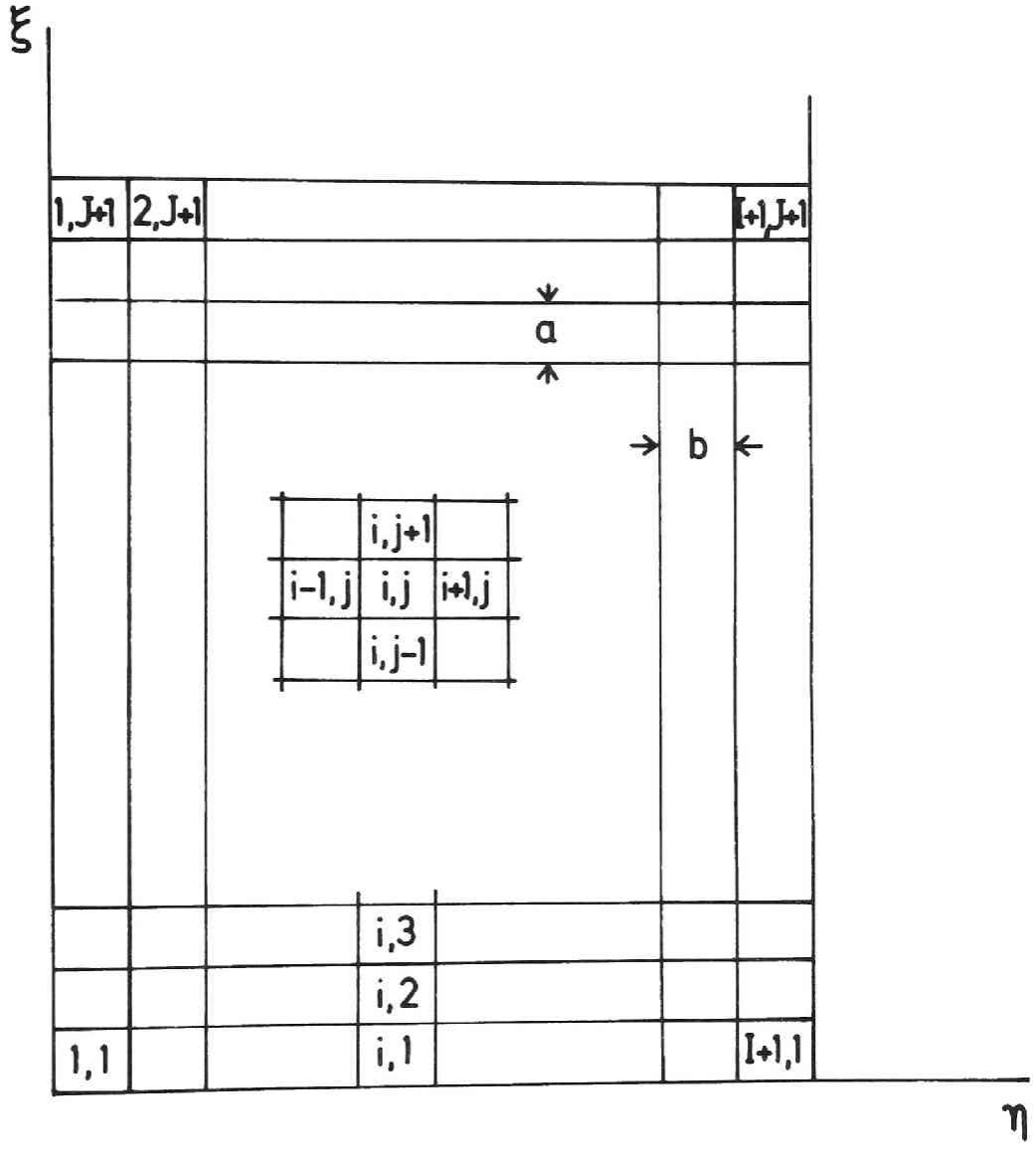

Fig. 5-2 The grid structure.

$$\zeta_{i,1} = \frac{8\,\psi_{i,2} - \psi_{i,3}}{2E^2 a^2} \tag{5-21}$$

The initial conditions for stream function and vorticity are assumed as follows,

$$\psi_{i,j} = e^{\pi\xi}\left(1 - \frac{1}{e^{\pi\xi}}\right) \sin \pi\eta \tag{5-22}$$

$$\zeta_{i,j} = 0 \tag{5-23}$$

The iterative procedure are performed for Eqs.(5-16) and (5-17) with the initial conditions of Eqs.(5-22) and (5-23) and with the boundery conditions of Eqs.(5-15),(5-18) and (5-21). In this procedure the relaxation factors are utilized to stabilize the computations. They are introduced as followed,

$$\psi_{i,j}^{(n)} = (1 - \beta_1)\,\psi_{i,j}^{(n-1)} + \beta_1\,\psi_{i,j}^{*} \tag{5-24}$$

$$\zeta_{i,j}^{(n)} = (1 - \beta_2)\zeta_{i,j}^{(n-1)} + \beta_2\zeta_{i,j}^{*} \tag{5-25}$$

where the superscripts (n) and (n-1) indicate the (n)th and (n-1)th iteration number and the asterik denotes the value calculated from Eqs.(5-16) and (5-17). The values of β_1 and β_2 such as $0.1 \leqq \beta_1 \leqq 1.5$ and $0.1 \leqq \beta_2 \leqq 0.5$ were used. The relative small values of β_1 and β_2 were needed to stabilize the computation at the initial stage of computations. The conditions of convergence are:

$$\left| \frac{\psi_{i,j}^{(n+10)} - \psi_{i,j}^{(n)}}{\psi_{i,j}^{(n)}} \right| \leq 10^{-2} \tag{5-26}$$

$$\left| \frac{C_D^{(n+10)} - C_D^{(n)}}{C_D^{(n)}} \right| \leq 10^{-3} \tag{5-27}$$

Drag coefficient and Nusselt number are calculated as follows. At the surface of a cylinder, next relationships are valid.

$$v_\theta = v_r = \frac{\partial v_\theta}{\partial \theta} = \frac{\partial v_r}{\partial \theta} = \frac{\partial^2 v_\theta}{\partial \theta^2} = 0 \quad \text{at} \quad r = 1$$

$$\zeta|_{r=1} = \frac{\partial^2 \psi}{\partial r^2}\Big|_{r=1} = -\frac{\partial v_\theta}{\partial r}\Big|_{r=1} \tag{5-28}$$

Substituting these equations into Eq.(5-8), the distribution of pressure gradient is given as,

$$\frac{\partial p}{\partial \theta}\Big|_{r=1} = -\frac{4}{Re} \frac{\partial \zeta}{\partial r}\Big|_{r=1} \tag{5-29}$$

The definition of pressure drag coefficient is

$$C_p = \int_0^\pi p \cos\theta \, d\theta \tag{5-30}$$

Thus from the relation of Eq.(5-29), C_p is given by partial integration as,

$$C_p = \frac{4}{Re} \int_0^\pi \sin\theta \frac{\partial \zeta}{\partial r}\Big|_{r=1} d\theta \tag{5-31}$$

The friction drag coefficient is given by,

$$C_f = \frac{4}{Re} \int_0^\pi \sin\theta \, \zeta|_{r=1} \, d\theta \tag{5-32}$$

Then the total drag coefficient is expressed as,

$$C_D = C_p + C_f = \frac{4}{Re} \int_0^{\pi} \sin\theta \left(\frac{\partial \zeta}{\partial r}\Big|_{r=1} - \zeta\Big|_{r=1} \right) d\theta \qquad (5\text{-}33)$$

The local Nusselt number may be obtained as the result of numerical solution of heat transfer equation in a similar way described in the preceding section. But, for the high Prandtl number range of this study the concentration boundary layer is so thin that even the finest grid which is possible to compute is not sufficient to detect the concentration profiles. So the approximate solution at $Pr \to \infty$ given by Acrivos (1) is used to calculate the distribution of local Nusselt number. This approximate solution is applicable only to the thermal or concentration boundary layer at large Prandtl number. The experimental condition of this study, i.e. at $Sc \fallingdotseq 1000$, may consistent with this assumption. Thus the local Nusselt number is calculated by,

$$Nu = Re^{1/2} \left(\frac{Pr}{9}\right)^{1/3} \frac{(\zeta|_{r=1}/\sqrt{Re})^{1/2}}{\Gamma(\frac{4}{3})} \times \left[\int_0^{x_1} (\zeta|_{r=1}/\sqrt{Re})^{1/2}\, dx\right]^{-1/3} \qquad (5\text{-}34)$$

The averaged Nusselt number is calculated from integrating the local Nusselt numbers.

5-3 Results of numerical calculation.

The numerical solutions were obtained for the cases of Re = 1.0, 10, 20 and We = 0 (Newtonian fluid) and We = 0.01 ∿ 0.25 (viscoelastic fluid). In all runs of computations the values of a and b in Fig. 5-2 were retained as constant values, i.e. a = 0.03 and b = 0.05. And the values of I and J in Fig. 5-2 were 20 and 30 respectively . Thus the value of r_∞ was 16.3xR. The computational results are given in Table 5-2 for Newtonian fluid and in Table 5-3 for viscoelastic fluid. The results of previous works for Newtonian fluid are also shown in Table 5-2, and compared with the results of this study in Fig. 5-3 and Fig. 5-4. From such a comparison, the results of this study have been confirmed to be valid.

The results of viscoelastic fluid given in Table 5-3 show the drastic change of viscoelastic fluid flow from the results of Newtonian fluid. This change is visualized in following figures. The results of equi-stream line are shown in Fig. 5-5, 5-6 and 5-7. The stream line of viscoelastic fluid show the expansion in front of a cylinder and the contraction at the back of a cylinder (see Fig. 5-5-b,c). At high Weissenberg number range of Re = 1.0, a stagnant region appears near the front

Table 5-2

Computational results for Newtonian fluid.

Re	1.0	10	20
C_D	13.50	3.031	2.092
	11.94*	2.084+	1.984*
			2.045+
			2.0**
C_f	6.96	1.375	0.861
	5.846*	1.246+	0.773*
			0.812+
C_p	6.55	1.656	1.231
	6.015*	1.600+	1.211*
			1.233+
L/2R	—	0.288	1.136
		0.285+	1.197*
			0.935**
θ_s	—	29.2	42.5
		29.6+	46.66*
			43.65**
			43.7+

* due to Yoshioka- Adachi (68)

** due to Takami-Keller (56)

\+ due to Dennis-Chang (13)

Table 5-3
Computational results for viscoelastic fluid.

Re	1.0				10.0			20.0			
We	0.1	0.15	0.2	0.25	0.01	0.03	0.05	0.01	0.02	0.03	0.05
C_D	7.105	5.298	3.729	2.147	2.145	1.302	0.7928	1.546	1.047	0.7676	0.3223
C_f	3.872	2.879	2.073	1.355	1.002	0.6358	0.3794	0.6586	0.4576	0.3530	0.1699
C_p	3.233	2.419	1.692	0.792	1.143	0.6662	0.4134	0.8874	0.5994	0.4146	0.1524
L/2R	—	—	0.33*	2.18*	0.288	—	—	0.67	0.42	0.27	0.091
θ_s	—	—	37.2*	62.5*	27.9	—	—	37.4	33.6	27.0	15.3

* ;These values are obtained from the front stagnation regions shown in Fig. 5-5-d and Fig. 5-5-e.

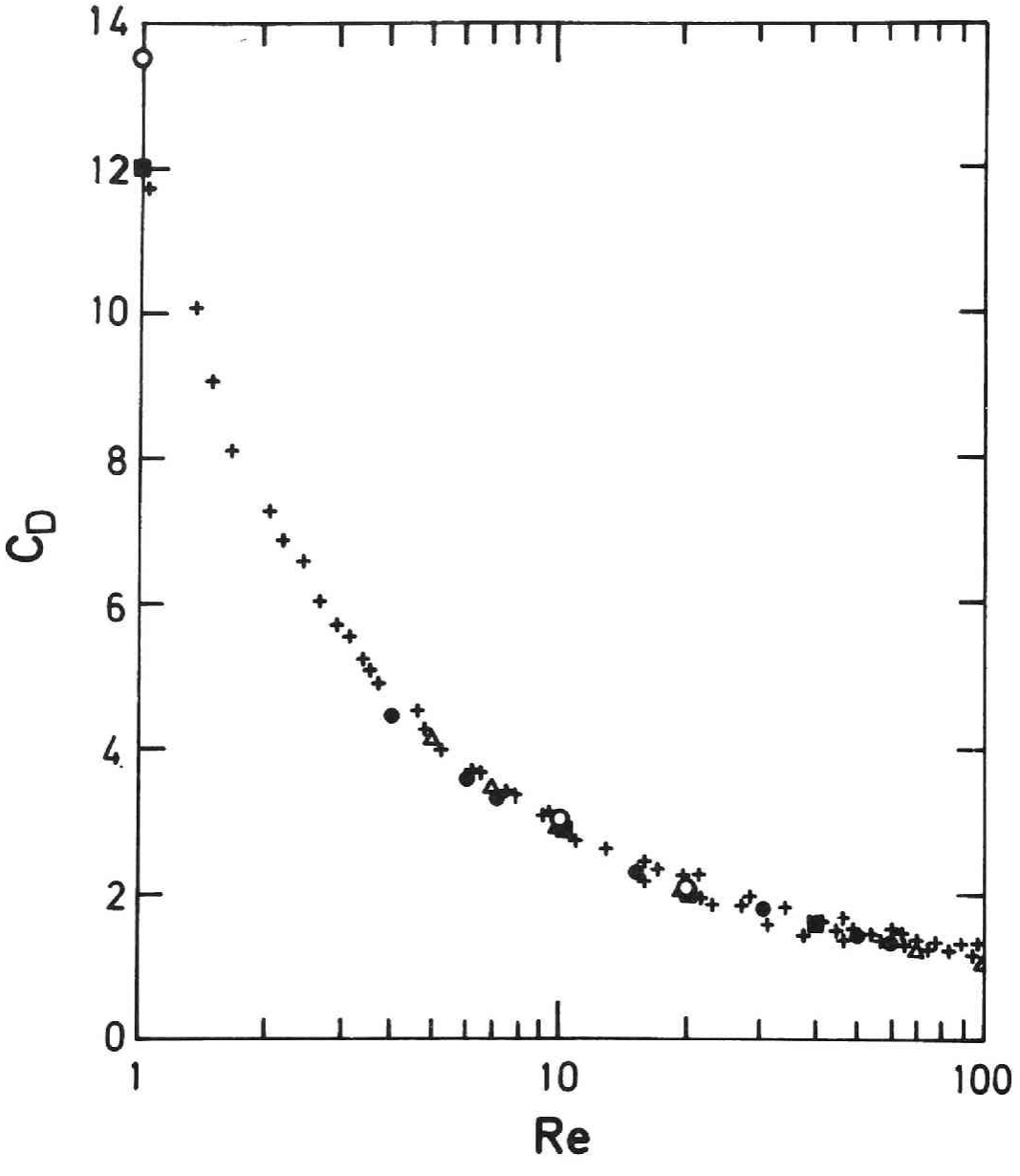

Fig. 5-3 Calculated and experimental values for drag coefficient.

Numerical solutions : ○, this work; △, Dennis-Chang (13)
●, Takami-Keller (56); ■, Yoshioka -Adachi (68)

Experimental measurement : +, Tritton (59)

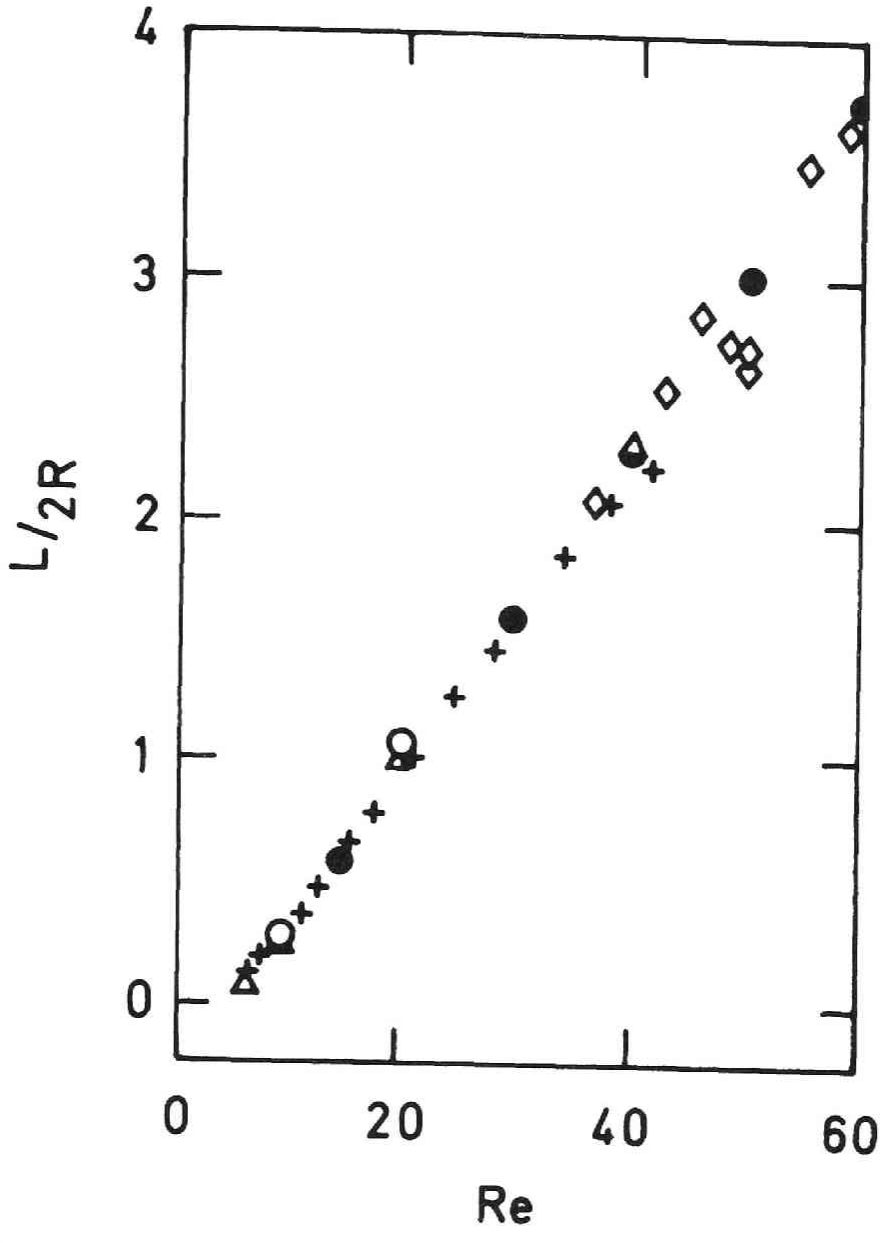

Fig. 5-4 Calculated and experimental values for wake length.

Numerical solutions : ○, this work
△, Dennis-Chang (13)
●, Takami-Keller (56)

Experimental measurement : +, Taneda (57)
◇, Acrivos et al. (2)

stagnation point (see Fig. 5-5-d,e). the appearance of stagnant region of this type has not been reported in any previous paper. But the observations by James et al. (28) and Ultman et al. (61) suggest the possibility of the existence of such a stagnant region in high Weissenberg number range. When the Reynolds number is equal to 10 and 20, the viscoelasticity causes a significant change in the wake of a cylinder even at small Weissenberg number range. In this case the expansion effect is same as mensioned above. At the back of a cylinder, the wake is suppressed because of the contraction effect and the separating point moves backward (see Fig. 5-6-b and Fig. 5-7-b,c), and finally the wake disappears (see Fig. 5-6-c ,d and Fig. 5-7-d,e). When Weissenberg number becomes large, the stream line of outer region (ψ = 0.2) is expanded even at the back of a cylinder because of the large expansion in front of a cylinder, but very near the cylinder (ψ = 0.005) the stream line is still contracted (see Fig. 5-6-d and Fig. 5-7-e). But when the product of Weissenberg and Reynolds numbers becomes larger than about unity, the wake appears again both in the cases of Re = 10 and 20. Once the wake reappears, the wake length becomes rapidly larger because of the expansion of outer region. So the outer boundary of numerical solution must be taken very large enough to satisfy the boundary

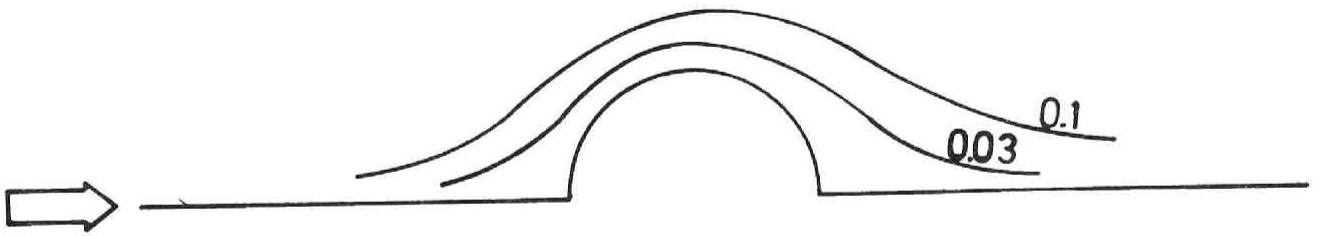

Fig. 5-5-a Streamlines at Re=1.0 , We=0.0
(Newtonian fluid)

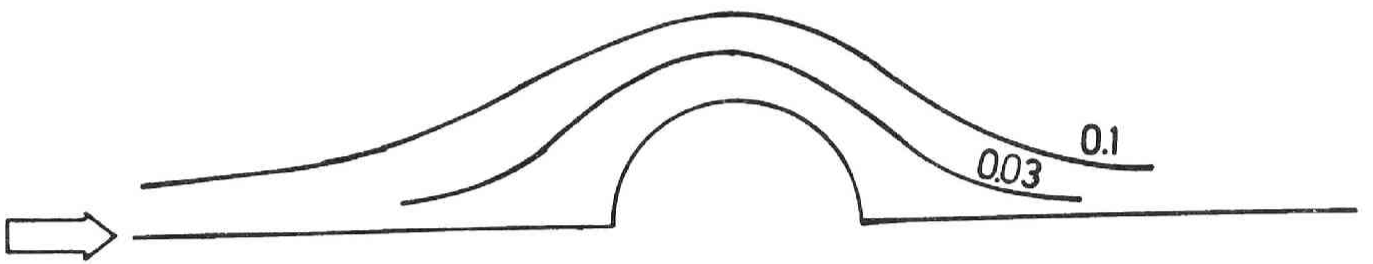

Fig. 5-5-b Streamlines at Re=1.0 , We=0.1

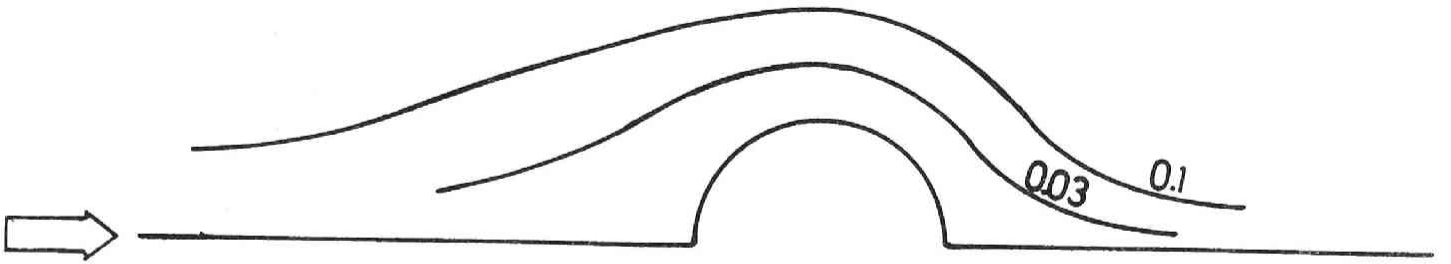

Fig. 5-5-c Streamlines at Re=1.0 , We=0.15

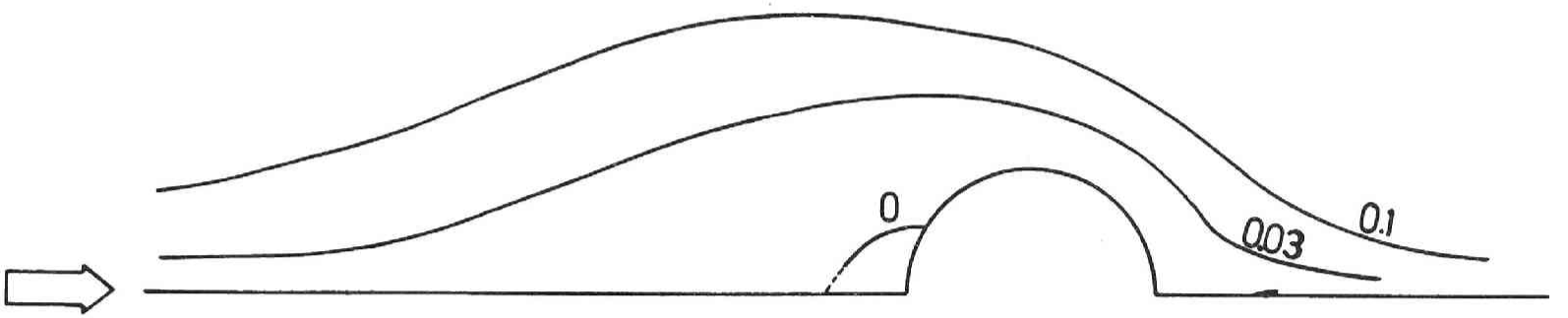

Fig. 5-5-d Streamlines at Re=1.0 , We=0.2

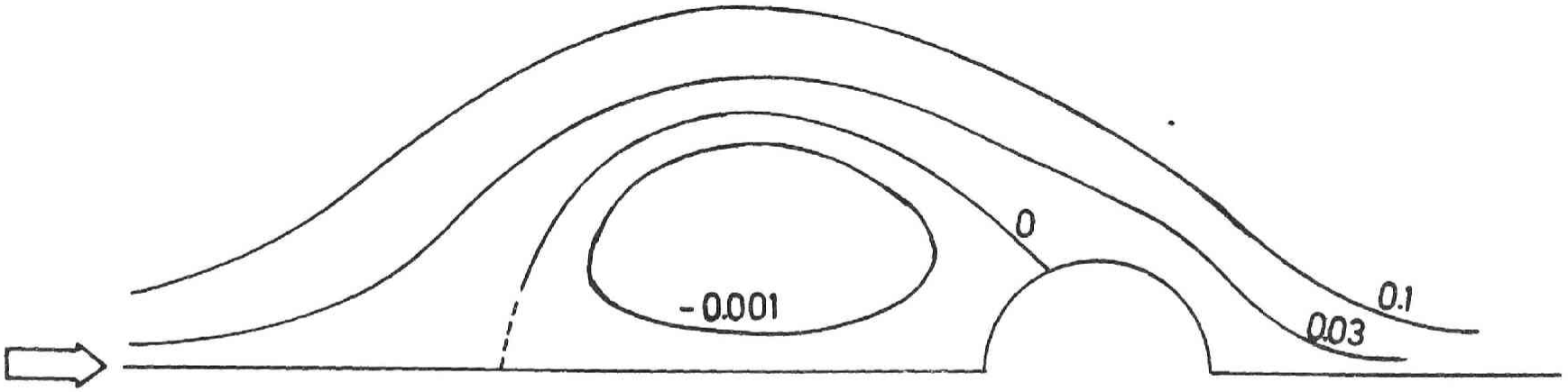

Fig. 5-5-e Streamlines at Re=1.0 , We=0.25

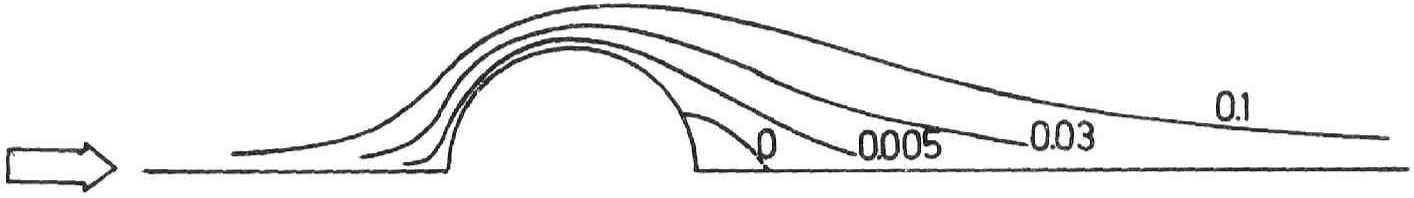

Fig. 5-6-a Streamlines at Re=10.0 , We=0.0
(Newtonian fluid)

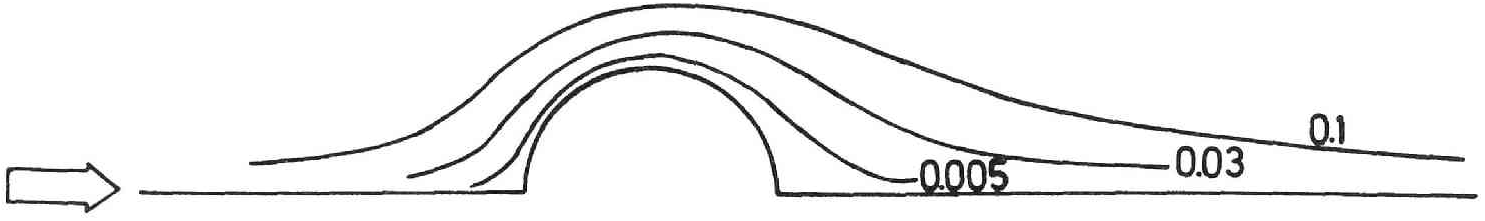

Fig. 5-6-b Streamlines at Re=10.0 , We=0.03

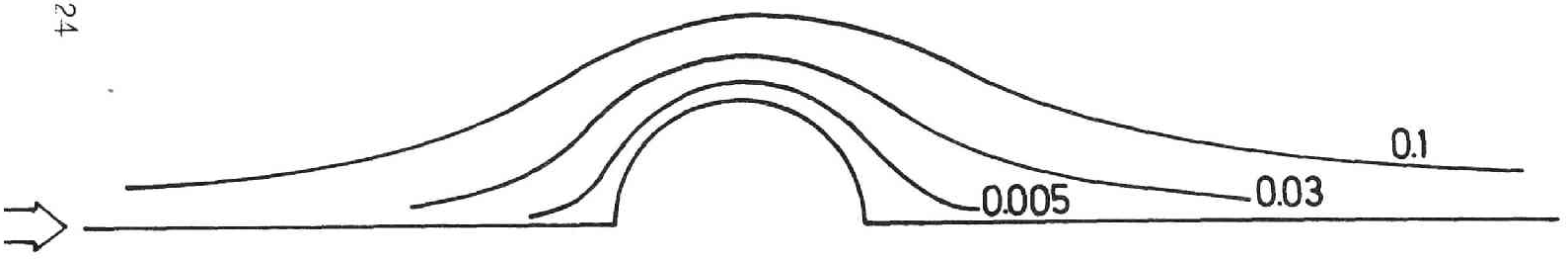

Fig. 5-6-c Streamlines at Re=10.0 , We=0.05

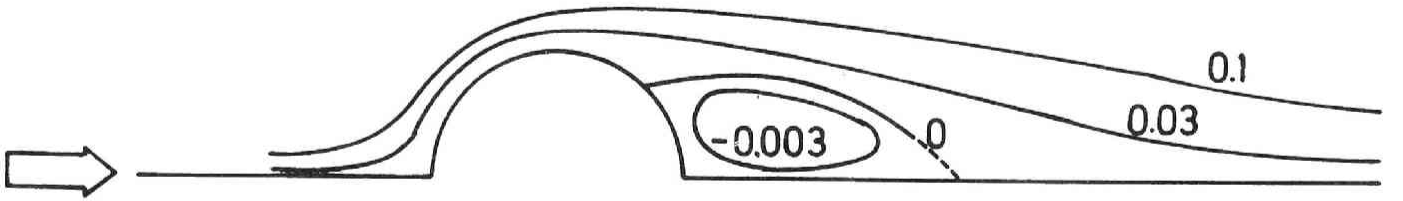

Fig. 5-7-a Streamlines at Re=20.0 , We=0.0
(Newtonian fluid)

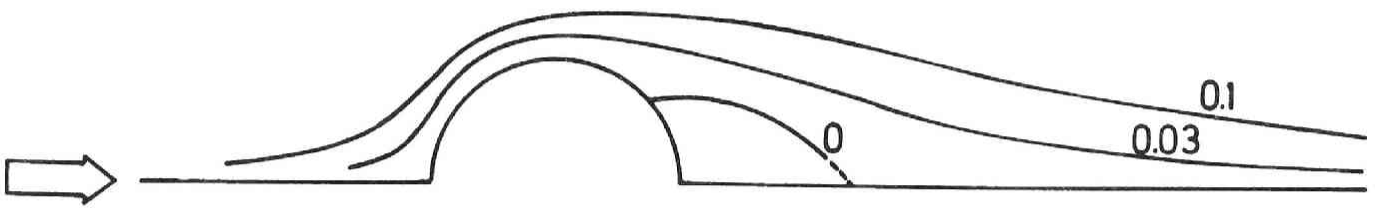

Fig. 5-7-b Streamlines at Re=20.0 , We=0.01

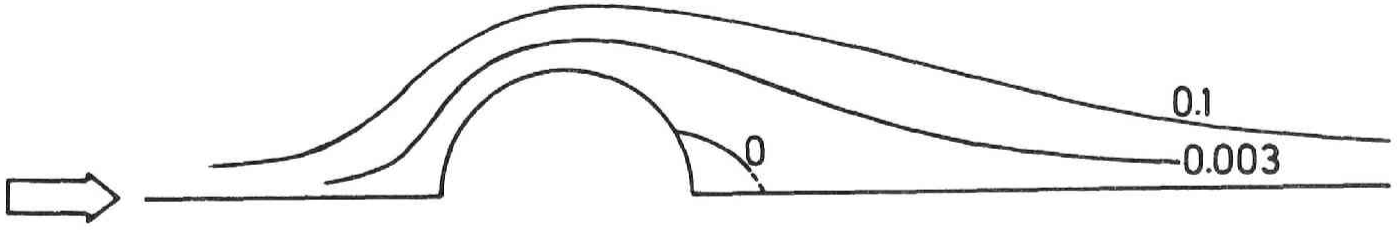

Fig. 5-7-c Streamlines at Re=20.0 , We=0.03

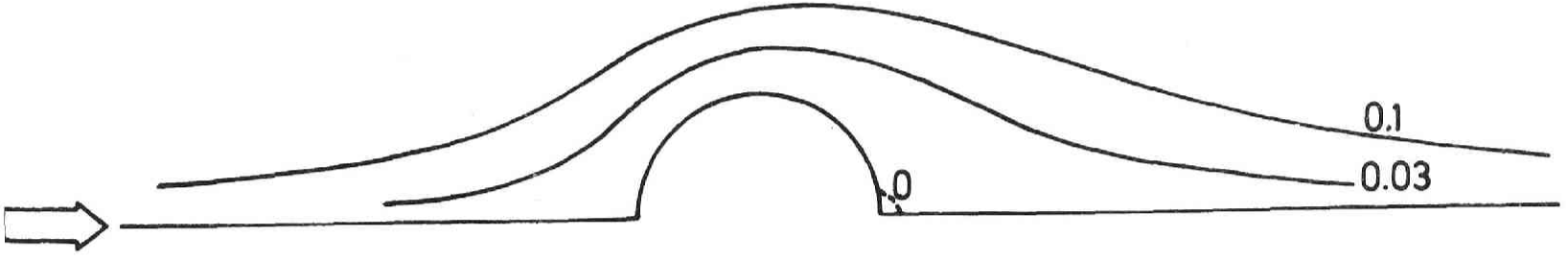

Fig. 5-7-d Streamlines at Re=20.0 , We=0.05

condition of Eq.(5-18). It spent so much time to take the outer boundary large enough that the calculation of large Weissenberg number range was impossible in this study. But some numerical calculations of larger Weissenberg number range before convergence suggested that the stagnant region appeared around a cylinder. Summarizing the results mentioned above, we may represent the change of flow patterns in viscoelastic fluid flow around a circular cylinder as those shown in Fig. 5-8. The appearance of discontinuous layer like a standing shock wave in supersonic flow was suggested by Ultman and Denn (60) in their analysis, and the results of this study shown in Fig. 5-8-e also suggest that the discontinuous layer may appear at high Weissenberg number range.

The availability of the assumption concerning the time derivative of Maxwell model, i.e. Eq.(5-5), may be most important in this calculation. Another assumption is possible for the region appart from a cylinder. In front and back of a cylinder, such assumption may be described by,

$$\frac{\delta}{\delta t} = U\frac{\partial}{\partial r} \tag{5-35}$$

The result of calculation based on this assumption is shown in Fig. 5-9 for the case of Re = 1.0 and We = 1.0. This diagram shows that the difference of assumption of

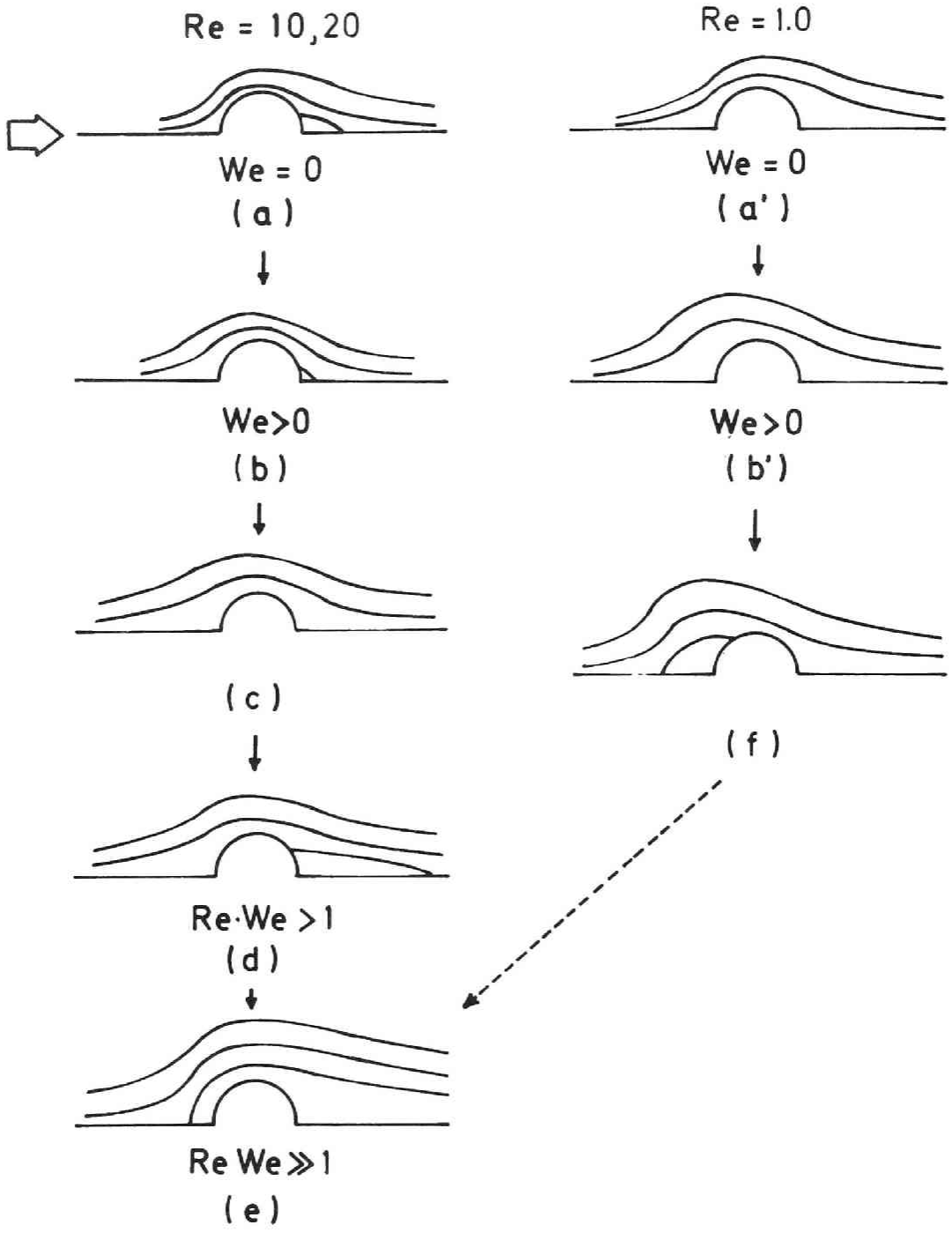

Fig. 5-8 Schematic representation of the flow patterns in viscoelastic fluid flow.

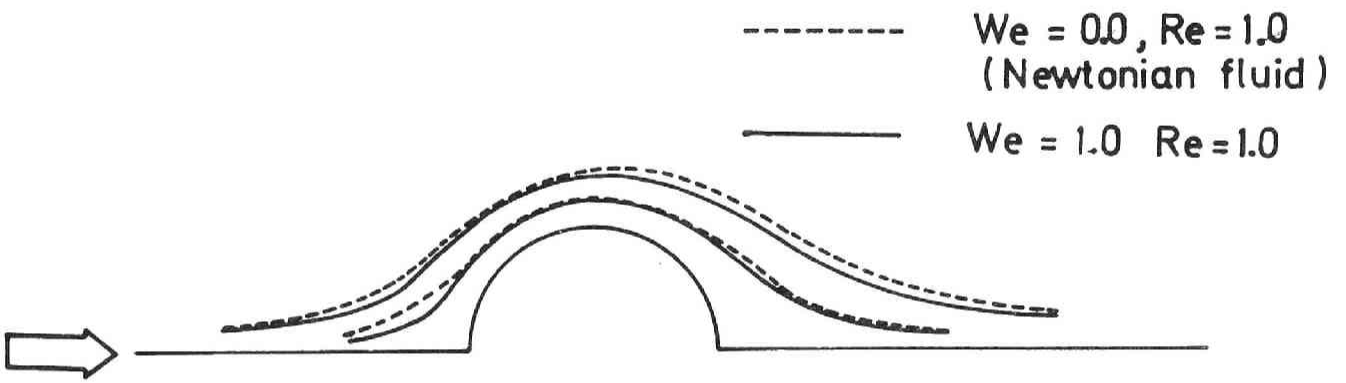

Fig. 5-9 Streamlines based on the assumption such as ; $\frac{\delta}{\delta t} = U\frac{\partial}{\partial r}$

Eq.(5-35) is not significant, and flow pattern is almost equal to those of Newtonian fluid flow. In the actual flow condition the time derivative of Maxwell model will be given by the combination of Eqs.(5-5) and (5-35). And near the cylinder surface the assumption of Eq.(5-5) is more important than the assumption of Eq.(5-35). Thus the calculation of this study may be correct qualitatively over the all flow region.

The distribution of wall shear stress is shown in Fig. 5-10-a,b,c. As the result of expanding effect of viscoelasticity, the wall shear stress becomes smaller than that of Newtonian fluid according to the increase of Weissenberg number. The appearance of a front stagnant refion is clearly observed in the case of We = 0.25 in Fig. 5-10-a. In Fig. 5-10-b,c it is shown that the separating point moves backward when Weissenberg number becomes larger.

Finally the distribution of local Nusselt number calculated by Eq.(5-31) is shown in Fig. 5-11-a,b,c. The heat transfer reduction is significant at the front part of a cylinder. The averaged Nusselt number calculated from these distributions of local Nusselt number are listed in Table 5-1. The reduction rate of heat transfer reached 40% of Newtonian fluid when Weissenberg number was 0.25 at Re = 1.0 . These results of numerical

calculation given in this section will be compared with the experimental results of this study and previous works in later sections.

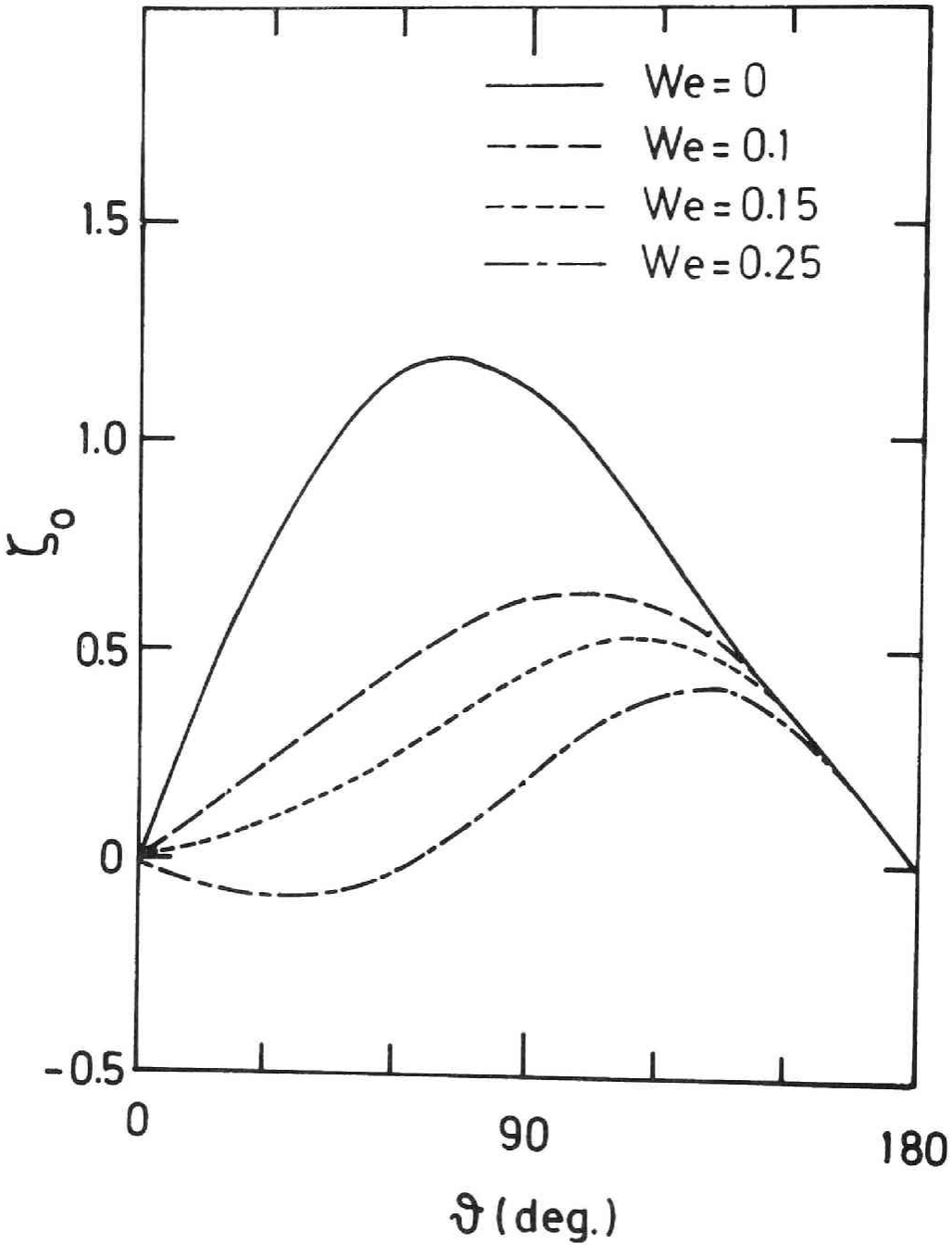

Fig. 5-10-a Distribution of surface vorticity at Re = 1.0 .

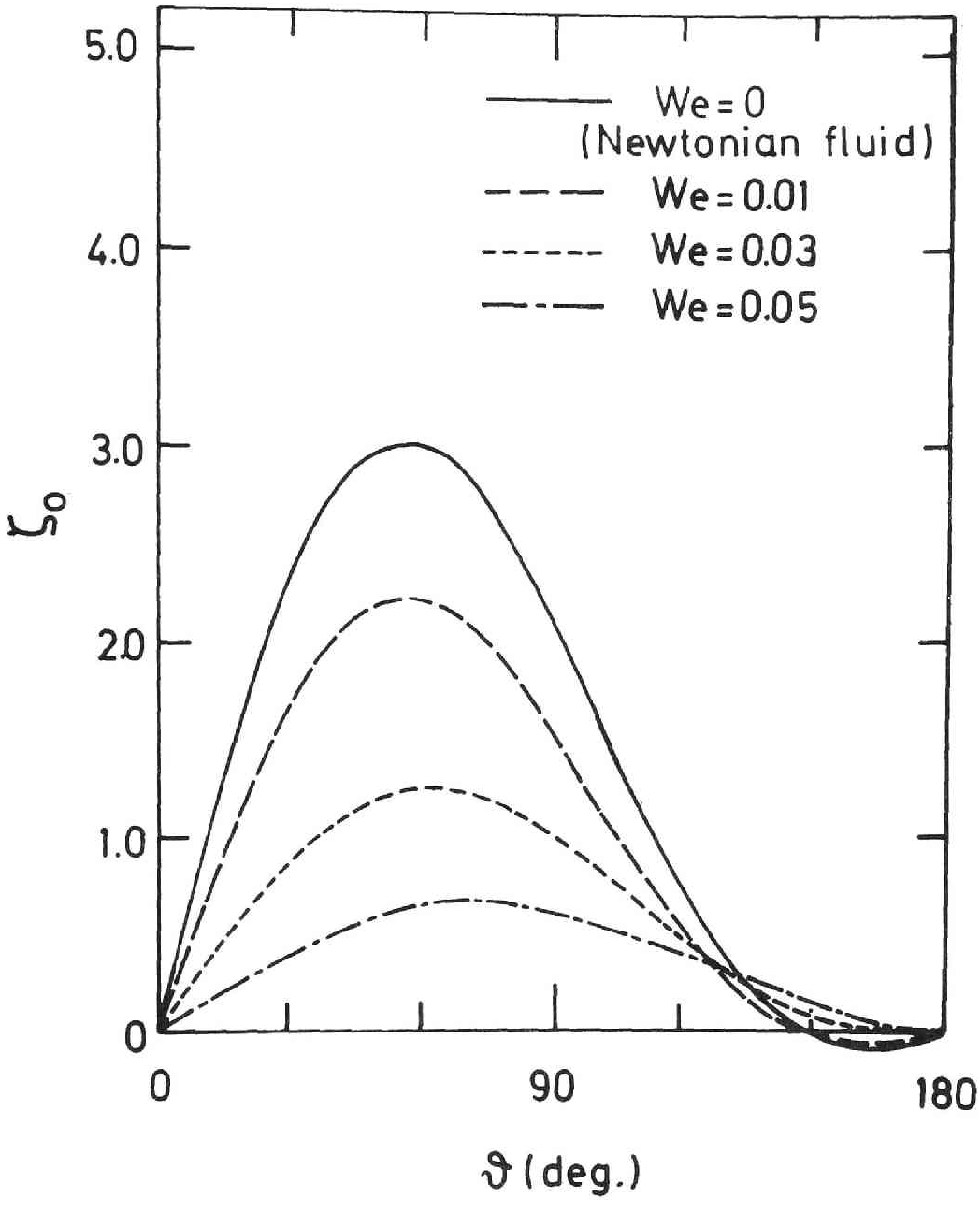

Fig. 5-10-b Distribution of surface vorticity at Re = 10 .

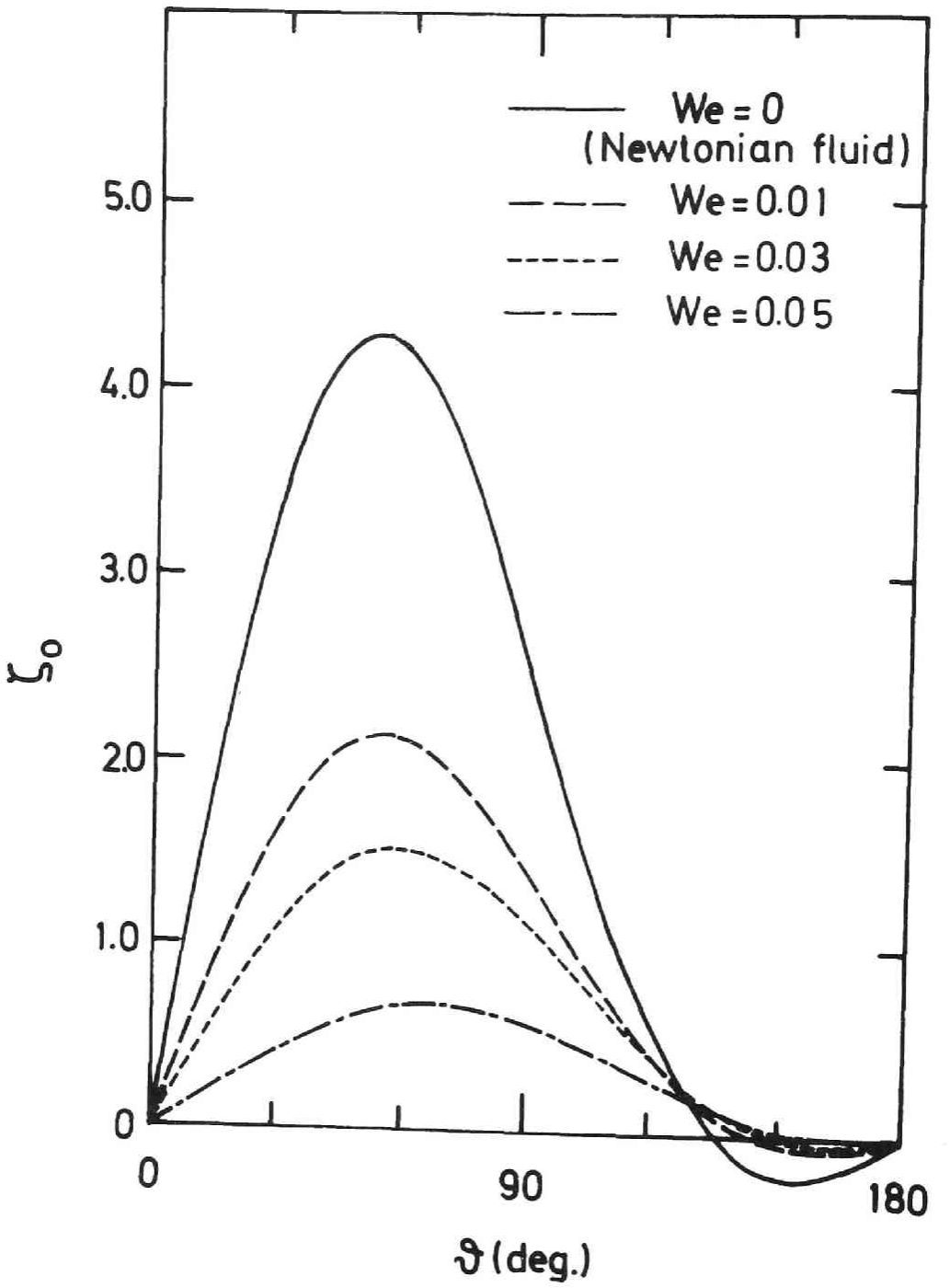

Fig. 5-10-c Distribution of surface vorticity at Re = 20 .

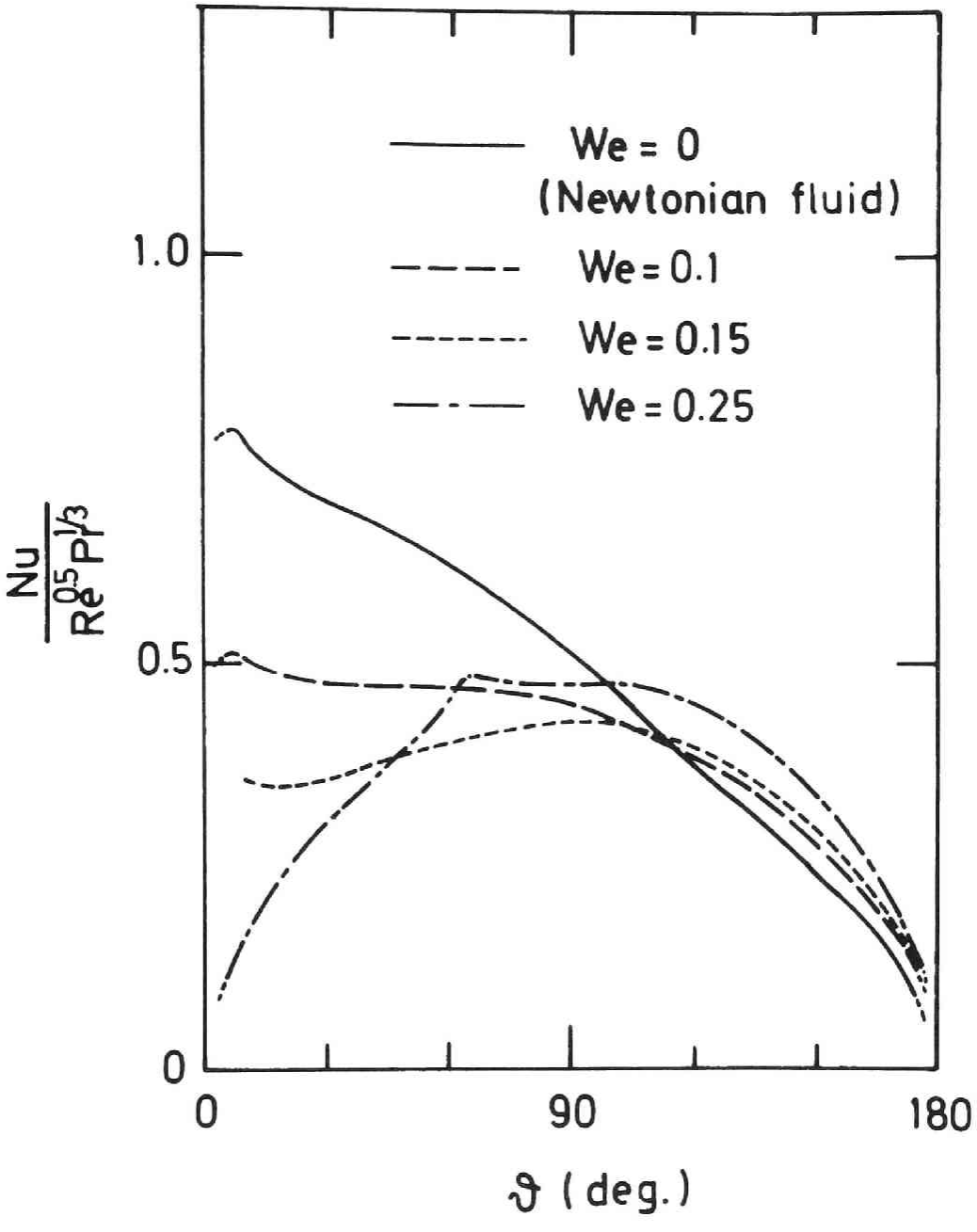

Fig. 5-11-a Distribution of local Nusselt number at Re = 1.0 .

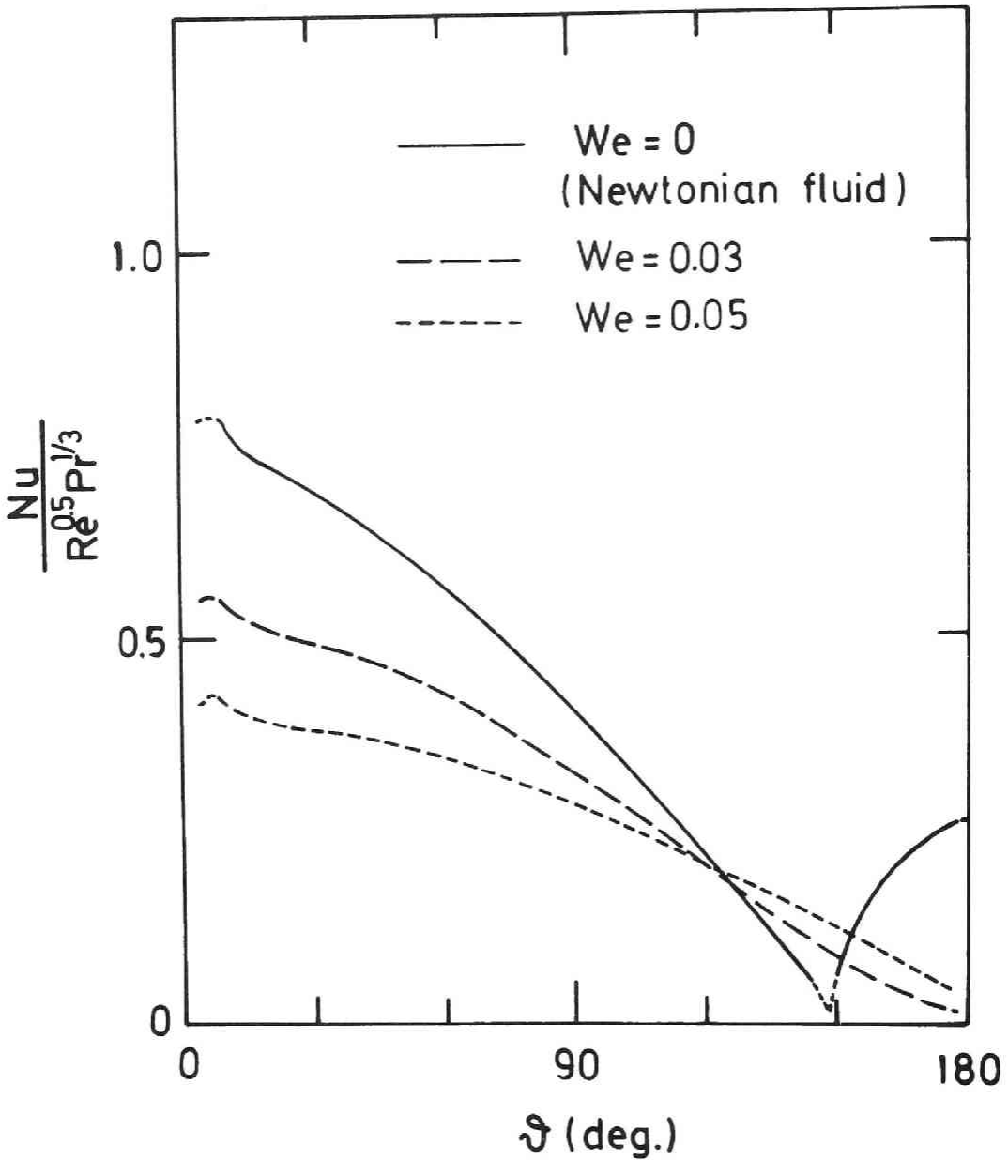

Fig. 5-11-b Distribution of local Nusselt number at Re = 10 .

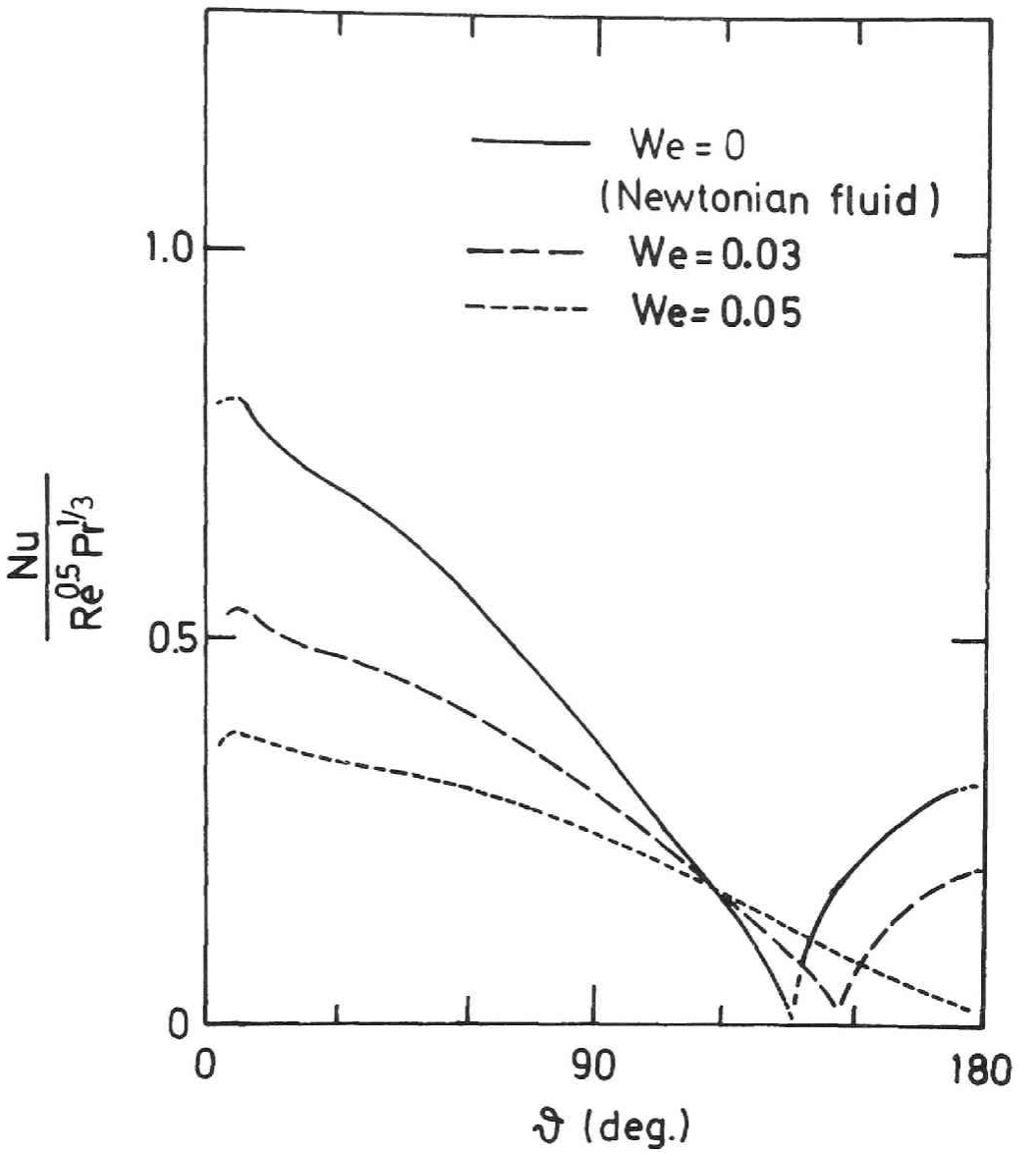

Fig. 5-11-c Distribution of local Nusselt number at Re = 20 .

Table 5-4

Calculated values of heat transfer reduction for various Weissenberg numbers.

Re	We	$Nu_{av.}/Pr^{1/3}$	Nu/Nu_o
1.0	0.0	0.4827	—
	0.1	0.3952	0.8187
	0.15	0.3511	0.7275
	0.25	0.3399	0.7042
10.0	0.0	1.3437	—
	0.01	1.2202	0.9081
	0.03	0.9743	0.7251
	0.05	0.8416	0.6263
20.0	0.0	1.9125	—
	0.01	1.7352	0.9073
	0.02	1.5090	0.7890
	0.03	1.3604	0.7113
	0.05	1.0086	0.5274

5-4 Experimental apparatus and procedure.

The results obtained by previous investigators (28), (52) were restricted only to heat transfer of viscoelastic fluids. They used the hot wire type probe, so the diameter of cylinder was not changed in a wide range. Thus the electrochemical method was employed in this study . The diameter of cylinder was easily changed, so the Reynolds number and Weissenberg number were varied in a wide range.

The whole experimental set-up is shown in Fig. 5-12. The variable motor was used to control the speed of the moving arm. The cylindrical platinum cathode probe was designed as shown in Fig. 5-13. Four sizes of platinum wire of nominal diameter of 800, 300, 100 and 50 μ were used. The probe was attached to the tip of the moving arm and submerged in the test fluids in a circular tank. The nickel plate strip curved around the tank was used as the anode. The electrochemical method summarized by Mizushina (38) was used for the measurement of over all Sherwood number of a circular cylinder. The redox system of ferro-ferri cianide was used in this study. The electrolitic polymer solution was prepared with 0.005N $K_3Fe(CN)_6$, 0.005N $K_4Fe(CN)_6$ in 0.5N NaOH. The polymer

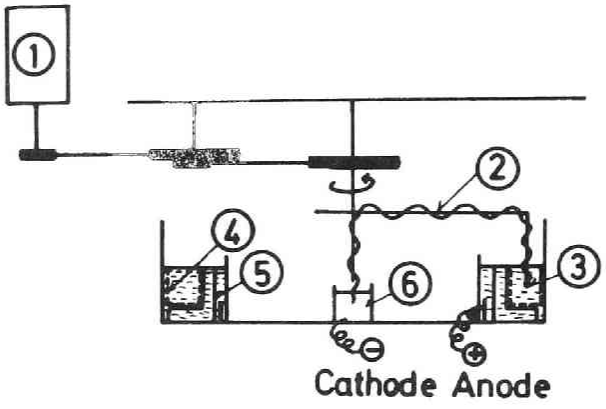

1 Variable speed moter
2 Moving arm
3 Probe
4 Stainless net
5 Buffle
6 Mercury contact point

Fig. 5-12 Experimental apparatus.

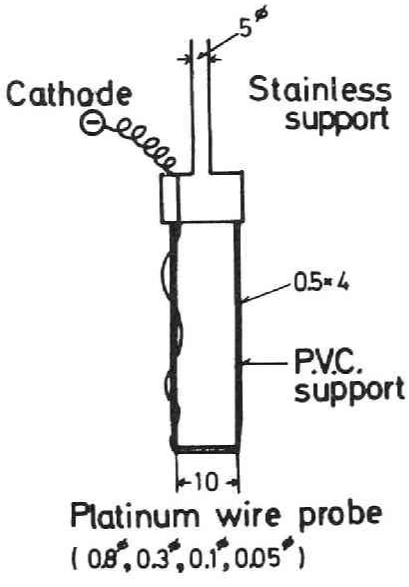

Fig. 5-13 Cathode design.

species used in this study was P.E.O. and its concentration varied from 0 to 100 ppm. The mechanical degradation of polymer was negligible in this experimental apparatus. But the chemical degradation reduced the molecular weight of polymer to some extent. So the intrinsic viscosity in electrolyte was measured, and the molecular weight of P.E.O. was calculated by Eq.(2-22). The relaxation time of polymer solutions was also calculated by Eq.(2-24). The results of measurement were , $[\eta]$ = 10.1 (dl/g) and M = 2.51×10^6. The molecular weight of the same polymer species in water was 3.50×10^6. Thus the degradation of polymer was considerable. The diffusivity was assumed to be equal to the Newtonian case because of the diluteness of polymer solutions.

5-5 Experimental results and discussions.

The experimental results of Sherwood number are shown in Fig. 5-14. The measurements of Newtonian fluid obtained with cylinders of 800 and 300 μ dia. coincided with the results of previous investigators. The correlation given by Mcadams (34) is,

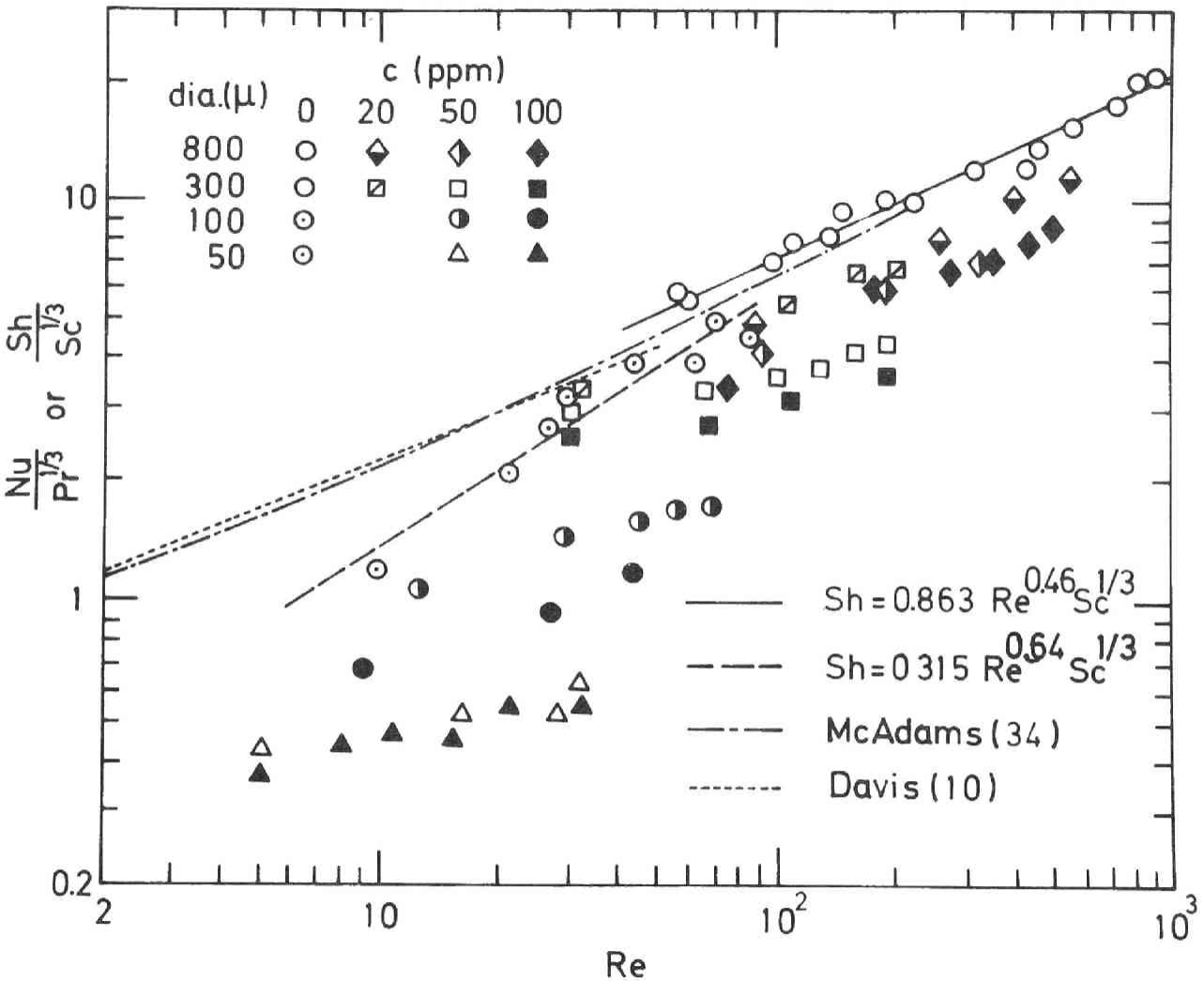

Fig. 5-14 Experimental results of mass transfer from a circular cylinder in cross flow.

$$Nu = (0.35 + 0.56\ Re^{0.52})\ Pr^{0.3} \qquad (5\text{-}36)$$

and experimental results of Davis (10) is given by,

$$Nu = 0.91\ Re^{0.345}\ Pr^{0.31} \qquad (5\text{-}37)$$

The results of this experiments obtained by the 100 and 50 μ dia. probes were slightly lower than the previous results. In case of 100 and 50 μ dia. probes, the mechanical strength of wires were so weak that it was impossible to polish the surface of the cylinders. The fall down of surface activity of platinum wire seems to be the reason of this deviation. Thus the following two correlations which were contributed to 800 and 300 μ dia. probes, and 100 and 50 μ dia. probes, were obtained. For 800 and 300 μ dia. probes, the correlation was given as;

$$Sh = 0.863\ Re^{0.46}\ Sc^{1/3} \qquad (5\text{-}38)$$

, and for 100 and 50 μ dia. probes, the correlation was given as;

$$Sh = 0.315\ Re^{0.64}\ Sc^{1/3} \qquad (5\text{-}39)$$

Next, the reduction of Sherwood number in the polymer solutions will be compared with these Newtonian correlations. The experimental results show that the mass transfer rate of polymer solutions is reduced in the whole

range of this experiments. Moreover the experimental results are clearly devided into two types. In the range of $Re < 60$, Sherwood number is nearly constant, and in the range of $Re > 60$, Sherwood number begins to increase again with the increase of Reynolds number. The dependency of Sherwood number on Reynolds number in the second region was determined from this diagram to be same as Newtonian fluid.

The ratio of Sherwood number of viscoelastic fluid, Sh, to the value of Newtonian fluid, Sh_0, is compared in Fig. 5-15 with the calculated value which was given in previous section. Weissenberg number varies along the equi-concentration line, so the extrapolated values or interpolated values should be taken for the comparison. From this diagram the present analysis based on Maxwell model is shown to be able to explain the heat transfer reduction of viscoelastic fluid in cross flow nearly quantitatively at $Re = 10 \sim 20$.

Ultman and Denn (60) introduced in their analysis the propagation velocity of a shear wave given by,

$$a = \sqrt{\upsilon/\lambda} \qquad (5\text{-}40)$$

And they discussed about the flow patterns of viscoelastic fluids employing the critical Reynolds number at the shear wave velocity, i.e.

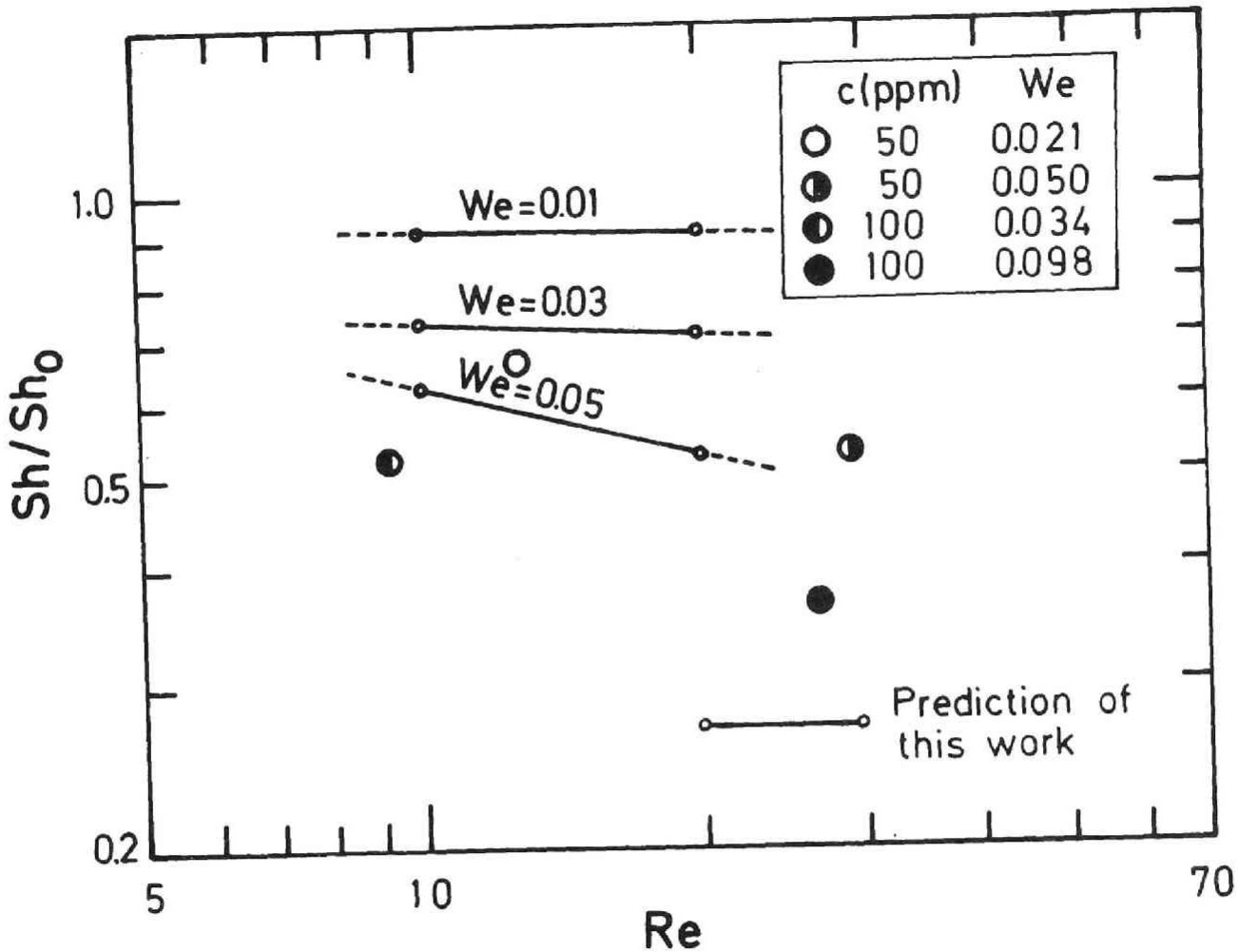

Fig. 5-15 Comparison of mass transfer reduction with calculated values.

$$Re_c = 2R / \sqrt{\lambda \nu} \qquad (5\text{-}41)$$

They showed from the analysis at the front stagnation point that the Nusselt number of viscoelastic fluid in supercritical flow region, i.e. Re · We > 1.0, was given by,

$$Nu = (2\ Pr/\pi)^{1/2}\ Re_c \qquad (5\text{-}42)$$

But this equation failed to explain the results obtained by James et al. (28). The correlation of the experimental results of James et al. is ;

$$Nu = 0.40\ Re_c^{0.34}\ Pr^{1/3} \qquad (5\text{-}43)$$

The calculated values of Nusselt number shown in Table 5-4 are correlated with the critical Reynolds number defined by Eq.(5-41) as;

$$Nu = 0.215\ Re_c^{0.52}\ Pr^{1/3} \qquad (5\text{-}44)$$

The scatter of the calculated values shown in Fig. 5-16 seems to be caused by the change of flow patterns shown in Figs. 5-5, 5-6 and 5-7. The above expression of this study corresponds to the subcritical region, i.e. Re · We < 1.0. Thus the expression may be impossible to apply to the case of supercritical region. But the comparison of this equation with experimental results shows that

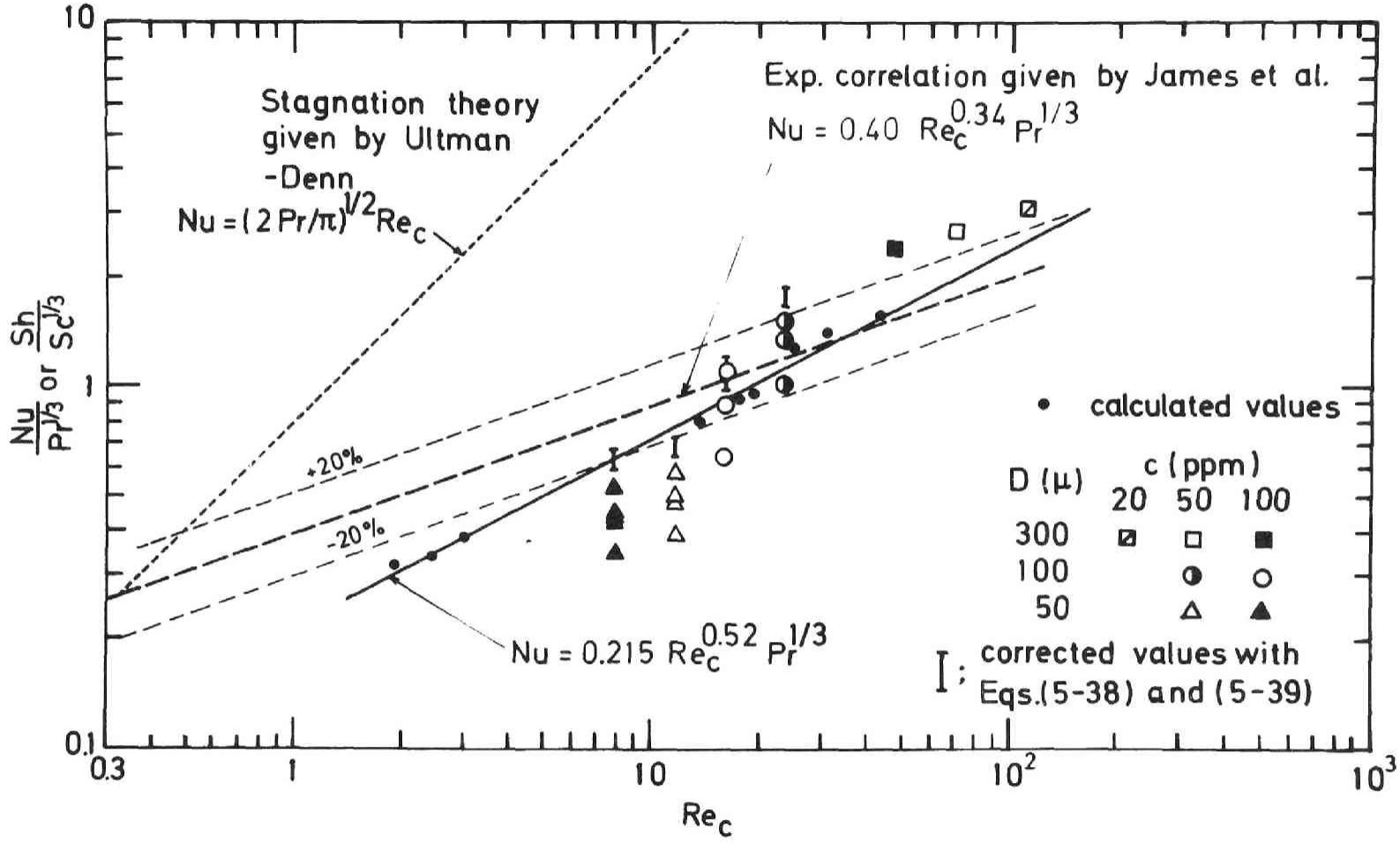

Fig. 5-16 Correlation of Nusselt number of viscoelastic fluids by critical Reynolds number.

this expression is applicable to almost all the data in the both regions, i.e. supercritical and subcritical regions. This comparison shown in Fig. 5-16 shows a good accordance between the prediction of Eq.(5-44) with experimental results of this study and of James et al. Thus it may be concluded that the heat transfer reduction of viscoelastic fluid in cross flow at $1 < Re < 60$ can be estimated by Eq.(5-44).

In the case of $Re > 60$, the problem of the heat transfer reduction may be somewhat different because of the appearence of vortex street. The correlation of the experimental results in the range of $60 < Re < 600$ was obtained as;

$$Sh = 0.096\ Re^{0.46}\ Sc^{1/3}\ Re_c^{0.34} \qquad (5\text{-}45)$$

, and is shown in Fig. 5-17 with experimental results. In this case, the reduction rate of heat transfer can be expressed by $Re_c^{0.34}$. It is interesting that the power indexes of Re_c in both Eqs.(5-43) and (5-45) are equal. But it is not clear why the dependency of Nu on Re_c is same in both cases.

The nondimensional parameter Re_c^2 is same as Re/We, so this nondimensional parameter is interpretted as the ratio of inertial force to elastic force. Thus in the region, in which representative length scale is very

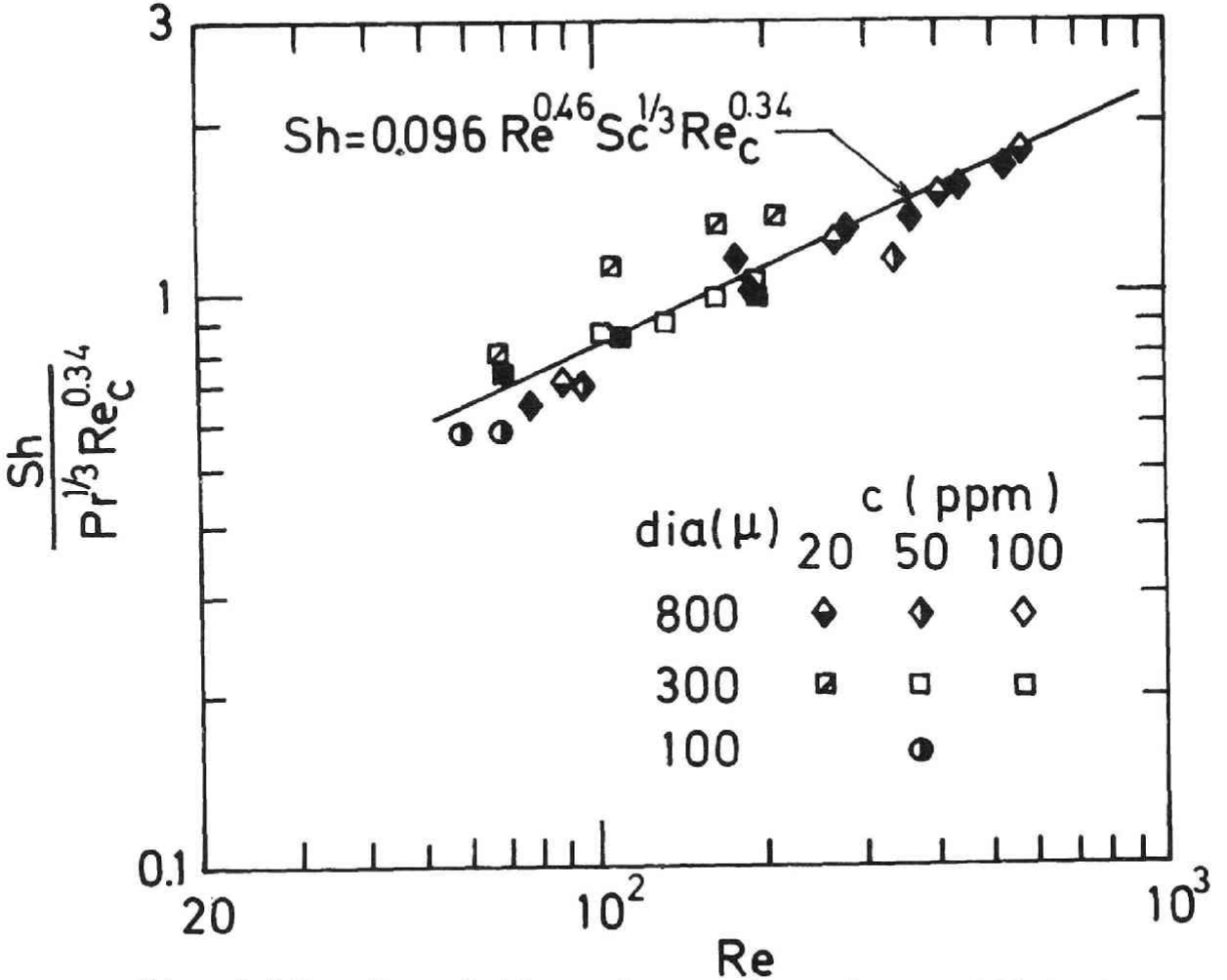

Fig. 5-17 Correlation of mass transfer coefficient for the region of $60 < Re < 600$.

small compared with elastic parameter, the parameter (Re/We) seems to be preferable to the usual nondimensional parameter, i.e. Weissenberg number which is the ratio of elastic force to viscous force.

If one make use of hot wire anemometry in viscoelastic fluids, the range of Reynolds number based on the diameter of hot wire must exceed the value, 60. Then the averaged velocity will be measurable if the appropriate caliblation is available. The condition that Reynolds number must be larger than 60 will make the diameter of hot wire probe larger, so the accuracy of measurements will be decreased. The measurement of fluctuating velocity may bring a more complicated problem which was not dealt with in this study. This problem must be connected with the dynamic behavior of viscoelastic fluids and will become an important problem in future study of viscoelastic fluids.

5-6 Concluding remarks.

Numerical solution of Navier-Stokes equation with generalized Maxwell model was obtained for the case of Re = 1, 10, 20 and We = 0 ~ 0.25. The results of calculation showed that the elasticity expanded the stream lines in front of a cylinder and contracted them at the back of a cylinder. So the separating point was forced to move backward in case of Re = 10 and 20. It was also found that the elasticity reduced the drag coefficient and averaged Nusselt number.

The measurements of over all Sherwood number around a circular cylinder was carried out by means of electrochemical method. Drastic reductions in mass transfer rate were observed. The rate of mass transfer reduction at Re = 10 ~ 20 was explained by the results of numerical calculation.

The results of calculation gave the relationship between Nusselt number and critical Reynolds number as;

$$Nu = 0.215\ Re_c^{0.52}\ Pr^{1/3}$$

This equation gave a good prediction for the case of $1 < Re < 60$. The experimental results of $60 < Re < 600$ were correlated as;

$$Sh = 0.096\ Re^{0.46}\ Sc^{1/3}\ Re_c^{0.34}$$

The conditions for the application of hot wire anemometry to viscoelastic fluids were discussed and some remarks were obtained.

CHAPTER 6

CONCLUSIONS AND RECOMMENDATIONS FOR FURTHER WORKS.

6-1 Conclusions.

(1) Tracsport phenomena of viscoelastic fluids in turbulent pipe flow.

Eddy diffusivities of momentum and heat for viscoelastic fluids were obtained from the damping factor model as ;

$$\frac{\varepsilon_M}{\nu} = f_n(y^+ , R^+)^2 \{1 - \exp(\frac{-y^+}{26}\sqrt{-\alpha + \sqrt{\alpha^2 + 1}})\}^2 \frac{du^+}{dy^+}$$

$$\frac{\varepsilon_H}{\nu} = 1.5\, f_n(y^+, R^+)^2 [\{1 - \exp(\frac{-y^+}{42 + \frac{120}{\sqrt{Pr}}})\} / \{1 - \exp(\frac{-y^+}{26})\}] \times \{1 - \exp(\frac{-y^+}{26}\sqrt{-\alpha + \sqrt{\alpha^2 + 1}})\}^2 \frac{du^+}{dy^+}$$

where

$$\alpha = \frac{2\lambda_t}{\nu} (\frac{u^*}{26})^2$$

The turbulent relaxation time was defined and determined

from the experimental results of pressure drop measurements for unsaturated region of drag reduction as ;

$$\frac{\lambda_t}{\lambda_\ell} = 3.76 \times 10^{8}\ We^{1.34}$$

, and for maximum reduction region we obtained,

$$\alpha = 60 \quad .$$

The validity of this damping factor model was checked by means of the several experiments in this study. Velocity profiles were measured by pitot tube method in unsaturated reduction region, and by Laser Doppler anemometry at maximum reduction asymptote. Temperature distribution and Nusselt number in the fully developed region were measured by thermo-couples both in unsaturated and maximum reduction region.

From the results obtained by the experiments, the availability of the damping factor model for viscoelastic fluids was ascertained. It was found that this model was able to express the effects of various sources on drag reduction, such as concentration, molecular weight, pipe diameter and saturation effects. Moreover the reduction of heat transfer rate was explained by this model. The damping effect caused by the elasticity of polymer solu-

tion was interpletted as the reason of Toms phenomenon.

(2) Transport phenomena of viscoelastic fluids in cross flow around a circular cylinder.

Numerical solution of Navier-Stokes equation with generalized Maxwell model was obtained. The results of calculation showed that the elasticity caused a significant change of the flow pattern in cross flow around a cylinder. Main effects of elasticity were the expansion effect in front of a cylinder and the contraction effect at the back of a cylinder. As the result of these effects, the drag coefficient and Nusselt number were reduced and the separating point was forced to move backward. The results of numerical calculation gave a relation between Nusselt number and critical Reynolds number as ;

$$Nu = 0.215\ Re_c^{0.52}\ Pr^{1/3}$$

The measurement of overall Sherwood number around a circular cylinder was carried out by means of electrochemical method. The experimental results of mass transfer reduction at low Reynolds number coincided with prediction given by numerical solution. The experimental results at middle Reynolds number region were correlated

as ;

$$Sh = 0.096\ Re^{0.46}\ Sc^{1/3}\ Re_c^{0.34} \qquad \text{at} \quad 60 < Re < 600$$

It was found that the reduction rate of heat and mass transfer was evaluated by the nondimensional parameter ; Re_c $(=(Re/We)^{1/2})$, which was the ratio of inertia force to elastic force.

6-2 Recommendation for further works.

(1) It seems to be important for the understanding of the turbulent pipe flow of viscoelastic fluid to make clear the physical meaning of turbulent relaxation time defined in this study. For this purpose the observation of the mechanism of turbulent shear flow at the wall region will be most important. Recently the visual technique has been applied to the turbulent shear flow of Newtonian fluid by many investigators. The extension of these investigations to the viscoelastic fluid flow is recommended. The estimation of representative shear rate of turbulent eddy, which may be the combined shear of simple and elongational shear, will be the key for under-

standing the turbulent shear flow of viscoelastic fluids.

(2) The viscoelastic fluid flow around a circular cylinder showed a typical effect of elasticity in external flow . The solution of this study is only the approximate solution with Maxwell model. More detailed study with other precise models is recommended, and the accumulation of more experimental results in viscoelastic fluid flow is expected. It was pointed out that the effect of elasticity could not be described only by Weissenberg number, but the nondimensional parameter Re_c was suitable for the case of cross flow around a cylinder. The effect of elasticity seems to appear strongly in the external flow to a body of a very small representative length scale. Therefore, the precise measurements of viscoelastic fluid flow around a body of very small length scale is recommended for revealing the effect of elasticity.

NOMENCLATURE

A^+ : constant defined by Eq.(2-11)

a : latice spacing in the radial direction

a_o, a_1 : constants defined by Eq.(3-4)

$B_{(1)}^{ij}$: first Rivlin-Ericksen acceleration tensor

$B_{(2)}^{ij}$: second Rivlin-Ericksen acceleration tensor

b : latice spacing in the angular direction

C : velocity of light, cm/sec

C_D : drag coefficient

C_f : frictional coefficient

C_p : pressure coefficient

C_o : constant defined by Eq.(3-15)

c : concentration, ppm or g/cm^3

c_p : heat capacity, cal/g ^oC

D : pipe diameter, cm

DF : damping factor

f : Fanning friction factor

G(s) : transfer function

g^{ij} : conjugate metric tensor

H : half height of rectangular channel, cm

j_H : Chilton-Colburn's j-factor for heat transfer

K : parameter in Ostwald-de Waele model, $g \cdot sec^{n-2}/cm$

k : thermal conductivity, $cal/cm \cdot sec \cdot {}^oC$

k_i : unit direction vector of incident beam

k_s : unit direction vector of scattered beam

L : wake length, cm

ℓ : mixing length, cm

M : molecular weight of polymer, g/g-mole

Nu : Nusselt number

n : power index of Ostwald-de Waele model

n_r : refraction index

Pr : Prandtl number

p : pressure, $g/cm \cdot sec^2$

p' : fluctuating pressure, $g/cm \cdot sec^2$

q_w : wall heat flux, $cal/cm^2 \cdot sec$

R : pipe radius or cylinder radius, cm

Re : Reynolds number ($= D\bar{u}/\nu$, $4H\bar{u}/\nu$, $2R\bar{u}/\nu$)

Re_c : critical Reynolds number

r : radial distance from the center of a tube or a cylinder, cm

Sc : Schmidt number

St : Stanton number

T : temperature, ^oC

T_A : amplitude of temperature oscillation, ^oC

T_w : wall temperature, ^oC

t : time, sec

U : approaching velocity, cm/sec

U_A : amplitude of velocity oscillation, cm/sec

u : velocity in the x-direction, cm/sec

$\bar{u}$: averaged velocity over a flow cross section, cm/sec

u^* : friction velocity, cm/sec

u_i : i-component of velocity vector, cm/sec

u' : fluctuating velocity in x-direction, cm/sec

v : velocity vector

v' : fluctuating velocity in y-direction, cm/sec

v_r : velocity in radial direction, cm/sec

v_θ : velocity in angular direction, cm/sec

W : width of rectangular duct, cm

We : Weissenberg number

w' : fluctuating velocity in z-direction, cm/sec

x : longitudinal co-ordinate in flow direction, cm

y : lateral co-ordinate, cm
y=0 corresponds to channel wall

z : vertical co-ordinate, cm

Greek symbols

α : dimensionless parameter in Eq.(2-13)

β_1 : relaxation factor defined by Eq.(5-24)

β_2 : relaxation factor defined by Eq.(5-25)

ε : eddy diffusivity, cm^2/sec

ζ : vorticity

η_s : solvent viscosity, g/cm sec

$[\eta]$: intrinsic viscosity, dl/g or cm^3/g

Θ : dimensionless temperature defined by Eq.(3-15)

Θ_b : dimensionless bulk temperature defined by Eq.(3-19)

θ : angle in cylindrical co-ordinate, degree or radian

θ_d : scattering angle, degree

θ_s : separation angle, degree

λ : relaxation time of Maxwell model, sec

λ_ℓ : relaxation time by Rouse, sec

λ_t : turbulent relaxation time, sec

λ' : material constant of Denn model

λ_i : wave length of incident beam, cm

λ_s : wave length of scattered beam, cm

λ_o : vacuum wave length, cm

μ : viscosity, g/cm sec

ν : kinematic viscosity, cm^2/sec

ν_i : frequency of incident beam, sec^{-1}

ν_p : frequency observed by scattering particle, sec^{-1}

ν_s : frequency of scattered beam, sec^{-1}

$\Delta\nu$: frequency shift of Doppler beat signal ($= \nu_s - \nu_i$), sec^{-1}

ρ : density, g/cm^3

ρ : fluctuating density, g/cm^3

σ : eddy diffusivity ratio ($= \varepsilon_H/\varepsilon_M$)

$\tau (=\tau_{xy})$: shear stress, $dyne/cm^2$

τ_{ji} : deviatoric stress tensor

τ_w : wall shear stress, $dyne/cm^2$

ψ : stream function

ω : representative frequency, sec^{-1}

superscript

$+$: nondimensionalized by wall parameter

subscript

H : for heat transfer

M : for mass transfer

o : for Newtonian fluid

REFERENCES

(1) Acrivos, A.; Phys. Fluids, 3, 657 (1960)

(2) Acrivos, A., L. G. Leal, D. D. Snowden and F. Pan; J. Fluid Mech., 34, 25 (1968)

(3) Arunahaham, Vr., R. L. Hummel and J. W. Smith; Canadian J. Chem. Eng., 50, 337 (1972)

(4) Astarita, G. and L. Nikodemo; Progress in Heat and Mass Transfer, 5, 37 (1972)

(5) Bazilevich, V. A.; J. Fluid Mech. Soviet Res., 3, 51 (1974)

(6) Berman, N. S. and V. A. Santos; A. I. Ch. E. Journal, 15, 323 (1969)

(7) Bizzel, G. D. and J. C. Slattery; Chem. Eng. Sci., 17, 777 (1962)

(8) Collinson, E., F. S. Dainton and G. S. McNaughton; Trans. Faraday Soc., 53, 489 (1957)

(9) Corman, J. C.; Ind. Eng. Chem. Process Des. Develop., 9, 254 (1970)

(10) Davis, A. H.; Phil. Mag., 47, 1057 (1924)

(11) Deissler, R. G.; NACA Report, 1210 (1955)

(12) Denn, M. M.; Chem. Eng. Sci., 22, 395 (1967)

(13) Dennis, S. C. R. and G. Chang; J. Fluid Mech., 42, 471 (1970)

(14) Dodge, D. W. and A. B. Metzner; A. I. Ch. E. Journal, 5, 189 (1959)

(15) Donohue, G. L., D. K. McLaughlin and W. G. Tiederman; Phys. Fluid, 15, 1920 (1972)

(16) Driest, E. R. van; J. Aeronaut. Sci., 23, 1007 (1956)

(17) Durst, F., A. Melling and J. H. Whitelaw; J. Fluid Mech., 56, 143 (1972)

(18) Elata, C., J. Lehrer and A. Kahanovitz; Israel J. Technol., 4, 87 (1966)

(19) Fortuna, G. and T. J. Hanratty; J. Fluid Mech., 53, 575 (1972)

(20) Goldstein, R. J., R. J. Adrian and D. K. Kreid; I. and E. C. Fundamentals, 8, 498 (1969)

(21) Goldstein, R. J. and D. K. Kreid; J. Appl. Mech., 34, 813 (1967)

(22) Gupta, M. K., A. B. Metzner and J. P. Hartnett; Int. J. Heat Mass Transfer, 10, 1211 (1967)

(23) Han, L. S.; J. Appl. Mech., 27, 403 (1960)

(24) Hartnett, J. P. and S. S. Yoo; 5th Int. Heat Transfer Congress, Tokyo, Japan, FC-5-8 (1974)

(25) Hasegawa, T. and Y. Tomita; Kikaigakkai ronbunshu , Japan, 35, 1277 (1969)

(26) Hsu, N. T., K. Sato and B. H. Sage; Ind. Eng. Chem ., 48, 2218 (1956)

(27) Isakoff, S. E. and T. B. Drew; Proc. of General Discussion on Heat Transfer, 405 (1951)

(28) James, D. F. and A. J. Acosta; J. Fluid Mech., 42 269 (1970)

(29) Karman, T. von; Trans. A. S. M. E., 61, 705 (1939)

(30) Krantz, W. B. and D. T. Wassan; Ind. Eng. Chem. Fundamentals, 10, 424 (1971)

(31) Krantz, W. B. and. D. T. Wassan; A. I. Ch. E. Journal, 17, 1360 (1971)

(32) Lin, C. S., R. W. Moulton and G. L. Putnum; Ind. Eng. Chem., 45, 636 (1953)

(33) Marrucci, G. and. G. Astarita; I. and E. C., 6, 470 (1967)

(34) McAdams, W. H.; "Heat Transmission" 2nd Ed. McGrow Hill Book Co., 222 (1942)

(35) Meek, R. L. and A. D. Baer; A. I. Ch. E. Journal, 16, 841 (1970)

(36) Metzner, A. B. and G. Astarita; ibid., 13, 550 (1967)

(37) Metzner, A. B. and P. S. Friend; Ind. Eng. Chem., 51, 879 (1959)

(38) Mizushina, T., Advances in Heat Transfer, 7, 87 (1971)

(39) Mizushina, T. and Y. Kuriwaki; Memoirs Fac. Eng.

Kyoto University, XXIX (2), 197 (1967)

(40) Mizushina, T. and F. Ogino; J. Chem. Eng. Japan, 3, 166 (1970)

(41) Mizushina, T. and T. Sasano; International Developments in Heat Transfer, 662 (1961)

(42) Mizushina, T. and H. Usui; Preprint of 5th Autum Meeting of S.C.E.J., E-205 (1971)

(43) Na, T. Y. and I. S. Habib; Appl. Sci. Res., 28, 302 (1973)

(44) Nikuradse, J.; Forsh. Arb. Ing.-Wes. No.356 (1932)

(45) Poreh, M. and U. Paz; Int. J. Heat Mass Transfer, 11, 805 (1968)

(46) Prutt, G. T., N. F. Whitsitt and H. R. Crawford; "Turbulent heat transfer to viscoelastic fluids" The Western Campany, Dallas, Texas (1966)

(47) Rouse, P. E.; J. Chem. Phys., 21, 1272 (1953)

(48) Rudd, M. J.; J. Fluid Mech., 5, 673 (1972)

(49) Seyer, F. A. and A. B. Metzner; A. I. Ch. E. Journal, 15, 426 (1969)

(50) Shah, M. J., E. E. Petersen and A. Acrivos; ibid., 8, 542 (1962)

(51) Shin, H.; Sc. D. thesis, M.I.T. (1965)

(52) Smith, K. A., E. W. Merrill, H. S. Mickley and P. S. Virk; Chem. Eng. Sci., 22, 619 (1967)

(53) Spalding, D. B.; Progress in Heat and Mass Transfer

5, 275 (1972)

(54) Son, T. S. and T. J. Hanratty; A. I. Ch. E. Journal, 13, 689 (1967)

(55) Son, J. S. and T. J. Hanratty; J. Fluid Mech., 35 369 (1969)

(56) Takami, H. and H. B. Keller; "Numerical solution of nonlinear differential equations," John Wiley, New York (1966)

(57) Taneda, S. ; J. Phys. Soc. Japan, 11, 302 (1956)

(58) Toms, A. B. ; Proc. 1st Int. Congress on Rheol. V2, 135 (1948)

(59) Tritton, D. J. ; J. Fluid Mech., 6, 547 (1958)

(60) Ultman, J. S. and M. M. Denn; Trans. Soc. Rheol., 14, 307 (1970)

(61) Ultman, J. S. and M. M. Denn; Chem. Eng. Journal 2, 81 (1971)

(62) Virk, P. S.; J. Fluid Mech., 45, 417 (1971)

(63) Virk, P. S., E. W. Merrill, H. S. Mickley and K. A. Smith; J. Fluid Mech., 30, 305 (1967)

(64) Wasserman, M. L. and J. C. Slattery; A. I. Ch. E. Journal 10 383 (1964)

(65) Wells, C. S; A. I. A. A. Journal, 3, 1800 (1965)

(66) Wells, C. S. ; A. I. Ch. E. Journal, 14, 406 (1968)

(67) Yeh, Y. and H. Z. Cummins; Appl. Phys, Letters, 4,

176 (1964)

(68) Yoshioka, N. and K. Adachi; J. Chem. Eng. Japan, 6, 134 (1973)

ACKNOWLEDGEMENTS

The author expresses his appresiation to Professor Tokuro Mizushina of Depertment of Chemical Engineering Kyoto University for his valuable suggestion and encouragements in this study.

The author wishes to acknowledge to Associate Professor Fumimaru Ogino and Lecturer Hiromasa Ueda of Department of Chemical Engineering, Kyoto University, and other persons in Mizushina laboratory for their helpful advices.

Many persons; Messrs Tian Chuan Shen, Taichi Yoshida, Toshiyuki Yamamoto, Naohiro Mitui and Hisatoshi Mitamura deserve many thanks for their technical helps to this study.

Also the author wishes to thank Miss Kumiko Yoshinari for her help in the preparation of this thesis.

H. Usui

Kyoto, December 1974